

Final Report
STUDY METHODS TO CHARACTERIZE AND IMPLEMENT THERMOGRAPHY
NONDESTRUCTIVE EVALUATION (NDE)

Contract Number: NAS8-97095
Task: H-28166D

Principle Investigator

James L. Walker
Center for Automation and Robotics
University of Alabama in Huntsville
Huntsville, AL 35899
(256)-890-6578*207

Submitted to

Samuel S. Russell
EH13
National Aeronautics and Space Administration
Marshall Space Flight Center, AL 35812
(256)-544-4411

October, 1998

TABLE OF CONTENTS

<u>Section</u>	<u>Page</u>
ABSTRACT.....	4
1.0 INTRODUCTION	5
2.0 THERMOGRAPHIC QUALIFICATION OF GRAPHITE/EPOXY INSTRUMENTATION RACKS.....	7
2.1 EXPERIMENTAL.....	8
2.1.1 IMPACT DAMAGE ASSESSMENT	8
2.1.2 POROSITY AND INCLUSIONS.....	10
2.2 DISCUSSION OF RESULTS	11
2.2.1 IMPACT DAMAGE ASSESSMENT	11
2.2.2 POROSITY AND INCLUSIONS.....	12
2.2.2.1 Results using the Amber Radiance 1/TWI system	12
2.2.2.2 Results Using The Bales Scientific Thermal Image Processor.....	16
2.3 CONCLUSIONS	17
3.0 THERMOGRAPHIC INSPECTION OF THE SPACE SHUTTLE MAIN ENGINE NOZZLE.....	18
3.1 DISBOND BETWEEN TUBES AND JACKET	18
3.2 DRILLED HOLE BETWEEN HAT BANDS 8 AND 9	19
3.3 INTERSTITIAL LEAKS AT THE NINTH HAT BAND.....	23
3.4 THERMOGRAPHY OF SSME4.....	25
3.4.1 INTENTIONAL WELD DEFECTS	25
3.4.2 COMPARISON OF THERMAL RESPONSE AT THREE PRESSURE LEVELS...27	
3.5 PAN, TILT AND FOCUS UNIT FOR INSPECTION OF SSME NOZZLE	29
4.0 TEST PANEL DESIGN FOR THE SPACE SHUTTLE CARGO BAY DOORS.....	34
4.1 TEST PANEL H1	34
4.2 TEST PANEL H2.....	36
4.3 TEST PANEL H3	38
5.0 MIKRON-AMBER CORRELATION.....	41
6.0 THERMOGRAPHIC INSPECTION OF GRAPHITE/EPOXY LOW PROFILE DOME	44
7.0 THERMOGRAPHIC INSPECTION OF GRAPHITE/EPOXY PANELS FOR THIOKOL ..	51

8.0 THERMOGRAPHIC INSPECTION OF GRAPHITE PANELS FOR LOCKHEED-MARTIN.....	58
9.0 SOLID ROCKET BOOSTER NOSE CAP	60
9.1 THERMOGRAPHY OF SRB COUPONS.....	60
9.2 THERMOGRAPHY OF GRAPHITE/CYANIDE ESTER PANEL	60
9.3 THERMOGRAPHY OF HG-10.....	61
9.4 HOT GAS PANELS (HG15, HG16, HG17, HG18, HG19, HG20).....	62
9.5 HOT GAS PANEL SC350 AND SCGLASS	65
9.6 HOT GAS PANEL EX1542 AND F650BMI (POST TREATMENT).....	66
10.0 X-38 PANEL #9	68
11.0 GRAPHITE/EPOXY DEBRIS IMPACT PANELS (PRE-IMPACT)	74

ABSTRACT

The limits and conditions under which an infrared thermographic nondestructive evaluation can be utilized to assess the quality of aerospace hardware is demonstrated in this research effort. The primary focus of this work is on applying thermography to the inspection of advanced composite structures such as would be found in the International Space Station Instrumentation Racks, Space Shuttle Cargo Bay Doors, Bantam RP-1 tank or RSRM Nose Cone. Here, the detection of delamination, disbond, inclusion and porosity type defects are of primary interest. In addition to composites, an extensive research effort has been initiated to determine how well a thermographic evaluation can detect leaks and disbonds in pressurized metallic systems "i.e. the Space Shuttle Main Engine Nozzles".

In either case, research into developing practical inspection procedures was conducted and thermographic inspections were performed on a myriad of test samples, subscale demonstration articles and "simulated" flight hardware. All test samples were fabricated as close to their respective structural counterparts as possible except with intentional defects for NDE qualification. As an added benefit of this effort to create simulated defects, methods were devised for defect fabrication that may be useful in future NDE qualification ventures.

1.0 INTRODUCTION

The process of taking infrared thermography (IRT) out of the lab and implementing it for the nondestructive evaluation (NDE) of advanced aerospace structures can be a complex task. Special attention must be given to determining the experimental limits and conditions which control the ability to perform a valid inspection. By characterizing and standardizing the thermal inspection process, factors such as measurement repeatability and reliability, defect size resolution and ease of data interpretation can be more effectively dealt with.

Thermographic NDE as it applies to structural “wellness” testing allows subsurface abnormalities to be visually detected through variations in surface temperature arising from the internal distortion of an externally applied “injected” heat field, such as from a flash lamp. The principle advantages of IRT over other NDE approaches is that the measurement can be made “at distance”, requiring no direct contact with the structure and can provide coverage over relatively large surface areas. The limitation on the size of the area to be tested varies primarily with the size of the defect to be located and the geometry/material of the structure.

The development of the thermographic method for application to inspection of aerospace structures is accomplished by first estimating the type, severity and location of the expected critical defects in the structure of interest. With this information the spatial resolution of the inspection can be estimated and required field of view determined. This in turn permits the development of an inspection grid, so as to provide optimal coverage of the structure. When no information is given as to the nature of the defects the inspection grid is normally determined based upon permitted inspection time and structural geometry. Next, a baseline must be established from the inspection of “thermally similar” test articles as to the conditions necessary to conduct a confident thermographic evaluation. Without this baseline the inspector has no way of telling if the inspection has caught all “critical” defects and also no way of quantifying the results obtained. To accomplish this task, test components are fabricated containing defects

simulating those found in real structures. By constructing test panels with various defect sizes, orientations and locations the threshold of detection for thermographic NDE of that specific aerospace structure can be determined.

The purpose of this project is to characterize the thermal inspection process such that IRT NDE can be efficiently implemented on a broad range of aerospace structures as well as be effectively tailored to specific applications. Emphasis has been placed upon developing standard methods for quantifying the resolution of the thermographic inspection with regard to defect size, type, orientation and depth into the structure. This in turn makes it possible to uniquely qualify thermography as a primary inspection tool for testing the structures of the next generation launch vehicles and other NASA aerospace hardware.

2.0 THERMOGRAPHIC QUALIFICATION OF GRAPHITE/EPOXY INSTRUMENTATION RACKS

A nondestructive evaluation method is desired for ensuring the “as manufactured” and “post service” quality of graphite/epoxy instrumentation rack shells. The damage tolerance models and geometry of the racks dictate that the evaluation method be capable of identifying defects, as small as 0.25 inch² in area, over large acreage regions, tight compound radii and thickness transition zones. The primary defects of interest include voids, inclusions, delaminations and porosity.

The potential for an infrared thermographic inspection to replace ultrasonic testing for qualifying the racks as “defect free” is under investigation. The inspection process is validated by evaluating defect standard panels built to the same specifications as the racks, except for the insertion of artificially fabricated defects. The artificial defects are designed to closely match those which are most prevalent in the actual instrumentation racks. A target defect area of 0.0625 inch² (a square with 0.25 inch on a side) was chosen for the defect standard panels to ensure the ability to find all defects of the critical (0.25 inch²) size.

One part of the qualification of an aerospace structure for service involves verifying that no defects were created during the manufacturing process and that no damage was produced during handling. This is normally accomplished with a combination of nondestructive evaluation (NDE) methods at various stages of the assembly. The graphite/epoxy instrumentation racks under investigation for this study are qualified through a series of ultrasonic inspections after fabrication. Ultrasonic testing (UT) provides 100 percent coverage of the rack shell and has the potential of locating all critically sized defects. The problem with UT though, is that it is time consuming and requires submersion of the shell in a water tank during the scanning operation. Therefore, the method is not suited for post flight or in-service inspections; i.e. a fully equipped rack. Infrared (IR) thermographic methods on the other hand have proven to be well suited for the inspection of monolithic “shell” structures.

As previously discussed, one of the principle advantages of IR thermography over conventional ultrasonic testing is that with thermography large regions are viewed in each inspection operation as opposed to the point by point coverage of UT. Also, no direct contact with the structure is required with thermography, such as the water coupling used with UT, therefore little disassembly of the structure is required. One of the main disadvantages of thermography is that in order for a defect to be detected it must interfere with an externally applied heat pulse in such a way as to develop a change in the normal surface temperature profile. A very tight defect or one that is thermally similar to the surrounding material has little chance of being detected.

The racks under investigation are constructed from an autoclaved graphite/epoxy with 18 ply acreage regions building up to 22 plies in the corners. A protective layer of fiberglass provides the finish layer and serves as a “tattle-tale” for in-service damage. The fiberglass shows as white

against the black graphite background when its surface is struck hard enough to produce significant internal damage. The defects of interest include voids, inclusions, delaminations and porosity with a critical area threshold of 0.25 inch².

2.1 EXPERIMENTAL

The work presented is divided into two segments. First, the issues of delaminations created by way of impact damage is covered then the ability to locate simulated porosity and inclusions are discussed. The thermographic methods and results from inspection of actual rack panels are also covered.

2.1.1 IMPACT DAMAGE ASSESSMENT

Damage created as a result of low energy blunt impacts are particularly troublesome for composite structures, since drastic reductions in strength can be produced even when little or no surface indications are present. The primary type of damage in low energy impacts are delaminations and matrix cracking. Very complex damage patterns can be produced from impact loads and quite often the extent of damage grows in size through the thickness of a sample beneath the impact site. In many cases little or no indication of damage may be present at the impact site while, serious back side and through thickness damage exists. For this reason it is important to be able to inspect the instrumentation racks, fully loaded and installed as well as between missions.

Selection of the impact energy level was determined by performing a series of tests with different impact tups, drop heights and boundary “panel support” conditions on a section of the instrumentation rack. Table 1 outlines the thirteen impact levels used to determine the correct drop height and Figure 1 shows their locations on the sample rack section. Figure 2 contains the resulting thermograms produced by flash heating the impacted panel. Note that in Figure 2, none of the 9 and 12 inch drop height impacts (impact numbers 5, 6, 9 and 10) produced any detectable thermal indications. These impacts also produced no visual indications and when tested ultrasonically gave no sign of damage. The smallest detectable impact level was produced from a 13.5 inch drop (impact number 3 and 4) using a rubber mat to support the panel at the impact site.

An impact produced by a 0.25 inch tup weighing 2.67 lb, dropped from a height of 13.5 inch (impact number 1), was found to best match the desired defect size and shape. A series of thirty impacts, in a 6 x 5 array, were performed on a section of rack (Table 2) to establish statistically the ability to thermographically locate and evaluate the damage zones. The visible damage area shown in the fiberglass cover ply was measured for reference. The areas ranged from 0.01 to 0.058 inch² on the outer “impact” side of the rack to between 0.015 to 0.078 inch² on the inner surface of the rack panel. In all, only four of the damage areas exceeded the desired defect size limit of 0.0625 inch².

Table 1. Check-out impact loads

Impact	Drop Height (inch)	Tup size (inch)	Support Backing	Outside Area (inch ²)	Inside Area (inch ²)
1	13.5	0.25	No	0.007	0.151
2	13.5	0.25	No	Not visible	0.144
3	13.5	0.25	Yes	0.004	0.040
4	13.5	0.25	Yes	0.031	0.040
5	12	0.25	No	Not visible	Not visible
6	12	0.25	No	Not visible	Not visible
7	15	0.25	No	0.012	0.131
8	15	0.25	No	0.021	0.160
9	9	0.25	No	Not visible	Not visible
10	9	0.25	No	Not visible	Not visible
11	23	0.25	No	0.342	0.650
12	13.5	0.5	No	0.017	0.176
13	21	0.5	No	0.016	0.225

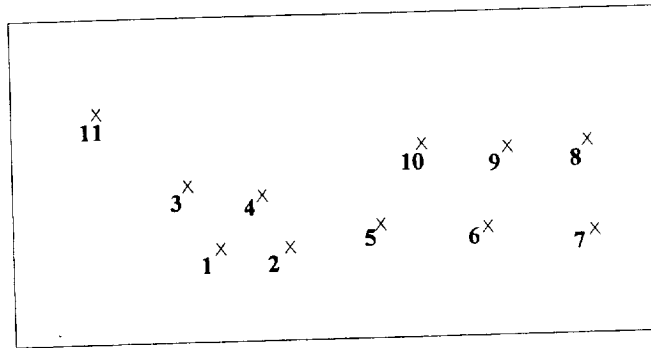


Figure 1. Impact locations for level determination.

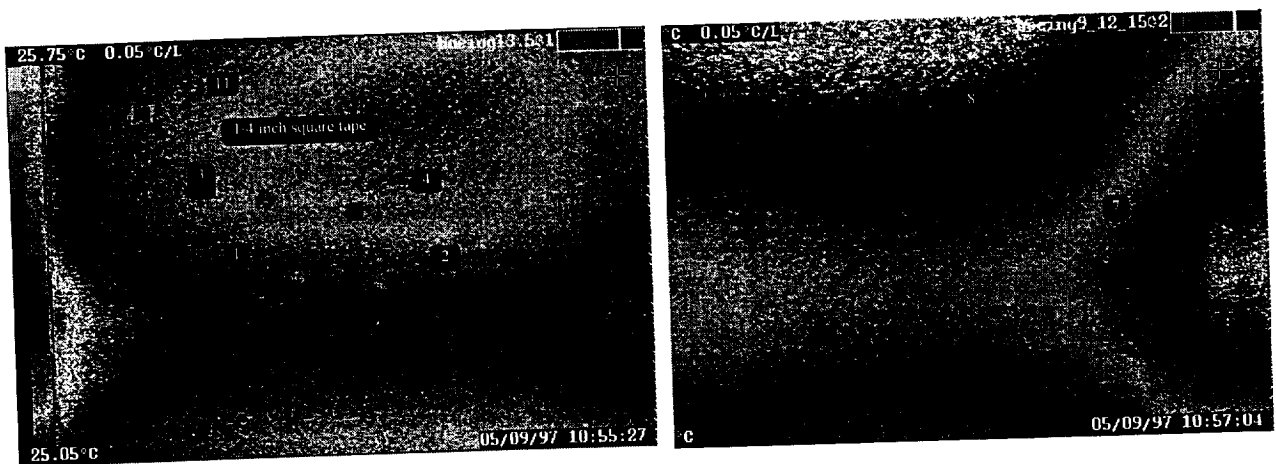


Figure 2. Thermograms of impact damage.

Table 2. Delamination size and impact energies.

Impact Number	Front Area (in ²)	Rear Area (in ²)	Impact Energy (ft-lbs)
1A	0.031	0.038	5.10
1B	0.038	0.030	4.16
1C	0.043	0.042	5.08
1D	0.057	0.034	5.06
1E	0.043	0.038	5.07
1F	0.047	0.038	4.30
2A	0.011	0.043	5.10
2B	0.044	0.034	5.08
2C	0.037	0.031	5.01
2D	0.036	0.045	5.05
2E	0.013	0.024	4.13
2F	0.058	0.026	5.12
3A	0.016	0.078*	4.94
3B	0.010	0.045	5.07
3C	0.033	0.041	4.25

Impact Number	Front Area (in ²)	Rear Area (in ²)	Impact Energy (ft-lbs)
3D	0.035	0.070*	5.01
3E	0.023	0.042	5.09
3F	0.029	0.039	5.05
4A	0.020	0.038	4.27
4B	0.010	0.026	4.46
4C	0.031	0.070*	5.08
4D	0.040	0.063*	5.04
4E	0.036	0.042	4.27
4F	0.042	0.042	5.06
5A	0.010	0.040	4.40
5B	0.012	0.026	5.06
5C	0.010	0.060	5.11
5D	0.048	0.037	5.07
5E	0.020	0.015	4.59
5F	0.013	0.044	5.05

2.1.2 POROSITY AND INCLUSIONS

During manufacture it is possible that regions within the laminate may contain tiny entrapped air bubbles, or porosity. The porosity can come from many sources including; degassing of contaminants (such as oils and silicones); improper debulking leaving air trapped between the plies; or poor ventilation restricting the removal of any degassing of the panel, to name a few. No matter what the source, porosity can have a detrimental effect on the performance of the structure by leaving regions of unsupported fibers and points of stress concentration. If the regions of porosity are large enough they may begin to interlink under stress and drastically weaken the load carrying capability of the fibers especially when put under compressive forces. For the racks under investigation in this paper a 0.25 inch² area of concentrated, or connected, porosity was set as the critical limit.

To determine the limits of thermographic NDE for detecting porosity two tests were performed. First, a section of a rack with known porosity documented through an ultrasonic map was thermographically examined. Second, a 24 ply monolithic test panel was created with simulated porosity of known size and depth into the laminate. The panel was constructed from bi-directional graphite/epoxy D683-29026 (22 plies) and E-Glass D683-29042 (2 cover plies) using a (0,45,45,0,45,0,0,45,0,0,45,0) lay-up schedule similar to that of the actual racks. The simulated defects were sized around the critical area by using 0.25, 0.50, 0.75 inch square regions yielding areas of 0.0625, 0.25 and 0.5625 inch². The pattern of planned defects is shown in Figure 3.

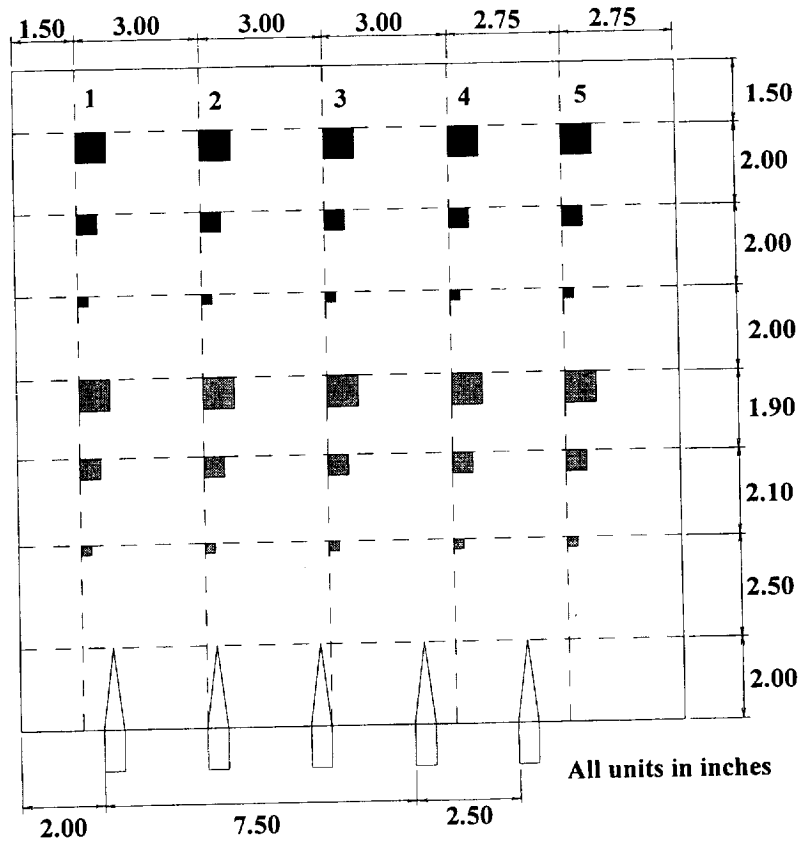


Figure 3. Fabricated test panel.

The light gray regions in Figure 3 depict where the simulated porosity “microballons” (7.0 nm diameter fused silica SiO₂ spheres) were placed in the panel. The dark Gray regions in Figure 3 are folded plastic backing material (0.001 inch thick polypropylene), used to simulate inclusions and disbond areas. Wedge shaped stainless steel shims (0.006 inch thick) were also inserted into the laminate to create void regions when they were removed after cure and are visible at the bottom of the panel. The defects were placed in five columns so that the depth of inspectability could be investigated. The defects were placed between plies (2-3), (5-6), (11-12), (16-17) and (21-22).

2.2 DISCUSSION OF RESULTS

2.2.1 IMPACT DAMAGE ASSESSMENT

The impacted panel was thermographically inspected using flash heating from the impact side. The coverage area for the imager dictated that the panel be inspected in two passes, each covering an area of the panel 18 inches wide by 12 inches tall. As evident in Figures 4 and 5, all thirty impact locations were identified thermographically. The extent of the damage between impact points as viewed by the thermography system remained fairly constant even though the visual measurements varied greatly between positions (Table 2). The thermograms indicate that the maximum damage area is approximately 0.25 inch square as seen by comparison with the foil

tape square in each image. As expected, yet not apparent in the two thermograms shown, the damage appeared to enlarge with depth away from the impact point.

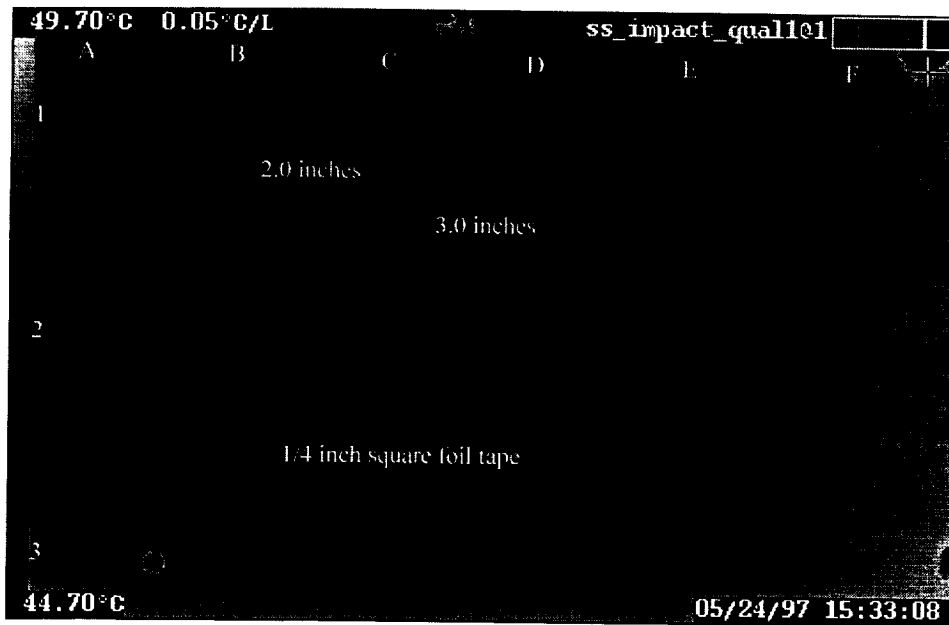


Figure 4. Rows 1, 2 and 3 of qualification impacts.

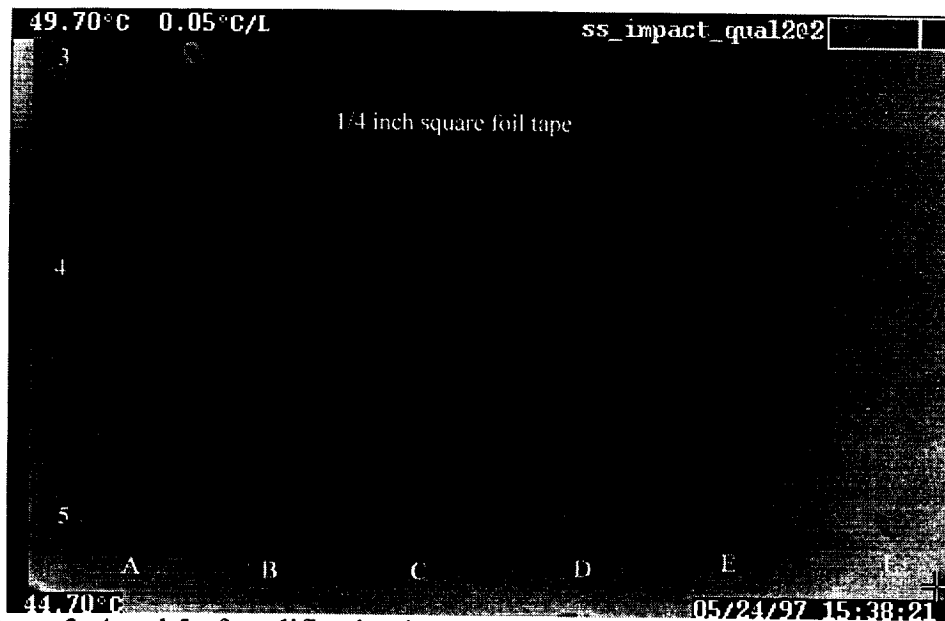


Figure 5. Rows 3, 4 and 5 of qualification impacts.

2.2.2 POROSITY AND INCLUSIONS

2.2.2.1 Results using the Amber Radiance 1/TWI system

A section of a rack panel with known porosity was inspected thermographically and compared against the UT results. As shown in Figure 6 a close match to the pattern of porosity is given

between the UT image and thermogram. In Figure 6 the porosity shows up as a dark patch for the UT image and as a white "hotter" zone on the thermogram. The single thermogram does not show all the details of the UT image since the porosity actually resides throughout the thickness. The UT image measures the complete thickness of the panel while the thermogram shows only the effects from a single slice the cross-section. When several thermograms are viewed over time though, by rastering through the scan history, most if not all of the details in the UT plot can be seen on the thermography image.

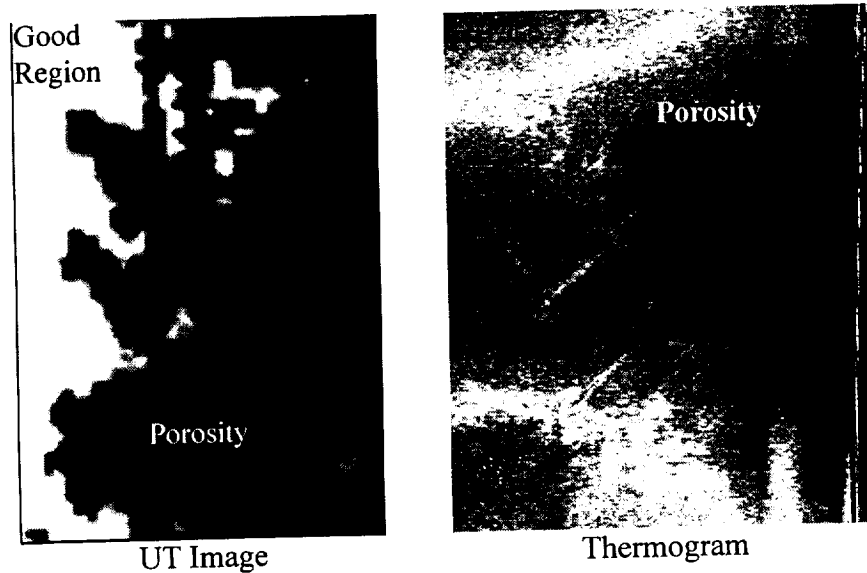


Figure 6. Comparison of Actual Porosity detected by UT and Thermography

In order to verify the depth of penetration of the thermography inspection a specially designed defect panel was constructed (see Section 2.1.2) and examined. The inspections were accomplished through the use of an Amber Radiance 1 camera with Thermal Wave Imaging software. The imager was positioned sixteen inches from the subject and though the use of a 25 mm lens gave a six inch square field of view. The flash unit used to thermally excite the sampled was set to deliver 1.6 kJ of energy to the surface of the panel.

The resulting thermograms indicate that the limits of the system are somewhere between the second and third column of defects, i.e. between the sixth and eleventh ply. Figures 7 and 8 show the defects from the first and second column from both sides of the panel (columns 1, 2, 4 and 5).

The primary drivers behind a successful thermal inspection lies in the ability to get heat into a structure uniformly and with sufficient intensity to create a temporary thermal imbalance around an anomaly as well as to resolve those temperature variations. The structure under test, although appearing to be a good color to absorb heat "black", is somewhat reflective. Due to the high reflectivity, even with a large heat pulse, most of the energy is reflected away from the panel. Possible solutions to this problem included spraying the surface with a flat black water soluble paint, using peal ply during manufacture to dull the surface, or increasing the number of flash

heat lamps (input heat energy). Of these solutions, increasing the number of heat lamps would have the least effect on production time but would require doubling the support hardware for the thermographic inspection. Dulling the surface during manufacture with peal ply would not be a likely choice since it would mean reevaluating the structural performance of the rack. The application of a water washable paint appeared to be the best choice for increasing the surface conductivity of the panel.

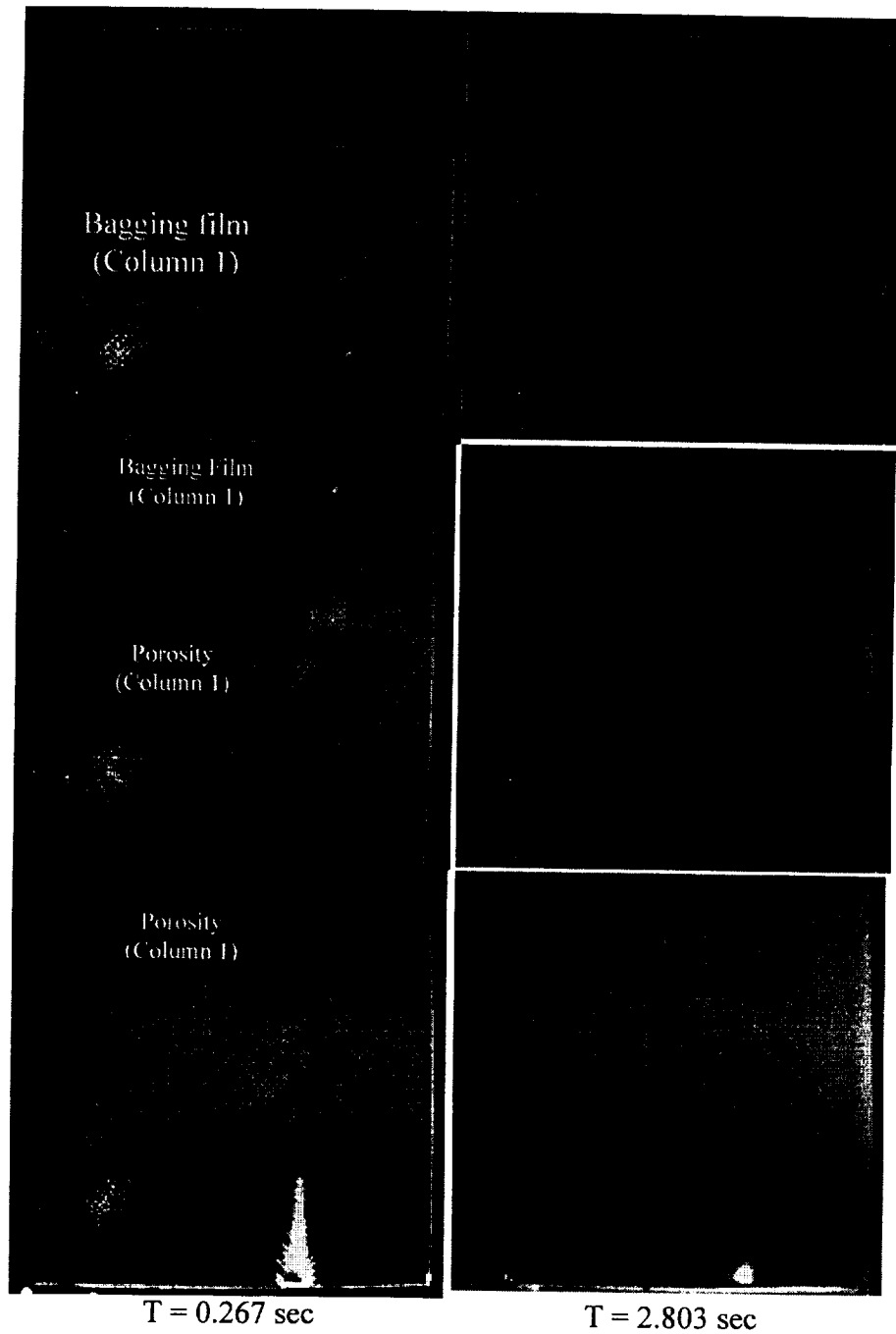


Figure 7. Results from test panel (Front side).

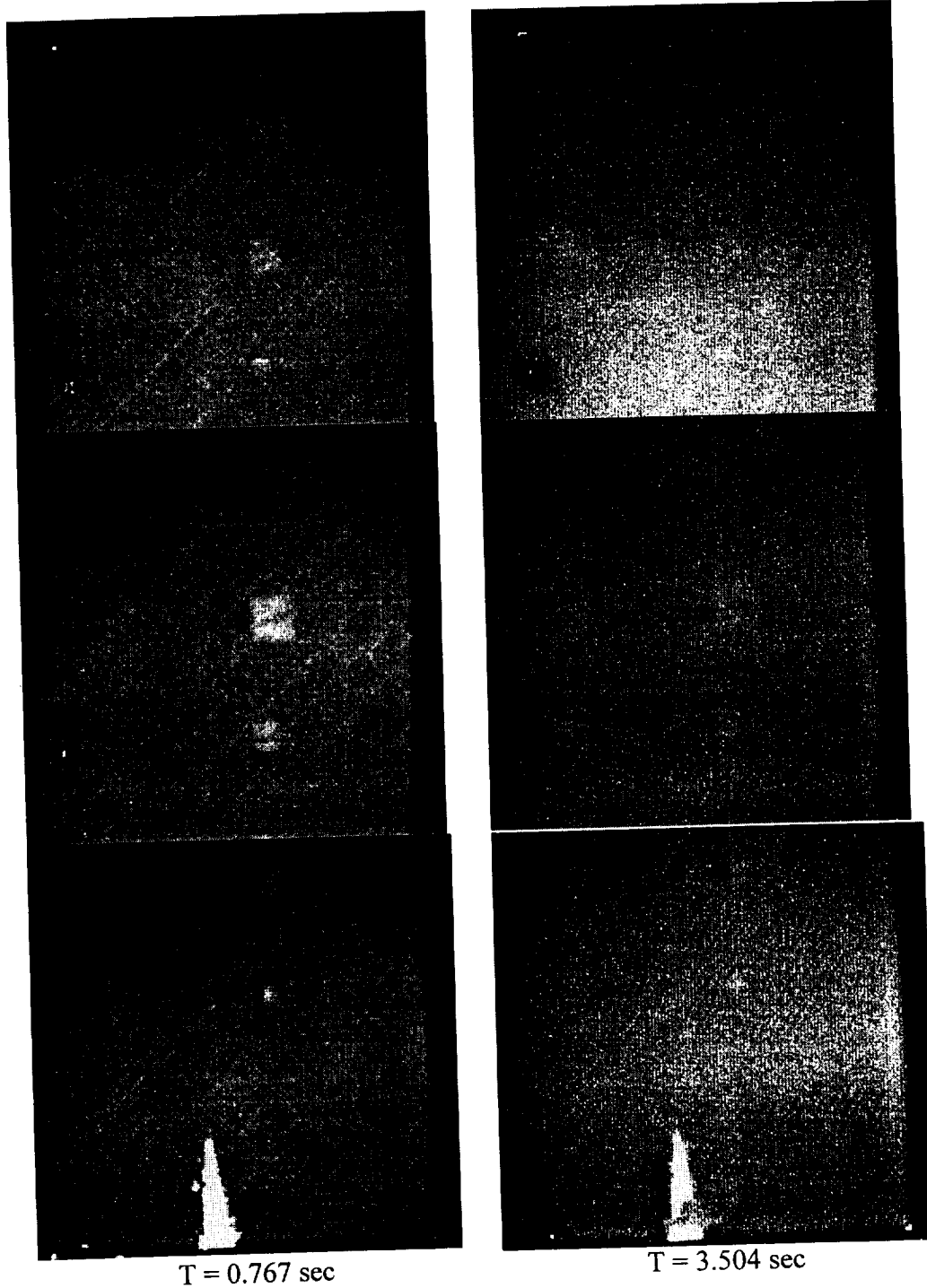


Figure 8. Results from test panel (Back side).

As shown in Figure 9, by spraying the surface with a water washable flat black paint it was possible to thermally penetrate to the midply of the laminate. The 0.25 inch square region of porosity is right on the edge of detectability, but can be seen when the thermograms are viewed in a series over time. Although this technique would require that the panel be inspected from

both sides and the rack be spayed and cleaned up after the inspection, it does demonstrate the potential to inspect the racks with thermography.

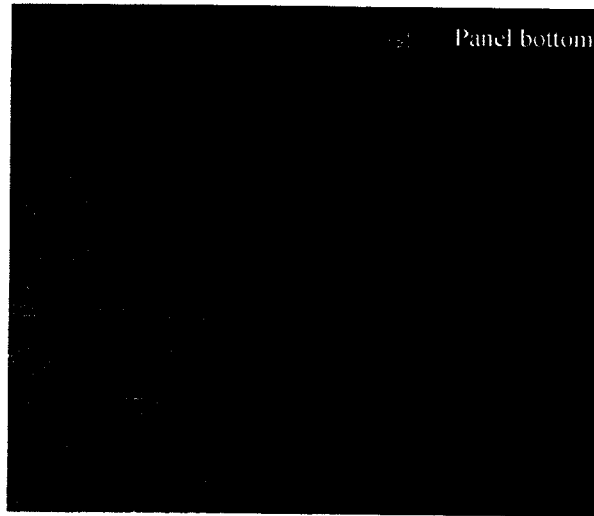


Figure 9. Midply porosity viewed when test panel was painted flat black.

2.2.2.2 Results Using The Bales Scientific Thermal Image Processor

For comparison, the Bales Thermal Image Processor was also used to inspect the panel. The imager was set 16 inches from the test panel and flashed with a power setting of 1400V (≈ 1.4 kJ)

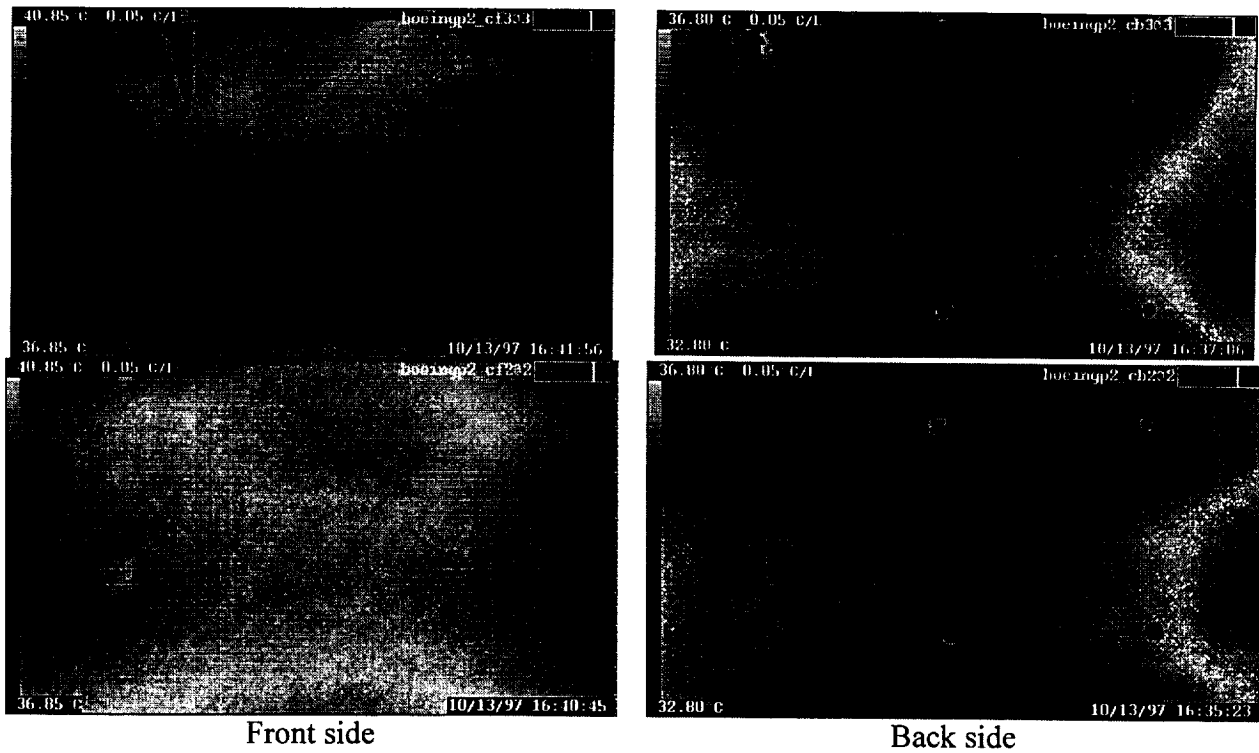
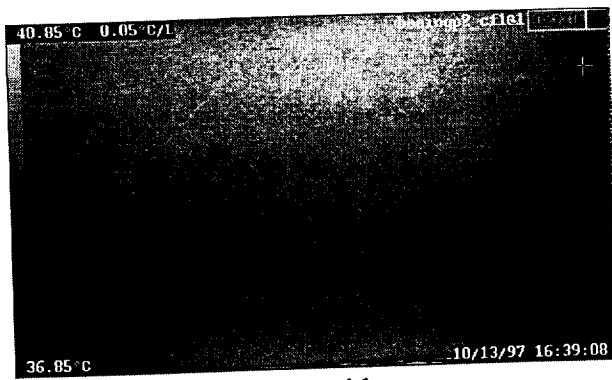
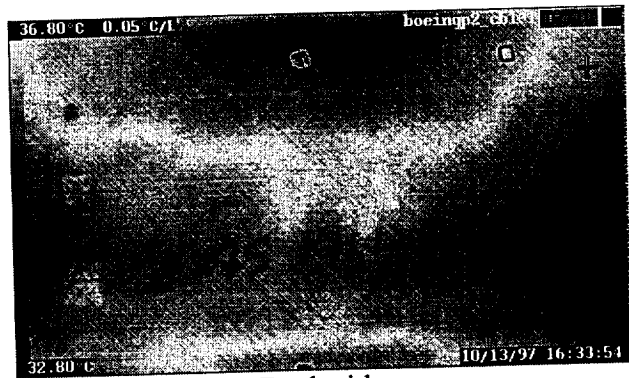


Figure 10. Bales TIP results.



Front side



Back side

Figure 10 continued.

2.3 CONCLUSIONS

Infrared thermography has been demonstrated to be capable of detecting impact damage “delamination”, porosity and inclusion type defects in the graphite/epoxy instrumentation racks. Good confidence was found for detecting delaminations related to impact damage. The thermographic technique was capable of detecting the subsurface effects of the impact loading that would have been missed with a visual inspection. Porosity close to the surface was found to also be a good candidate for location with thermography. When the porosity reached depths of six or more plies it is difficult to say with any confidence that it could be detected without some surface preparation of the racks. With the application of a flat black, water washable, paint the porosity at the midplane of the panel was able to be detected. Finally, embedded inclusions and voids were detectable down to about six plies into the laminate and deeper with the addition of a dulling agent to the panels surface.

Additional research will need to be performed to develop methods to raise the sensitivity of the thermographic inspections to a level that will permit one sided inspections without the need for altering the surface finish of the racks. Investigations into image enhancement to increase the sensitivity of the thermographic system, optional heating methods to better excite the defect and finite element methods to determine the theoretical limitations of the system are ongoing.

The primary drivers behind a successful thermal inspection is the ability to get heat into a structure uniformly and with sufficient intensity to create a temporary thermal imbalance around an anomaly and the means to resolve those temperature variations. Both systems are highly sensitive; the Bales system has a sensitivity of $0.05^{\circ}\text{C}/\text{level}$ of color and the Amber system can resolve $0.025^{\circ}\text{C}/\text{level}$. The main limitation for both systems is the ability to heat the part quickly and to a sufficient level to make the defects react.

The structure under test, although being a good color to absorb heat “black”, is somewhat reflective. Possible solutions to this problem would be to spray the surface with a flat black water soluble paint, use peel ply during manufacture to dull the surface, or increase the number of heat lamps. Of these solutions, increasing the number of heat lamps has the least effect on production time. By doubling the number of flash bulbs it may be possible to insert sufficient heat into the structure so that the cameras can detect the scheduled defects.

3.0 THERMOGRAPHIC INSPECTION OF THE SPACE SHUTTLE MAIN ENGINE NOZZLE

The nozzles of the Space Shuttle's main engines consist of approximately 1100 tapered Titanium tubes brazed to a Titanium structural jacket (Figure 11). Two potential problems occur within the SSME nozzles as a result of manufacturing anomalies and the highly volatile service environment. The first problem is the unbonding of the tubes from the jacket and the second is the leaking of fluid into the interstitial channels between the tubes as a result of tube fracture.

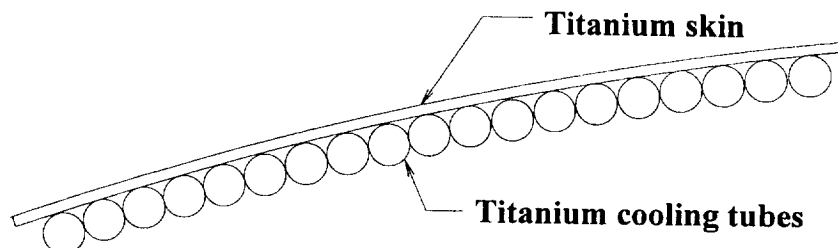


Figure 11. SSME nozzle cross section.

3.1 DISBOND BETWEEN TUBES AND JACKET

Initial experiments were performed to determine if it is possible to identify disbonds between the cooling tubes and shell of the SSME nozzle. The disbond was simulated by milling out a portion of the tubing with a moto-tool from the hot wall side of the nozzle as shown in Figure 12. The defect tapers from a 1 inch opening at the inner surface of the nozzle to the brazed edge of the skin. Although this did not produce a true disbond, the artificial defect did demonstrate the same thermal behavior that a disbond, i.e. both have the effect of reducing the effective flow path of heat.

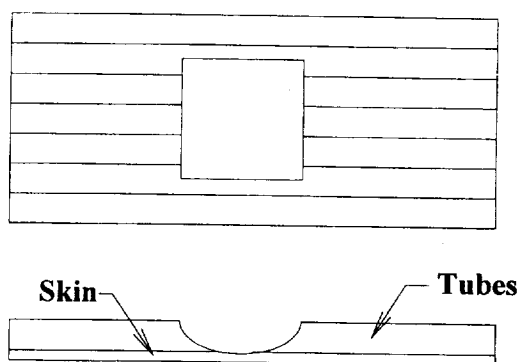


Figure 12. Artificial disbond.

The nozzle was then inspected by flash heating its cold wall side using the Amber Radiance 1 camera (25 mm lens) running under TWI software. Three surface treatments were investigated

including; none, flat white image developer, flat black spray paint and the thermograms gates set to 0.150, 0.584 and 1.485 seconds after flash

The images were all acquired by viewing the jacket side of the coupon after flash heating the same side. Areas of greatest structural integrity conducted the heat away from the jacket quite well, and appear dark in these images. Areas containing discontinuities (such as the programmed defect or the interstitial gaps between the cooling tubes and jacket) did not conduct the heat away from the jacket as well, and appear bright in these images.

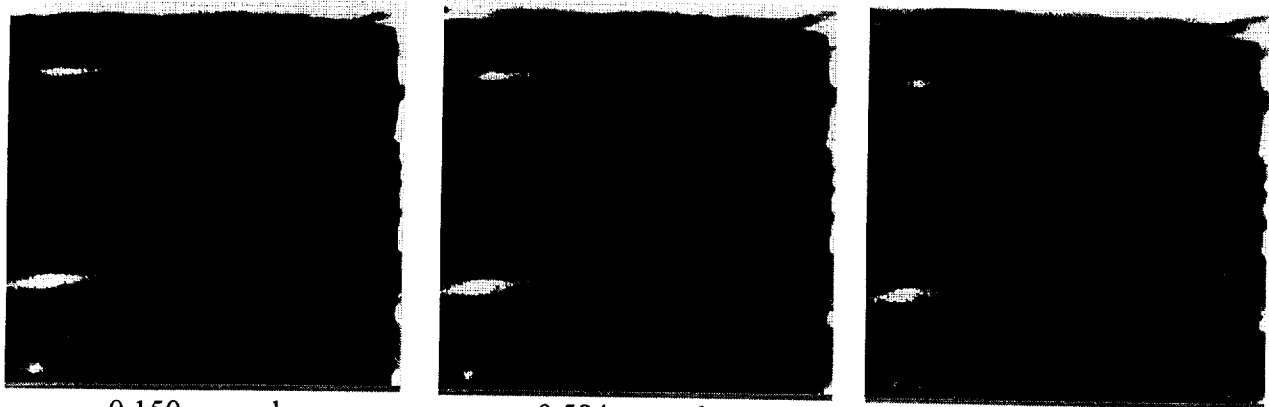
- **Figure 13a.** Obtained by viewing the unaltered jacket surface.
 - The dark (cold) spot is the thermal reflection of the cooled infrared camera.
 - The distinct horizontal bright (hot) “flares” are the thermal reflections of the residual heat in the lamps after flash.
 - The faint horizontal bright (hot) lines are the interstitial gaps between the coolant tubes and the jacket.
 - The faint horizontal dark (cold) lines are the regions where the coolant tubes are in contact with the jacket.
 - The diagonal bright (hot) line is a feature of unknown classification which is visible to the unaided observer on the coupon surface.
 - The vertical bright (hot) line is a feature of unknown classification which is not visible to the unaided observer on the coupon surface.
 - The extremely faint bright (hot) spot near the lower left “flare” is the thermal signature of the programmed defect.

- **Figure 13b.** Obtained by coating the jacket surface with a flat white powder (Adrox NQ1 liquid penetrant developer: non-aqueous solution of calcium carbonate).
 - The faint bright (hot) spot is the thermal signature of the programmed defect.
 - The faint horizontal bright (hot) and dark (cold) lines are the tubes and gaps.
 - The diagonal and vertical bright (hot) lines are the features of unknown classification.

- **Figure 13c.** Obtained by painting the jacket surface flat black.
 - The distinct bright (hot) spot is the thermal signature of the programmed defect.
 - The somewhat distinct horizontal bright (hot) and dark (cold) lines are the tubes and gaps.
 - The diagonal and vertical bright (hot) lines are the features of unknown classification.

3.2 DRILLED HOLE BETWEEN HAT BANDS 8 AND 9

As an initial attempt to create an interstitial leak in the nozzle a 1/16 inch diameter hole was drilled through the Titanium structural jacket into the interstitial region of the tubing. Using the same bit, a hole was started in the wall of a coolant tube. Once the wall was thinned sufficiently, a sharp pin was used to puncture the coolant tube (Figure 14). The resulting hole in the tube was then partially closed back off by forcing solder into the hole with a pointed chisel. The resulting defect was leak tested with a soap solution under 35 psi pressure. The leak produced a foaming indication similar to the class one or two defect. Finally the hole in the structural jacket was plugged with a piece of vacuum bag sealant tape.

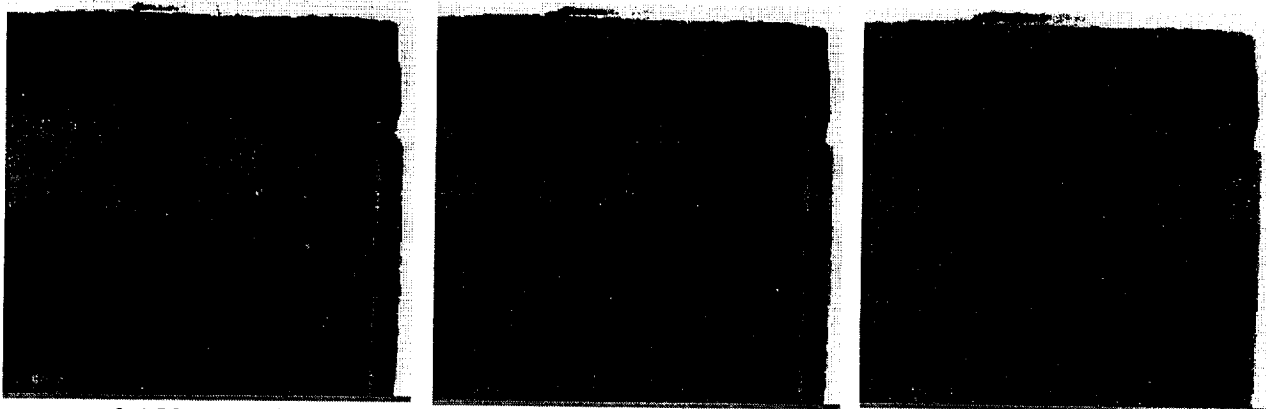


0.150 seconds

0.584 seconds

1.485 seconds

Figure 13a. No Surface Treatment

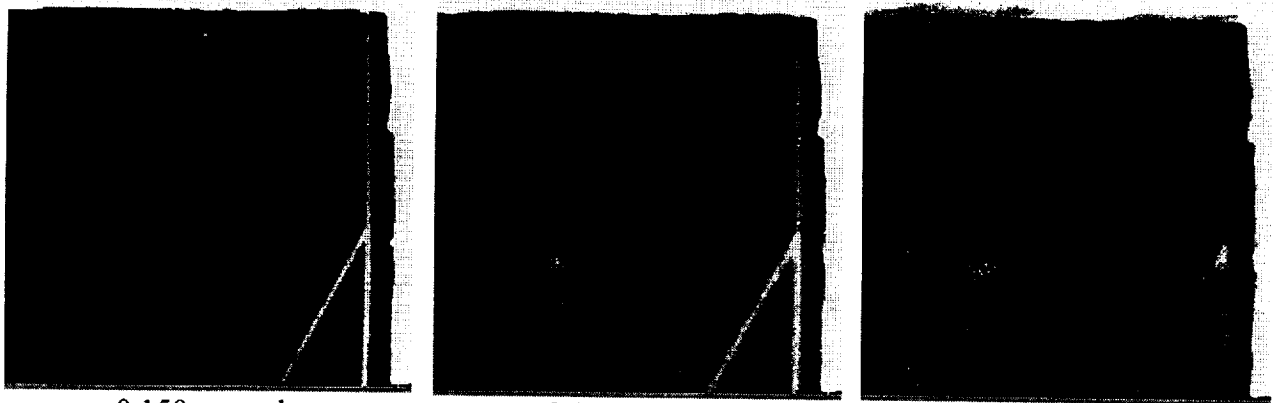


0.150 seconds

0.584 seconds

1.485 seconds

Figure 13b. Painted flat white (penetrant developer)



0.150 seconds

0.584 seconds

1.485 seconds

Figure 13c. Painted Flat Black (Water washable paint)

To verify that the thermographic inspection was seeing the leak and not the tacky tape, another piece of sealant tape was placed 2 inches away from the sealed hole.

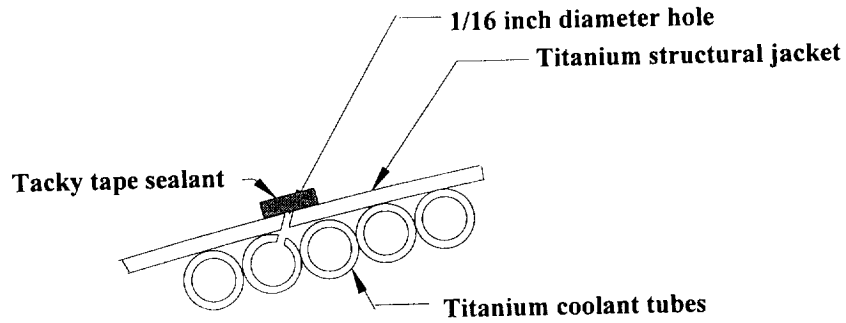


Figure 14. Artificial interstitial leak.

The defect was then inspected using the Amber Radiance 1 camera (25 mm lens) , running under the TWI software. The structure was viewed at a distance of 24 inches and no surface preparation was performed. Images were taken from the hot wall side at the defect location and below hat band 9 as shown in the following figures. The defective tube was connected to a nitrogen gas source and pressurized to 35 psi.

The affects of the leaking tube defect are apparent below the ninth hat band and in the acreage of the nozzle at the point were the tube is leaking. Inspection time may be saved by first conducting either a soap solution check or thermographic inspection below hat band 9 to locate which tube is defective. Once the defective tube is found thermography may be used to find the position along the tube where the defect exists.

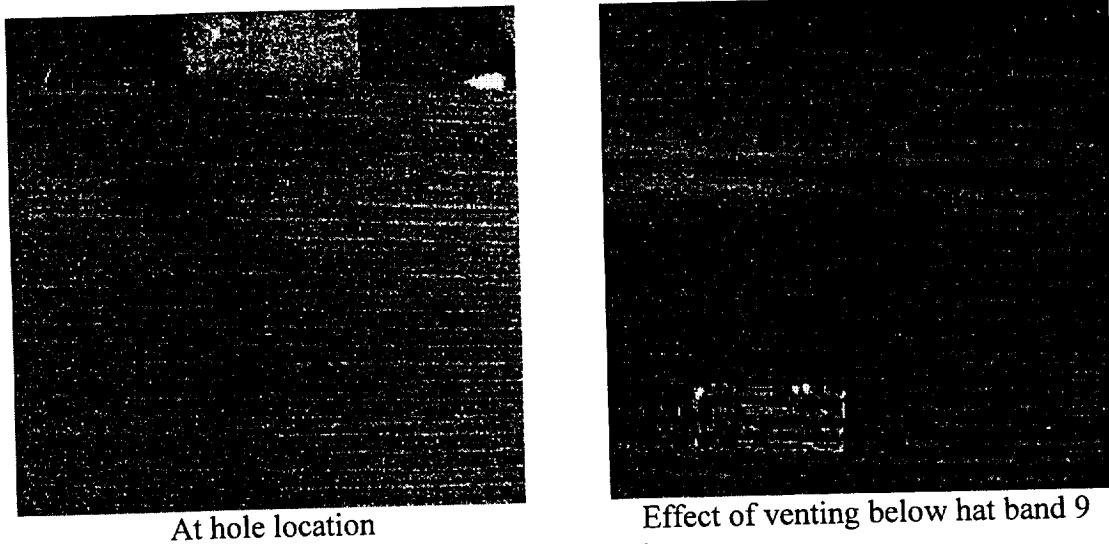


Figure 15. Thermograms of venting interstitial leak.

A second test was performed by pressurizing a series of tubes around the artificial defect in an attempt to simulate more closely an actual nozzle test. In the full nozzle test all the tubes would

be pressurized simultaneously. Figure 16 shows the manifold system used to pressurize eight tubes at a time from a common nitrogen bottle.

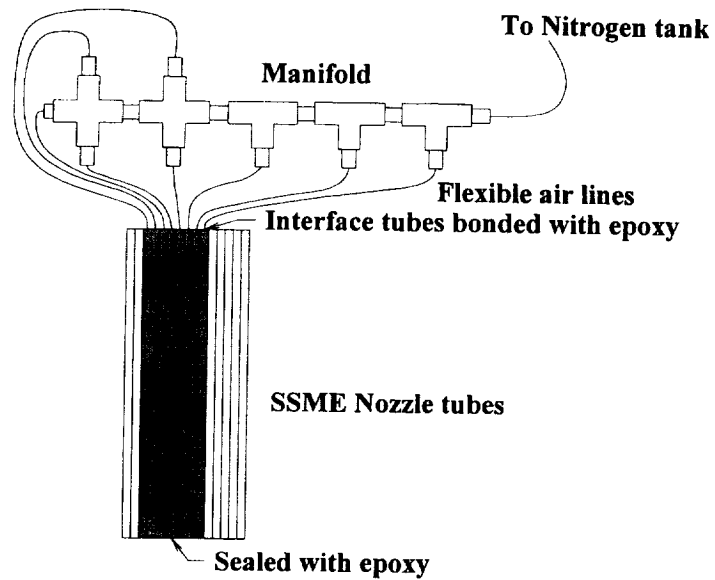


Figure 16. Pressurization manifold.

The resulting thermograms are provided in Figure 17 at a time of 6.1 seconds after initial pressurization. Note that in the unaltered image the defect is just barely visible. By subtracting the initial frame from all subsequent frames though the defect resolution is increased drastically. Upon pressurization the tubes are seen to increase in temperature while the leak produces a cold spot.

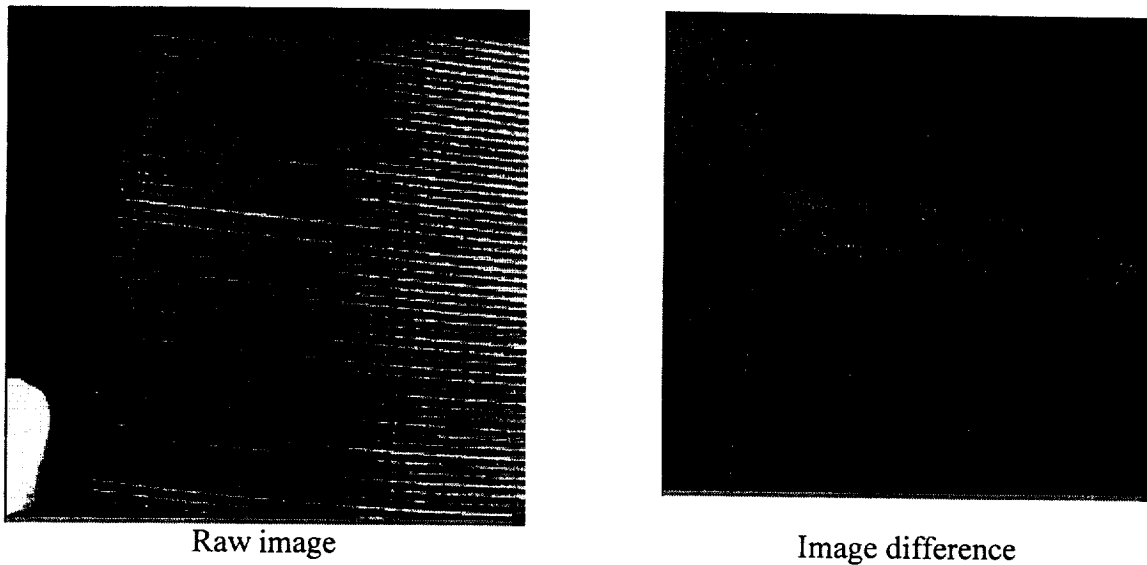


Figure 17. Comparison of raw image and image difference.

3.3 INTERSTITIAL LEAKS AT THE NINTH HAT BAND

A nozzle section was provided with a series of known interstitial leaks found by using leak check solution below the ninth hat band. These leaks were verified and divided into groups of 8 tubes so that they could be pressurized with the manifold system described in Section 3.2 of this report. A summary of the leaks and their locations is provided in Table 3. The thermograms are provided in Figure 18.

Table 3. Interstitial leaks

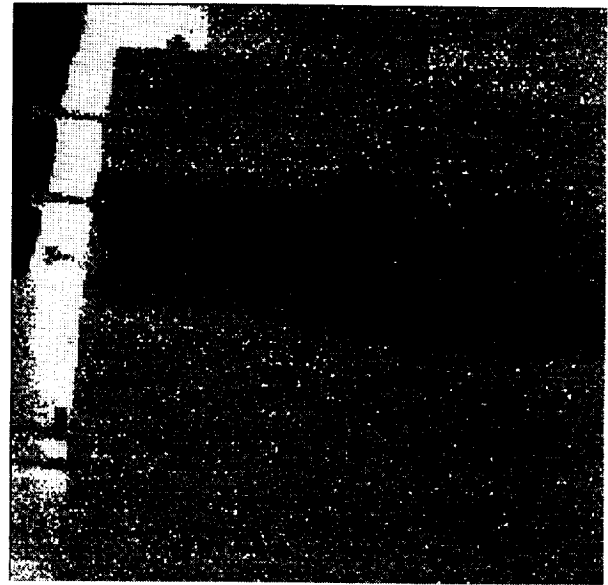
Tube Number	Region Number	Defect Class	Defect Location	
546	1	Type II	Both sides	
547		None		
548		Type I	Left	
549B		Type I	Right	
550		None		
551		None		
552		None		
553		None		
554		2	Type III	Centered
555B			Type III	Centered
556	Type III		Centered	
557	Type II		Right	
558	Type III		Centered	
559B	Type III		Centered	
560	None			
561	None			
562	3		None	
563			Type II	Right
564		Type III	Centered	
565		Type III	Centered	
566		Type III	Centered	
567		Type III	Centered	
568		Type III	Centered	
569		Type III	Centered	
570		Type III	Centered	
571B		4	Type II	Centered
572	Type III		Centered	
573B	None			
574	None			
575	None			

Type I => Frothy
 Type III => Blows out bubbles (audible)

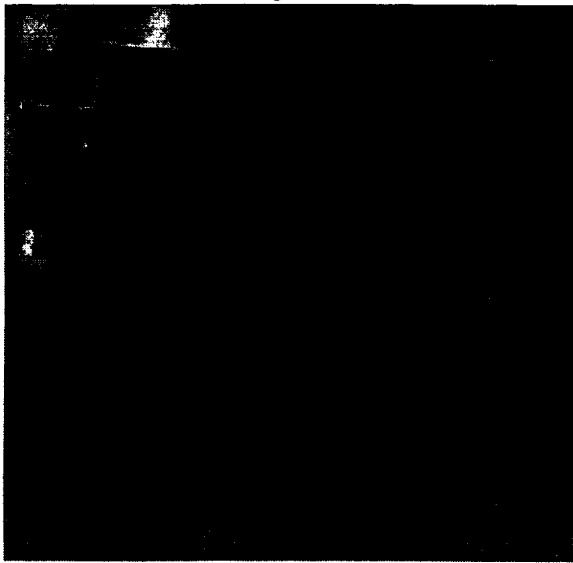
Type II => Bubble growth
 B => Bolt locations



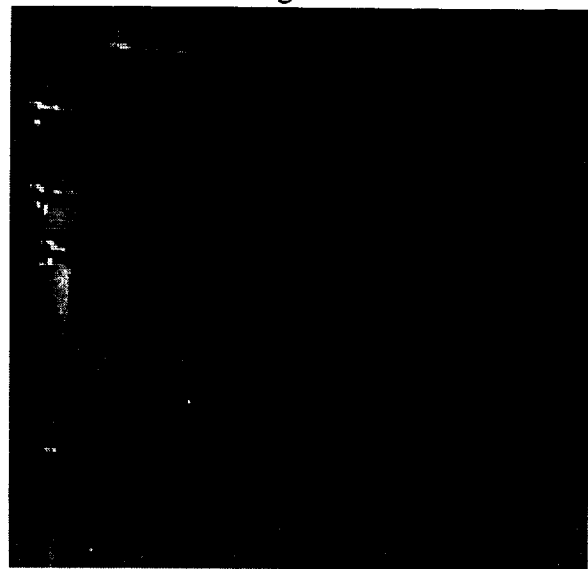
Region 1



Region 2



Region 3



Region 4

Figure 18. Thermograms of leaks at the ninth hat band.

3.4 THERMOGRAPHY OF SSME4

The nozzle segment known as SSME4 is a section of nozzle including the eighth and ninth hat bands that has artificial interstitial defects. The artificial defects were fabricated by cutting open the tubing on the hot wall side of the nozzle, then puncturing the tube into the interstitial region and finally resealing the tube through a welding operation.

During the reweld operation the hot wall surface of the tubes had to be cleaned with a wire brush. This left the surface shiny, which greatly limits the thermographic inspection capability. To dull the surface it was painted with a water washable flat black paint. As a side note, it is helpful to heat the metal surface with a hot air gun before painting. This provides a more consistent finish and permits a thinner coat of paint be applied and still have adequate dulling of the surface.

Unless otherwise noted all inspections were performed with the Amber Radiance 1 thermal camera (25 mm lens) and Thermal wave Imaging software at a distance of 18 inches. The system was pressurized to 35 psig Nitrogen and imaged

3.4.1 INTENTIONAL WELD DEFECTS

Two leak regions were manufactured in SSME4 as shown in Figure 19. The leak type and interstitial location were determined by individually pressurizing tubes and checking with leak solution (Tables 4 and 5). In all cases no surface leaks were detected with leak check solution

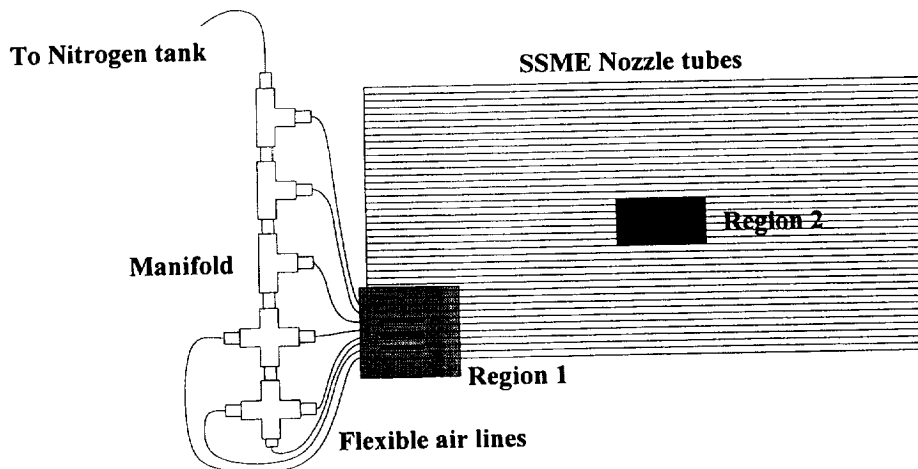


Figure 19. SSME4 defect regions.

Figures 20 and 21 show the resulting thermograms over 4 (gate)/time intervals. Also included in the figures are the Time-Temperature plots which provide an indication of the degree to which the defects can be detected.

Table 4. Region 1.

Defect number	Pressurized tube	Interstitial Leak location	Leak type
C	2	2-3	3
B	4	4-5	2
A	6	6-7	3

Table 5. Region 2.

Defect number	Pressurized tube	Interstitial Leak location	Leak type
E	4	4-5	1 - 2
D	9	9-10	3

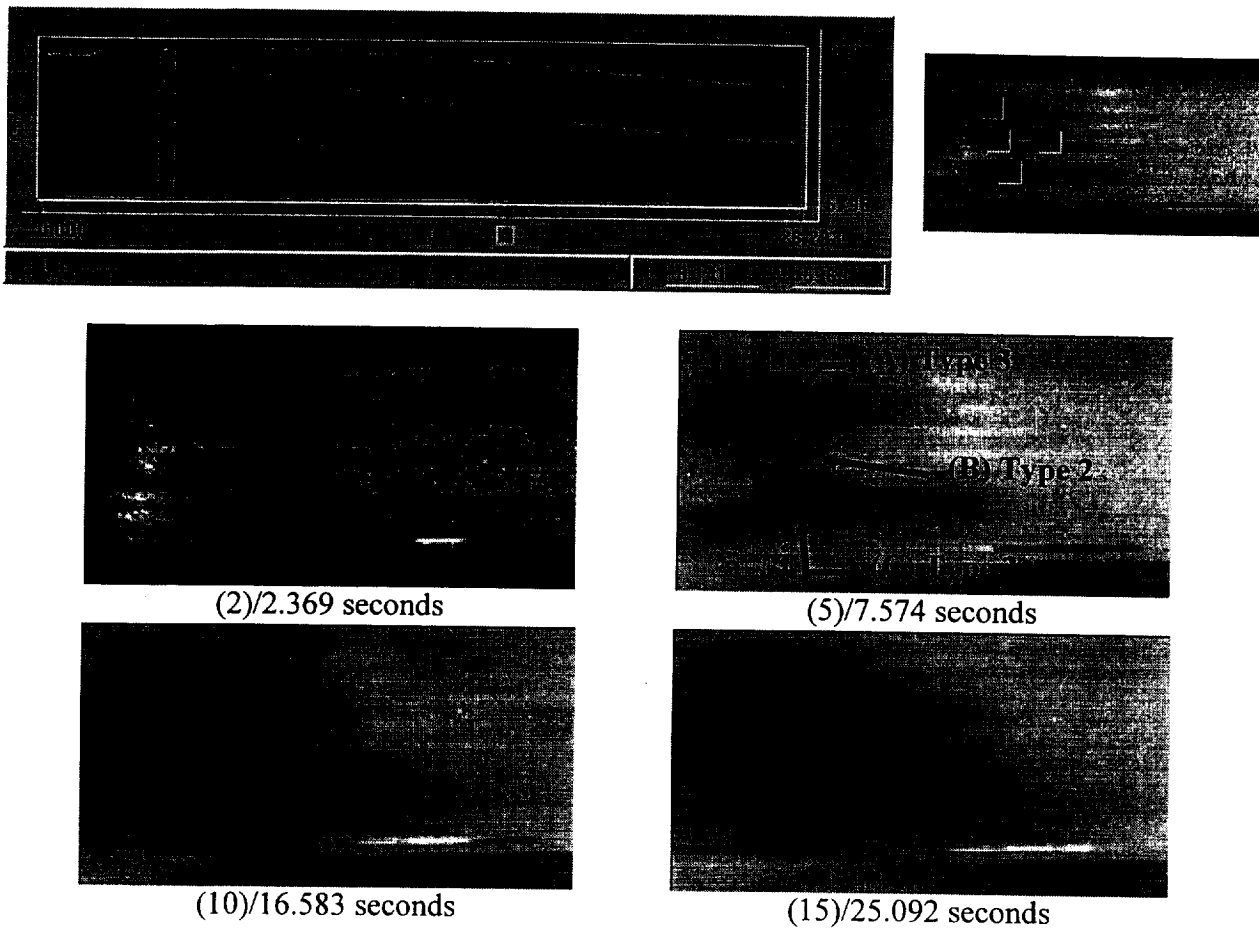


Figure 20. Region 1.

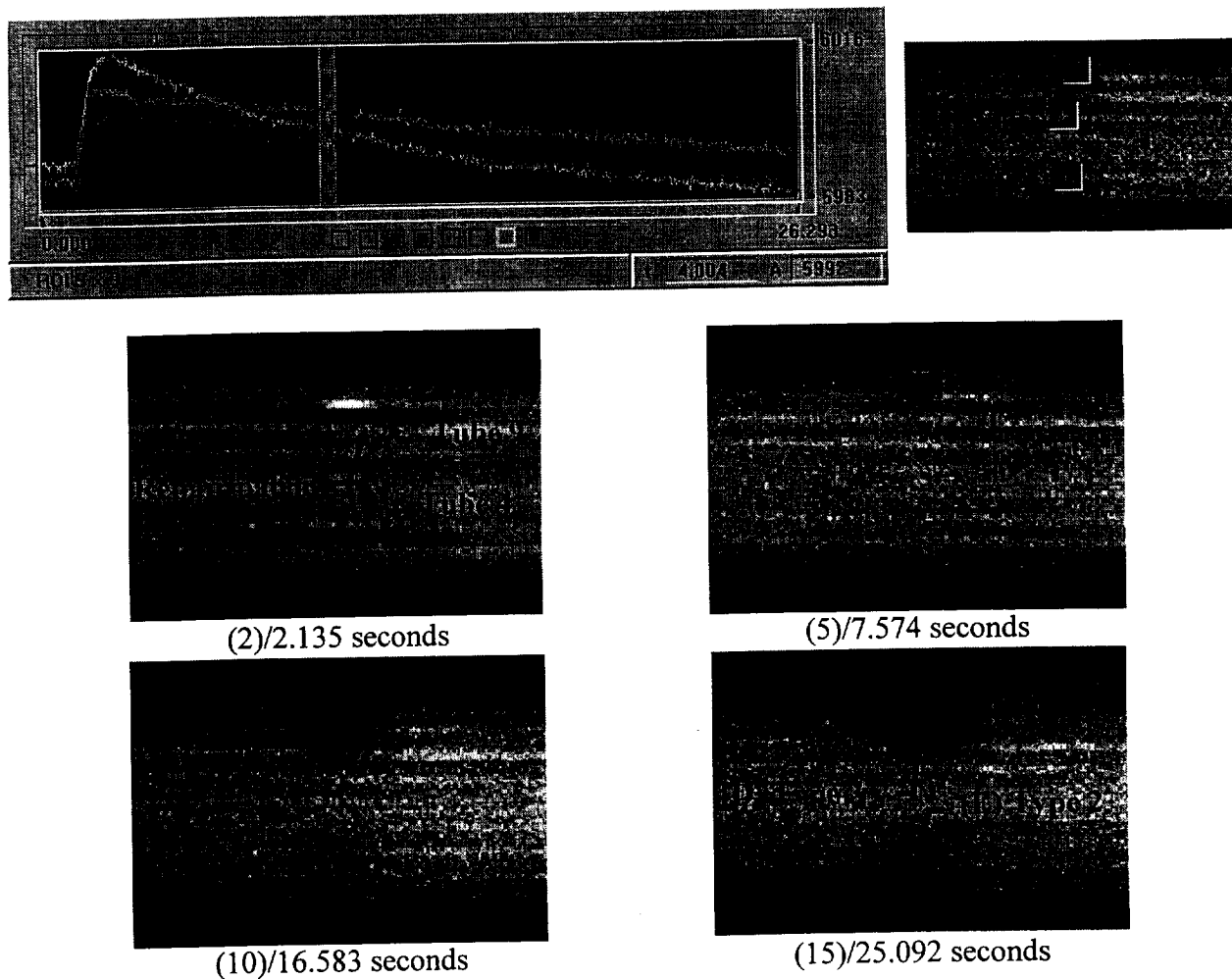


Figure 21. Region 2.

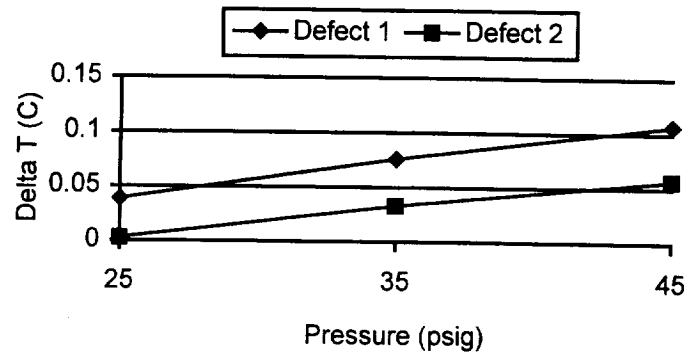
3.4.2 COMPARISON OF THERMAL RESPONSE AT THREE PRESSURE LEVELS

One question that arose from the previous testing was how much of an effect does the amount of pressure have on the ability to detect a leak. This question was answered by computing the delta temperature based upon maximum difference in IR camera values between defect region and acreage region assuming a conversion factor of 203 levels/°C. The results are given in Table 6 and Figure 22. All tests were conducted in region 2 of SSME4.

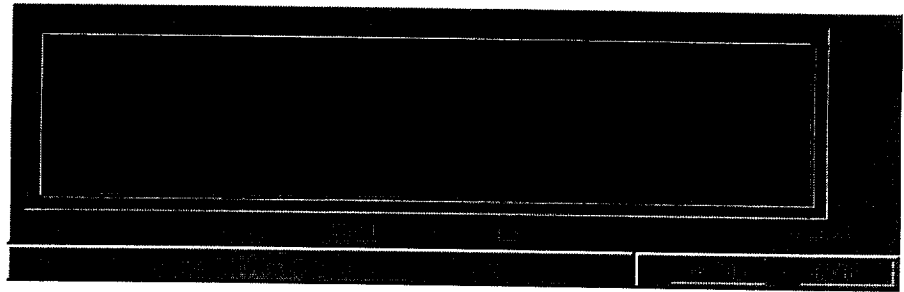
Table 6. Thermal responses.

Line color	Region	Defect Class
Blue	Defect 1	3
Green	Acreage	none
Pink	Defect 2	2

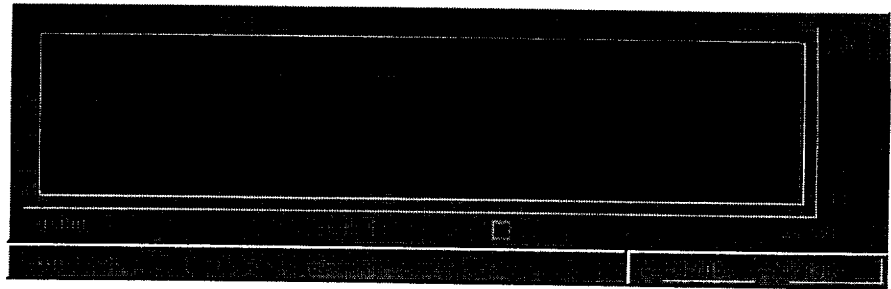
Defect	Pressure (psig)		
	25	35	45
1	.039 Δ°C	.076 Δ°C	.107 Δ°C
2	.003 Δ°C	.033 Δ°C	.057 Δ°C



25 psig



35 psig



45 psig

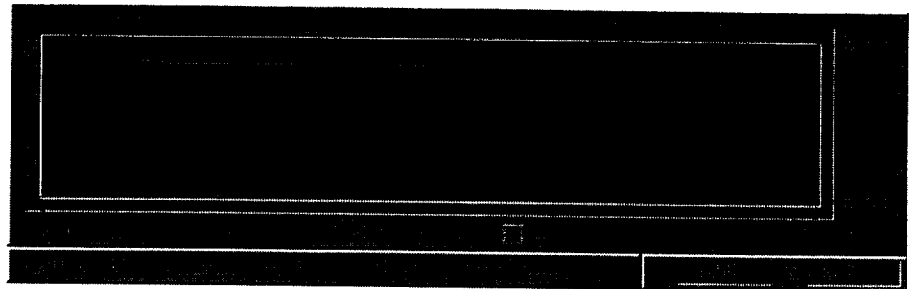


Figure 22. Thermal response at three pressures.

3.5 PAN, TILT AND FOCUS UNIT FOR INSPECTION OF SSME NOZZLE

In support of future inspections of complete nozzle assemblies a pan, tilt and focus unit was adapted to the Amber camera. The following sketches provide the descriptions of each component designed and fabricated in support of this effort.

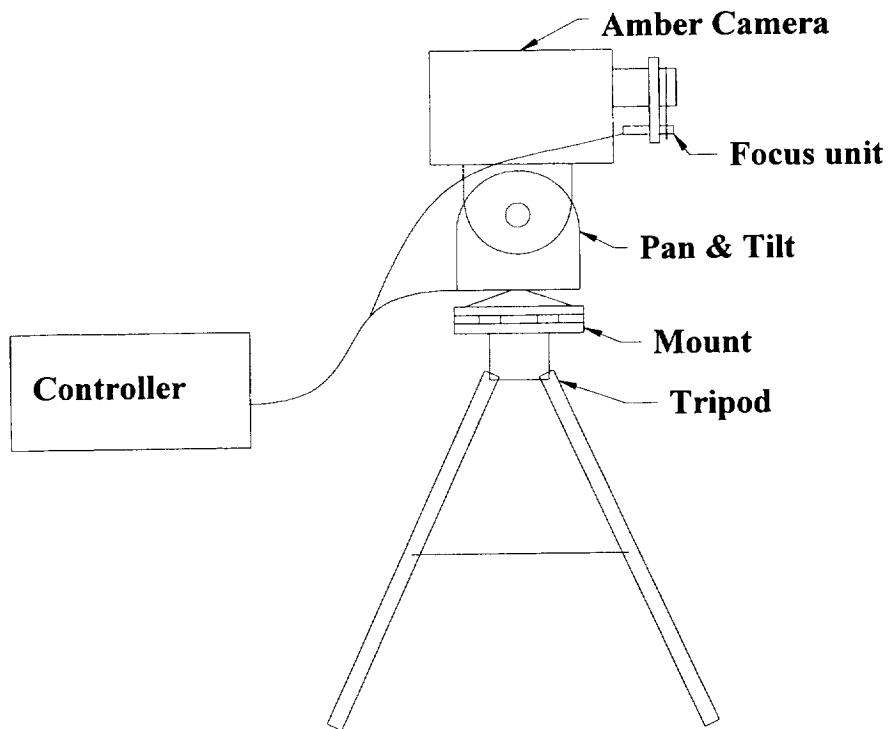
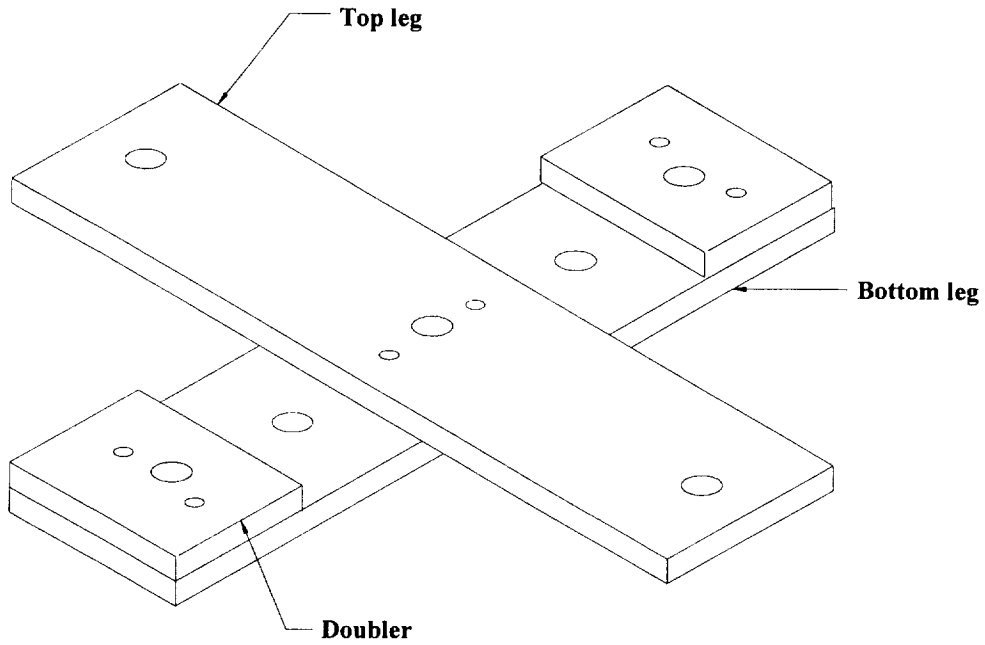
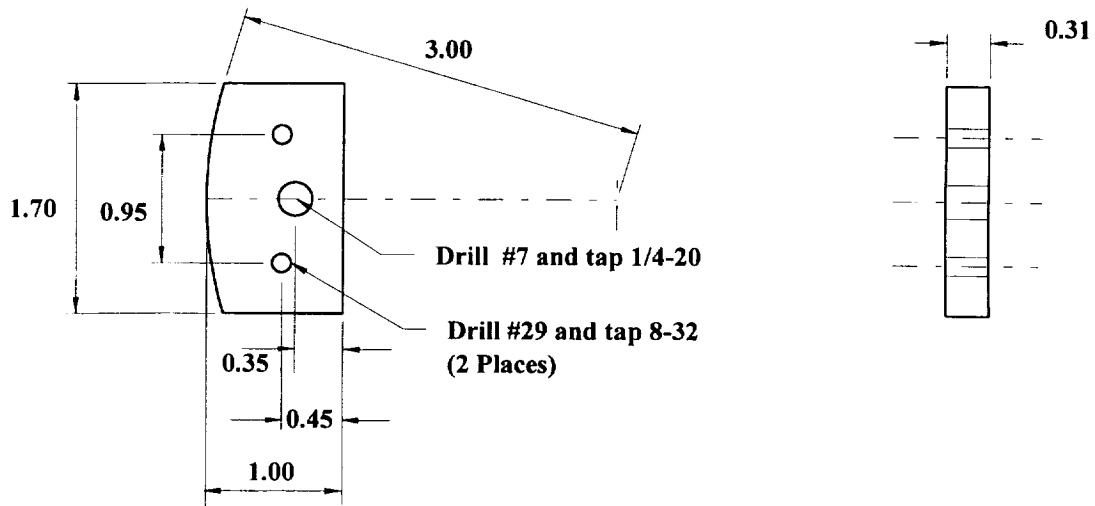


Figure 23. Pan, tilt and focus assembly.



- Material: 6061-T6 aluminum
 Hardware: 6 => 1/2 inch long 1/4-20 socket head cap screws
 6 => 1/2 inch long 8-32 countersunk socket head screws

Figure 24. Pan & Tilt Tripod Mount.



(Make 2)

Figure 24a. Doubler

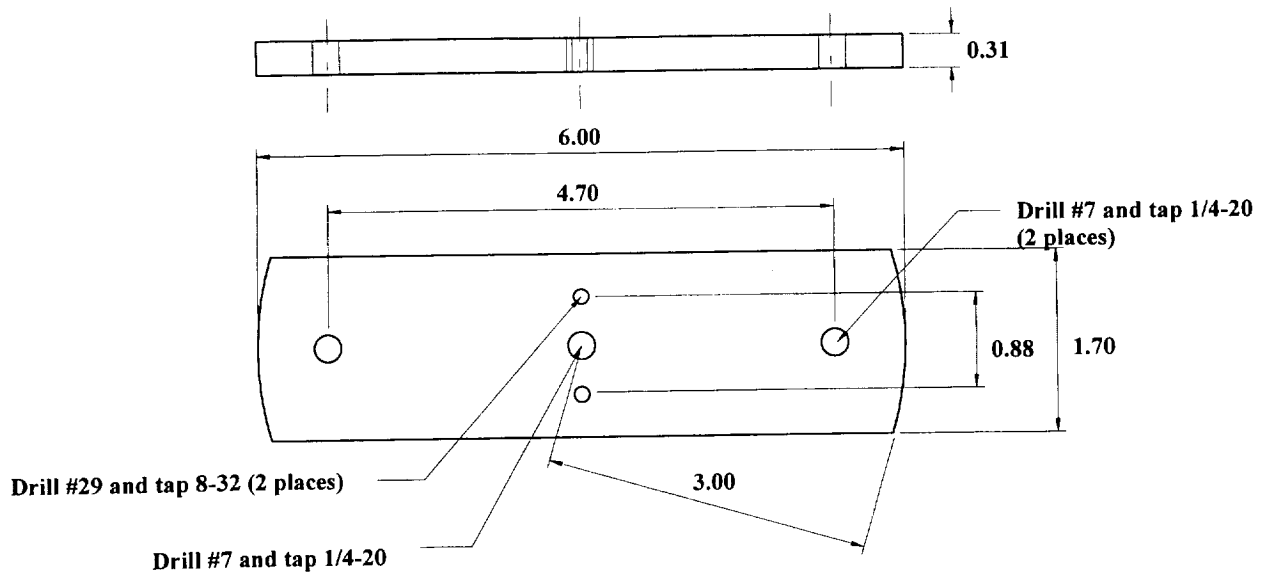


Figure 24b. Top leg.

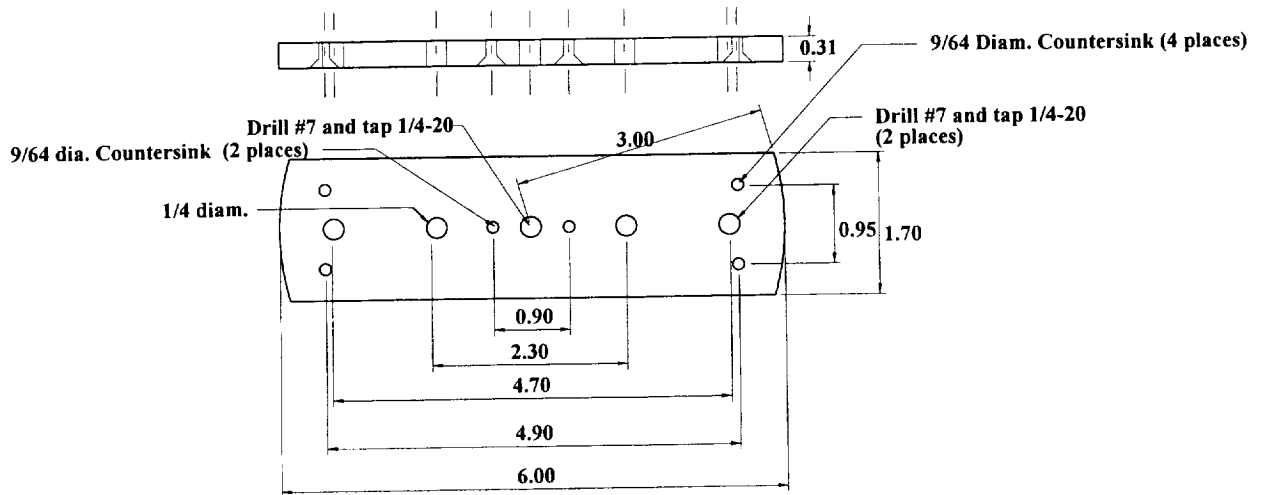


Figure 24c. Bottom Leg

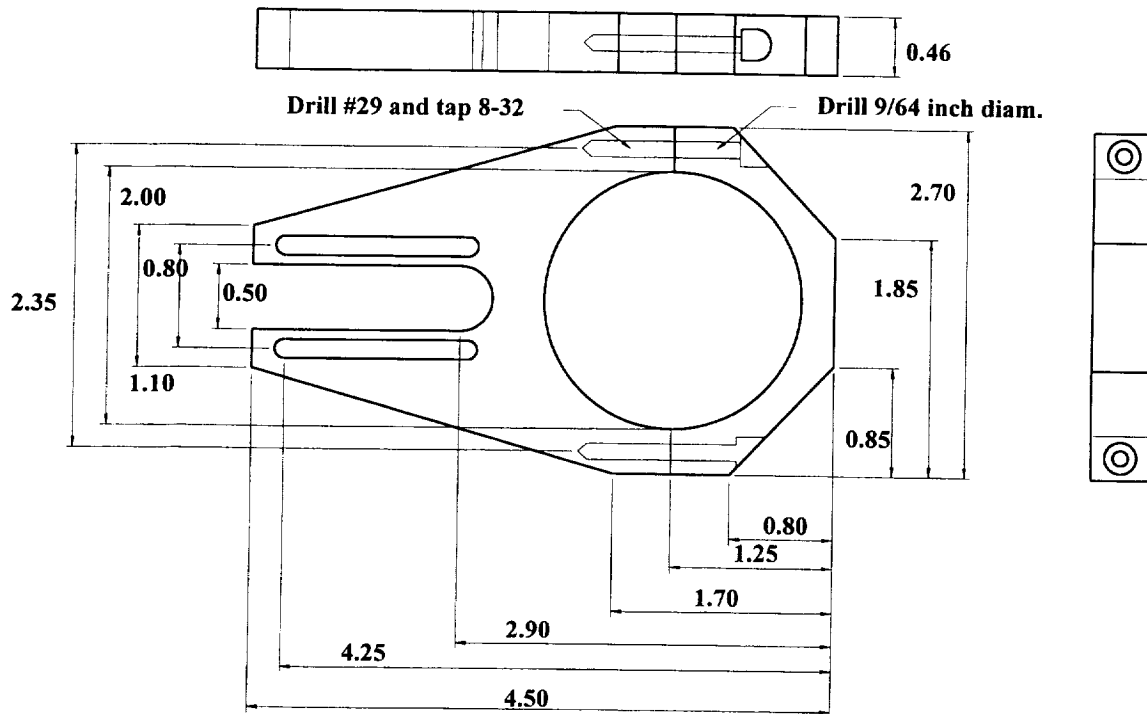


Figure 25a. Focus Unit Clamp

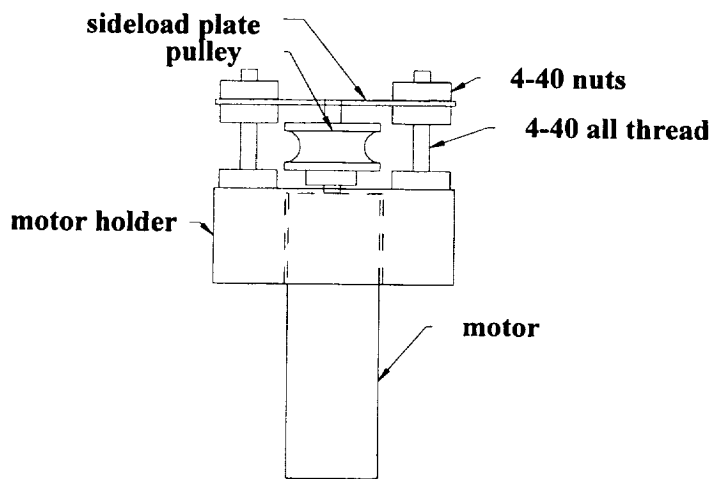


Figure 25b. Focus motor holder assembly

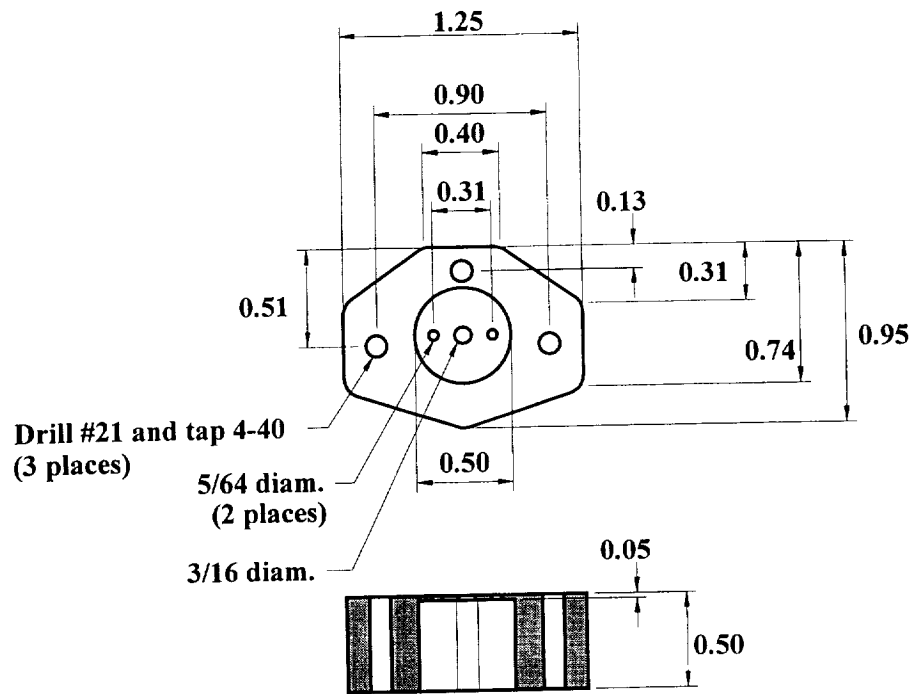


Figure 25c. Motor holder

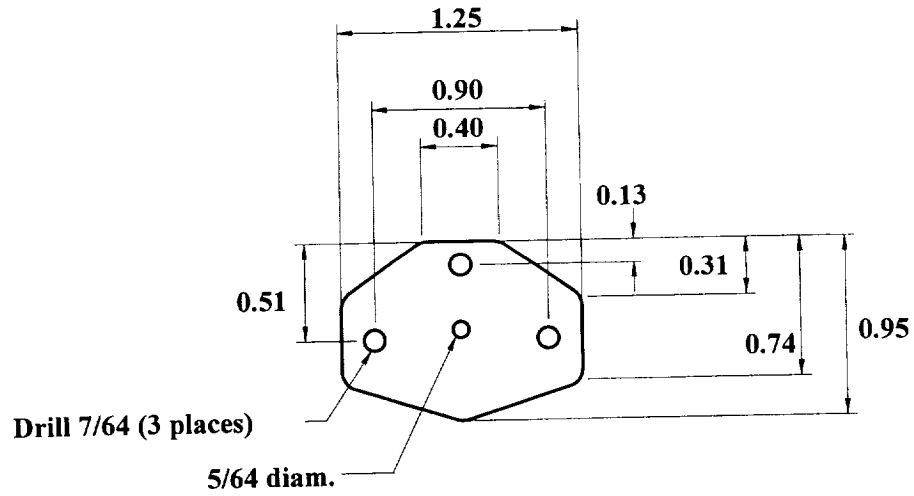


Figure 25d. Motor side load support

4.0 TEST PANEL DESIGN FOR THE SPACE SHUTTLE CARGO BAY DOORS

Three graphite/epoxy phenolic paper honeycomb panels were built for the Kennedy Space Center (KSC) in support of an effort to qualify shearographic and thermographic inspection methods for use on the Space Shuttle cargo bay doors. Each panel measures 18 inch square, with 3 ply (0,45,0) face sheets over a 0.6 inch core.

4.1 TEST PANEL H1

The first test panel was built to determine which methods of defect fabrication would be best suited for the given geometry. A summary of the defects built into the panel is provided in Table 7 and located on the panel in Figure 26.

Table 7. Defects for Panel H1.

Defect	Side	Description
A	Foil	Missing cobond layer between face plate and core
B	Foil	Shim indentations (0.004 in) in face plate
C	Foil	Missing foil
D	Back	Doubled bagging film between plies 2 and 3
E	Back	Microballons between plies 2 and 3
F	Back	Doubled bagging film between plies 1 and 2
G	Back	Microballons between plies 1 and 2
H	Back	Precured cobond adhesive between core and face plate

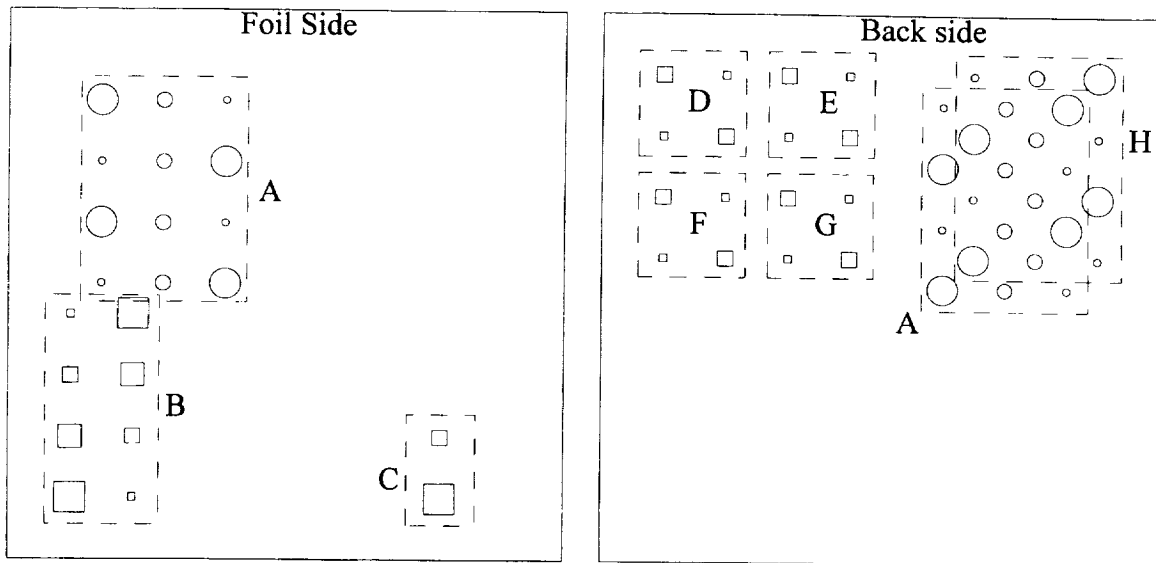


Figure 26. Defect map for panel H1.

The panel was fabricated by first precuring the face sheets at 350 °F for 2.5 hr. using conventional vacuum bagging procedures.. The stacking sequence for bagging included; (Tool\bagging film\release ply\gr/ep\release ply\bagging film\tool\bleader\bagging film). The core was precured with the built in defects for 2 hr. at 350 °F as it was sandwiched between two tooling plates and held under vacuum pressure. Finally the face sheets were cobonded to the core under vacuum pressure for 2 hr. at 350 °F.

The finished panel was inspected using the Amber Radiance 1 camera and front side flash heating before being sent to KSC. The heat source for this inspection was supplied by the Thermal Wave Imaging flash hood. The thermograms are given in Figures 27 and 28.

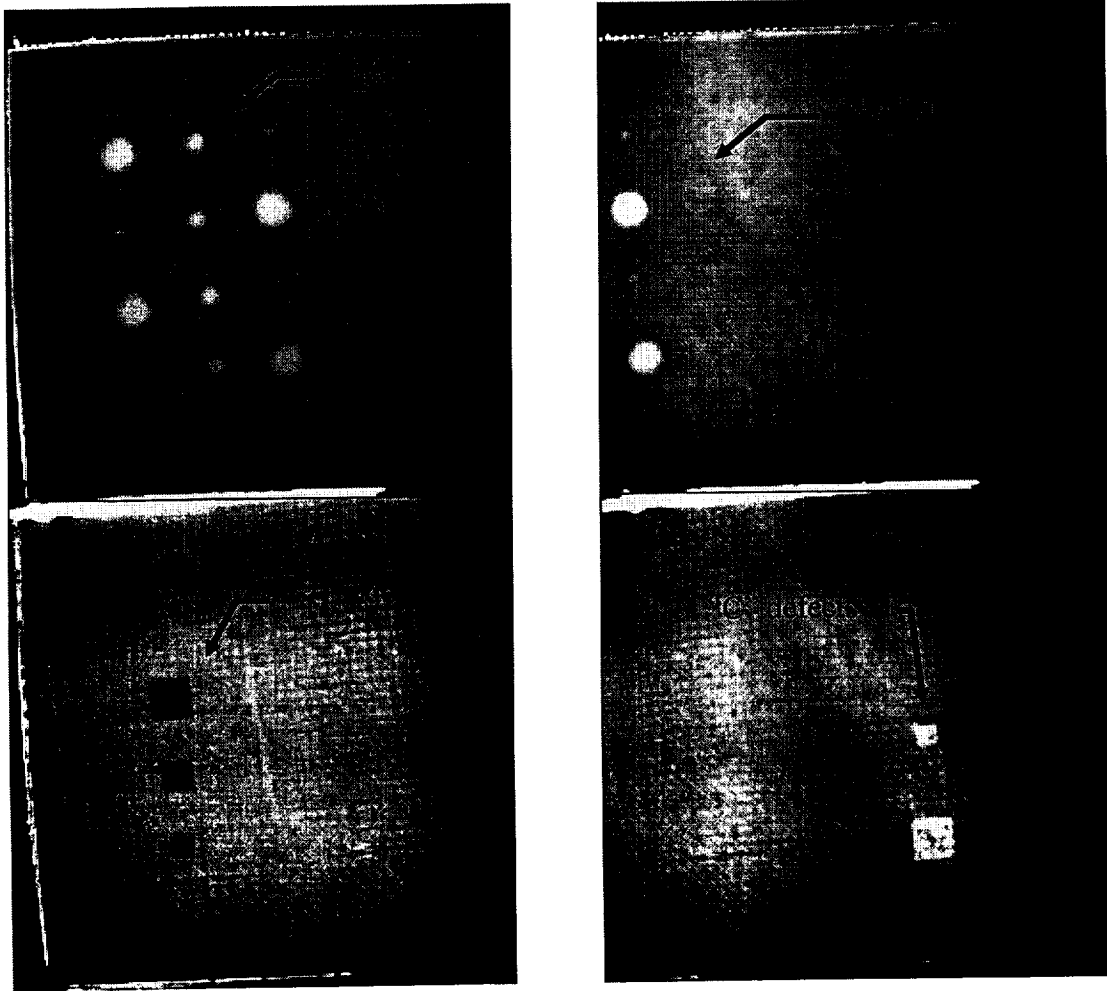


Figure 27. Foil Side of panel H1.

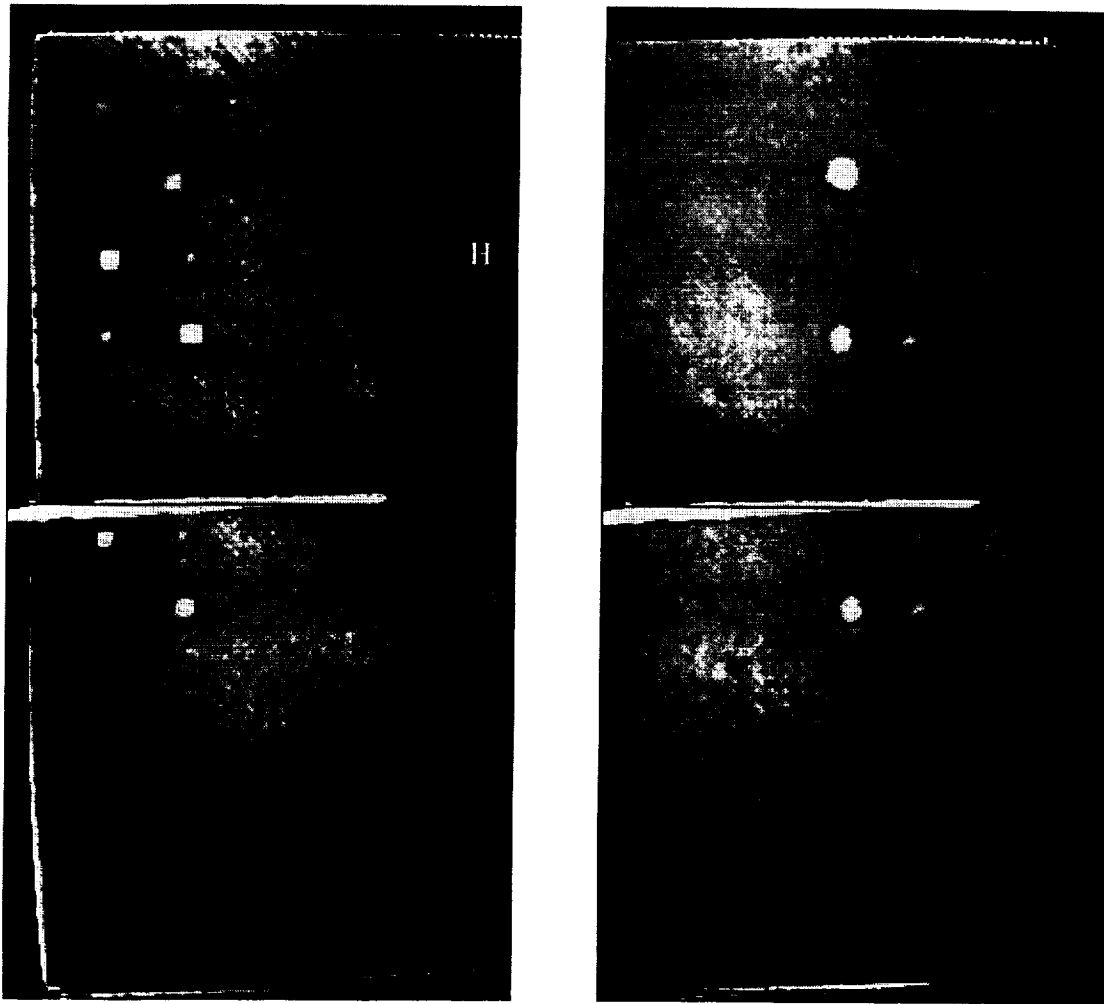


Figure 28. Back side of panel H1.

4.2 TEST PANEL H2

Panel H2 was fabricated in a manner similar to H1 except the defects were formed by precuring sections of cobond adhesive on the core as given in Table 8 and Figure 29. The resulting thermograms are given in Figure 30.

Table 8. Defect description for panel H2.

Defect	Side	Description
A	Foil	0.50 inch diameter precured cobond adhesive between core and face plate
B	Back	0.25 inch diameter precured cobond adhesive between core and face plate

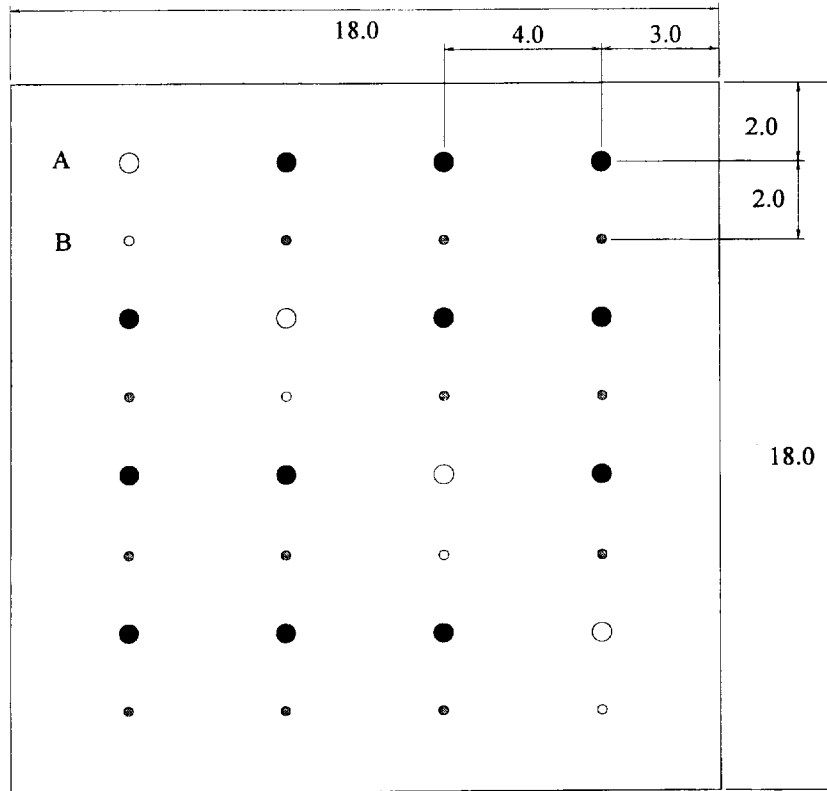


Figure 29. Defect map for panel H2.

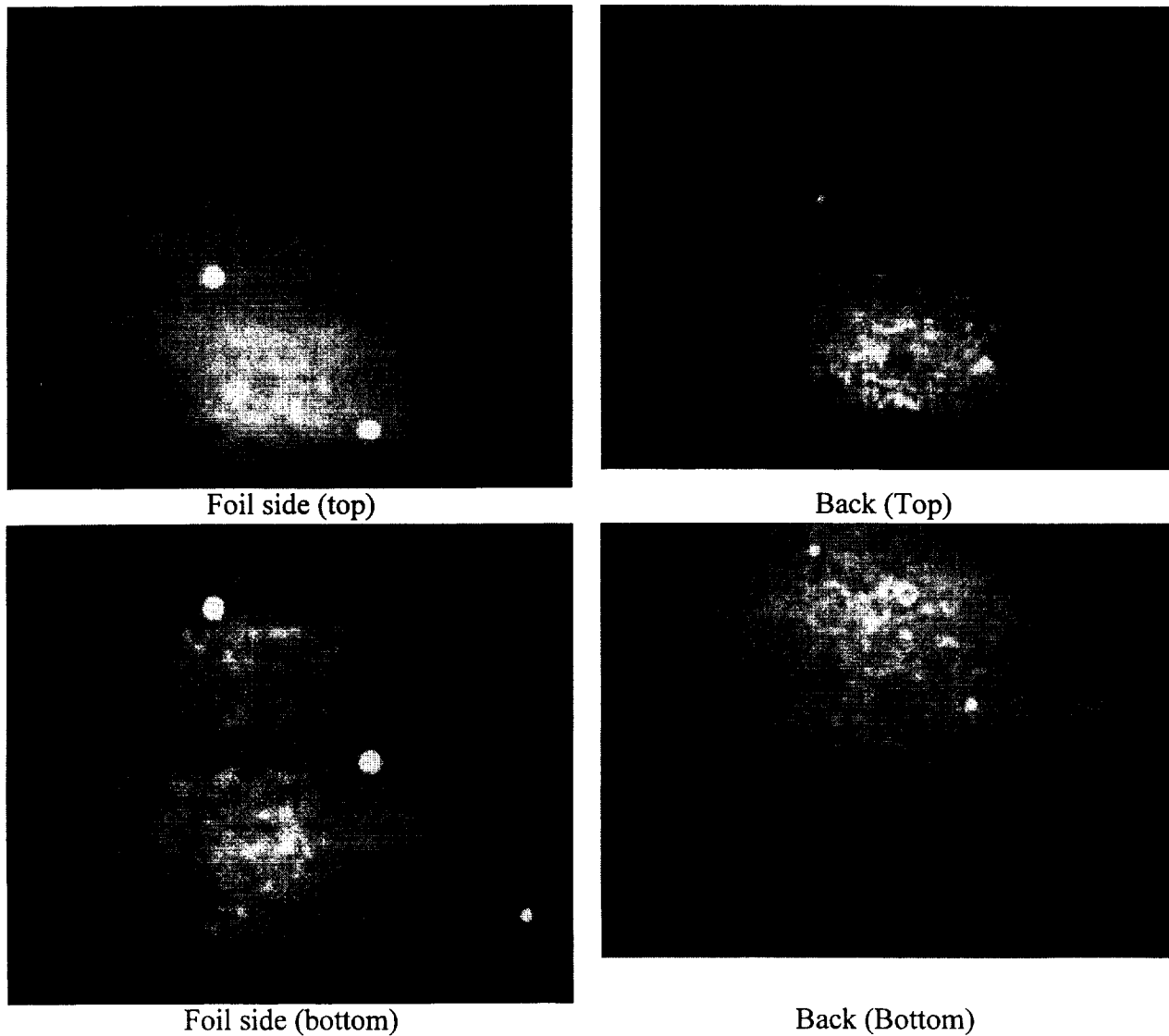


Figure 30. Thermograms for panel H2.

4.3 TEST PANEL H3

Panel H3 was constructed using the lessons learned from building and testing the first two panels. Due to physical constraints imposed by the shearographic system at KSC it was desired on panel H3 to group the main defects within a 9 inch box in the center of the panel. Milled core defects would be placed on the corners of the plate for thermographic inspection. The defect descriptions are given in Table 9 with a defect map given in Figure 31. The resulting thermograms are provided in Figure 32.

Table 9. Defect identification.

Defect Number	Characteristics
1	Milled core, 3/4 inch diameter, 0.2 inch deep
2	Milled core, 1/2 inch diameter, 0.2 inch deep
3	Missing cobond adhesive, 3/4 inch diameter
4	Missing cobond adhesive, 1/2 inch diameter
5	Missing cobond adhesive, 1/4 inch diameter
6	Doubled 0.001 inch thick plastic film with single ply tissue paper insert, 1/2 inch square film, 1/4 inch square paper
7	Doubled 0.001 inch thick plastic film, 1/2 inch square
6*	Doubled 0.001 inch thick plastic film with single ply tissue paper insert, 3/4 inch square film, 1/4 inch square paper
7*	Doubled 0.001 inch thick plastic film, 1/4 inch square

* glossy side of panel

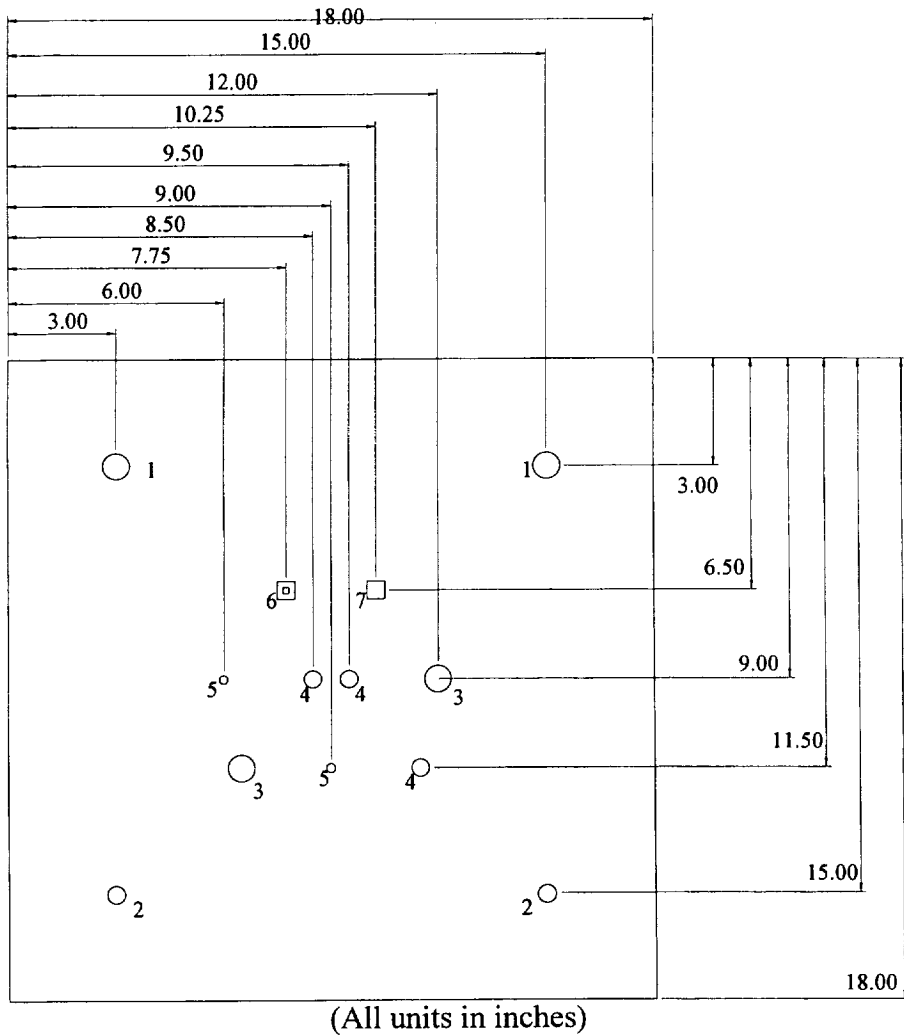
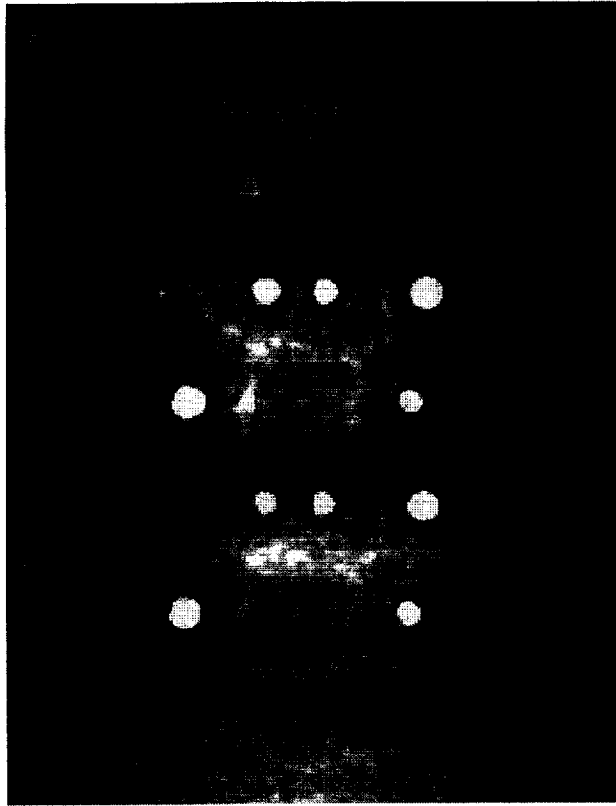
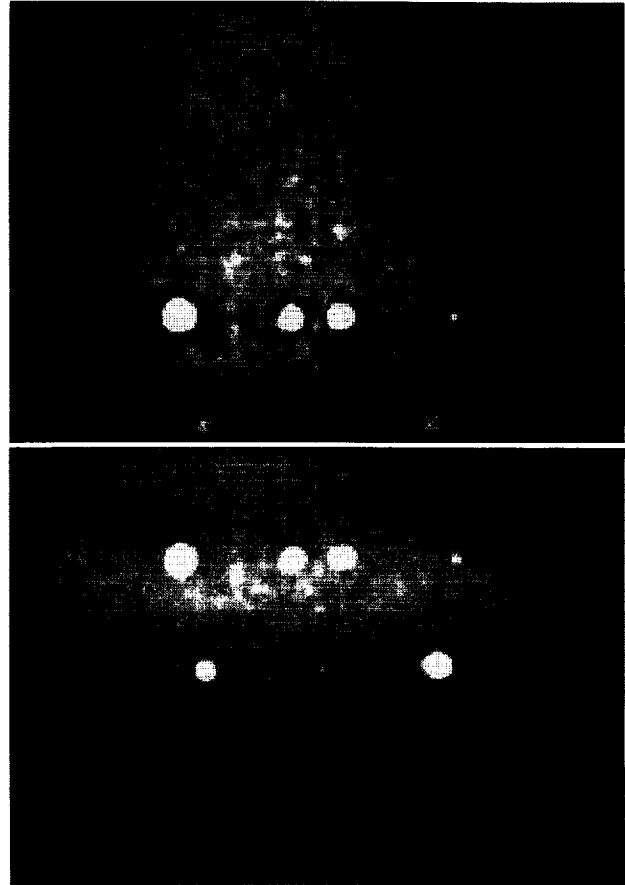


Figure 31. Defect map for Panel H3.



Top (Shiny)



Bottom (Dull)

Figure 32. Thermograms for panel H3.

1. The milled core defects are just barely visible. It appears that the ability of the core to conduct heat away is very similar to the ability of air to radiate the heat away.
2. One milled defect looks very similar to a missing cobond tape defects. It may be that the cobond tape on that milled core pulled away from the face plate.
3. The only insert defect that was clearly visible was number 6. Defects 6* and 7 are just barely visible. The insert defects were placed between the core and cobond tape. It is possible that a better defect would be made by placing the inserts between the cobond tape and the face plate. In this manner the inclusion, and air, would be trapped between the cobond tape and face plate. As the panel was built, the only thing one would expect to see is the lack of bond between the cobond tape and the core and the difference in thermal conductivity of the inclusion. The tightness to which the insert is held between the core and face plate may be helping the flow of heat through that region, i.e. making the region look “thermally” bonded.

5.0 MIKRON-AMBER CORRELATION

In an attempt to get a handle on the temperature differences that were being produced during the leak inspections of the SSME nozzles a study was initiated comparing the indicated values to temperatures given off by a blackbody source. The Amber Radiance 1 thermal camera using a 25 mm lens and the TWI software was set up to image the detector of the Mikron M310 Blackbody calibration source. The face of the camera lens was placed 3 inches from the blackbody source. The Mikron unit was then set to 20 °C, allowed to stabilize and then the indicated Amber temperature and TWI values recorded. This process was repeated in one degree increments up to 40 °C and Table 10 produced. With these vales a calibration factor for the Amber/TWI system was found to be 203 levels/°C. This implies that each unit increase of the TWI values corresponds to approximately 0.004 °C. A graph of the estimated error and calibration curve is given in Figures 33 through 35.

Table 10. Summary of correlation values.

Mikron SV	Mikron PV	Amber (C)	TWI	Slope	SV-PV	Fitted SV-	Fitted TWI
20	20	20.7	6011		0.7	0.862	203.0
21	20	20.8	6039	280	0.8	0.871	5768.6
22	22	23.3	6159	48	1.3	1.100	6276.0
23	23	24	6477	454	1.0	1.164	6418.0
24	24	25.6	6721	153	1.6	1.310	6742.8
25	25	26.6	6915	194	1.6	1.402	6945.7
26	26.5	27.9	7136	170	1.4	1.521	7209.6
27	27.5	29.1	7331	163	1.6	1.631	7453.1
28	28	29.5	7429	245	1.5	1.667	7534.3
29	29	30.9	7709	200	1.9	1.795	7818.4
30	30	31.5	7798	148	1.5	1.850	7940.2
31	31	33.3	8164	203	2.3	2.015	8305.5
32	32	34.3	8444	280	2.3	2.107	8508.5
33	33	35	8532	126	2.0	2.171	8650.5
34	34	36.2	8866	278	2.2	2.281	8894.1
35	35	37.4	9131	221	2.4	2.390	9137.6
36	36	38.7	9385	195	2.7	2.509	9401.5
37	37	39.9	9716	276	2.9	2.619	9645.0
38	38	40.4	9782	132	2.4	2.665	9746.5
39	39	41.6	10160	315	2.6	2.775	9990.0
40	40	42.9	10483	248	2.9	2.894	10253.9

slope	203	Rsq =	0.9911
Intercept	1547		
Slope	0.0915	Rsq =	0.9117
Intercept	-1.0331		

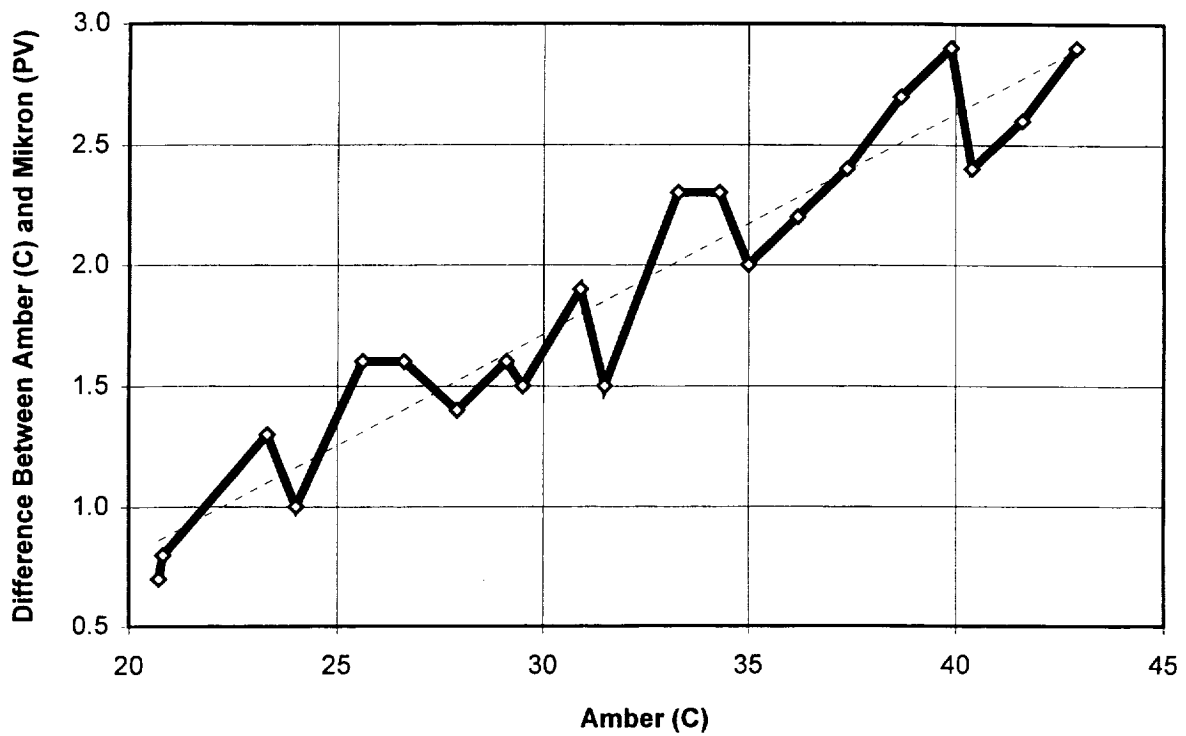


Figure 33. Error curve for Amber/TWI system.

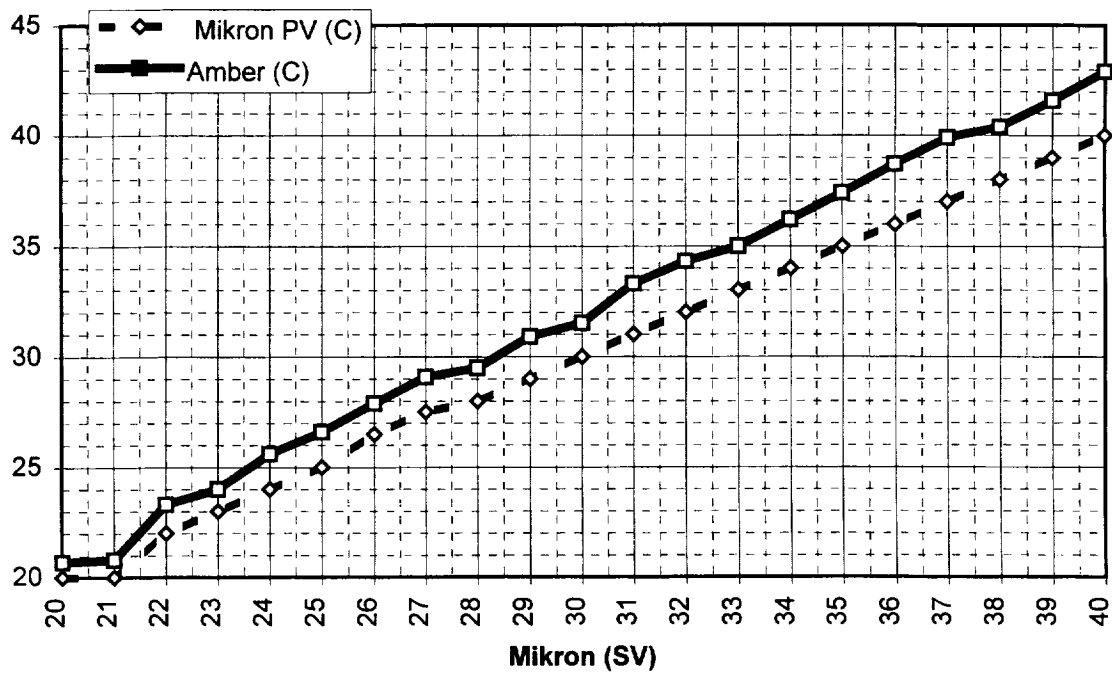


Figure 34. Correlation between Amber indicated values and Mikron set values.

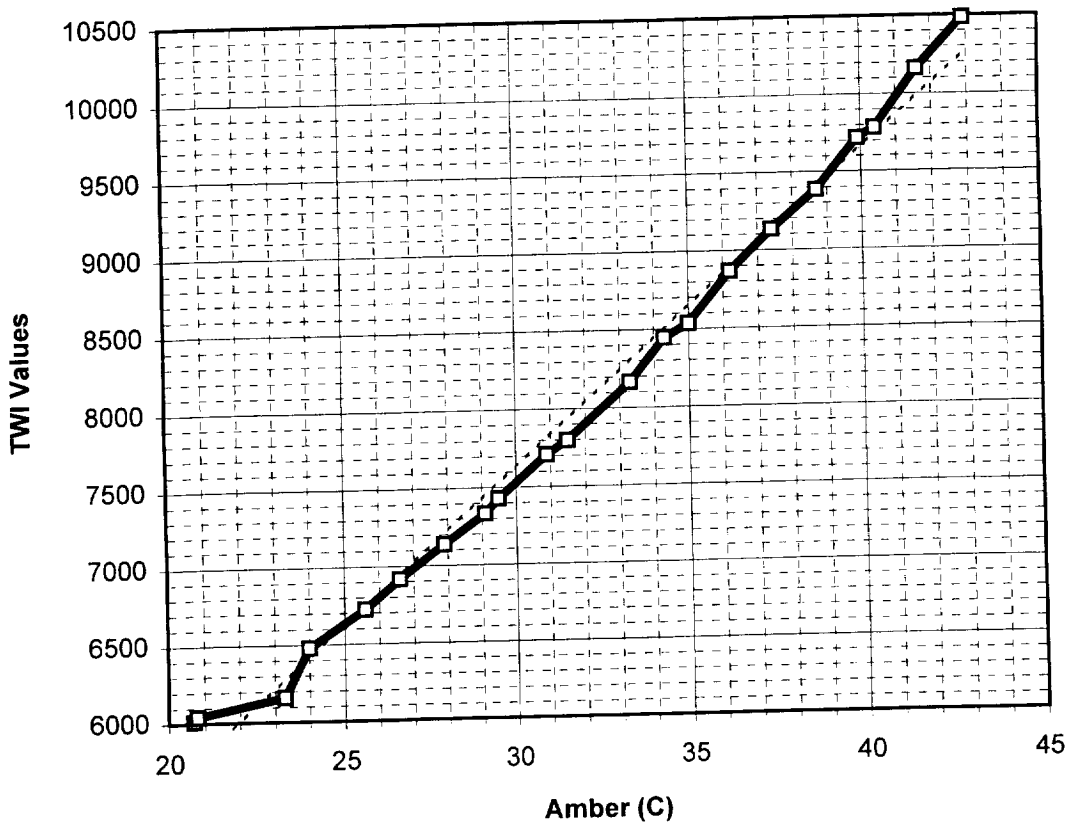


Figure 35. Calibration curve for Amber/TWI system.

6.0 THERMOGRAPHIC INSPECTION OF GRAPHITE/EPOXY LOW PROFILE DOME

A graphite/epoxy low profile dome structural test article was thermographically inspected prior to ultimate load testing. The lay-up schedule and critical defect size were not provided. The dome was inspected using flash thermography and long term exposure (LTE) lamps. A Bales Scientific thermal image processor was used for the inspections, configured to view a 12 inch by 18 inch section of the dome. A map showing the inspection regions is provided in Figure 36. The power setting for flash was set at 1400V while the LTE heating was induced by a 1000 W lamp.

Some thermal abnormalities were found at visible surface wrinkles as shown in the following thermograms. Due to the severity of the visible surface features it is difficult to identify individual subsurface defects.

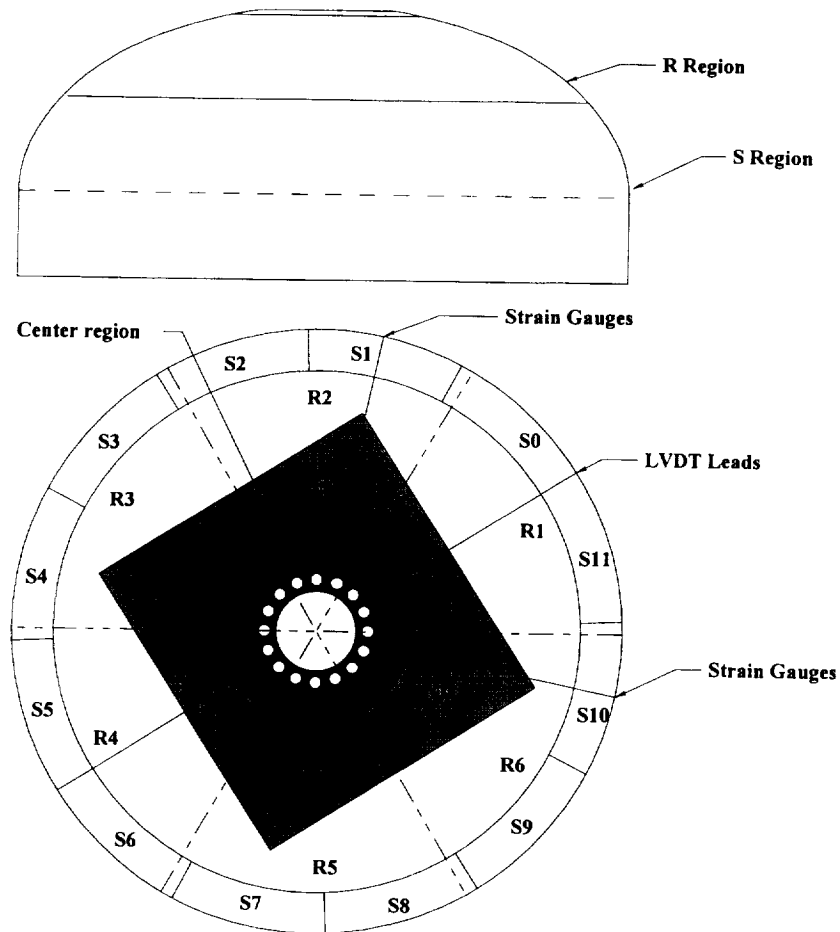
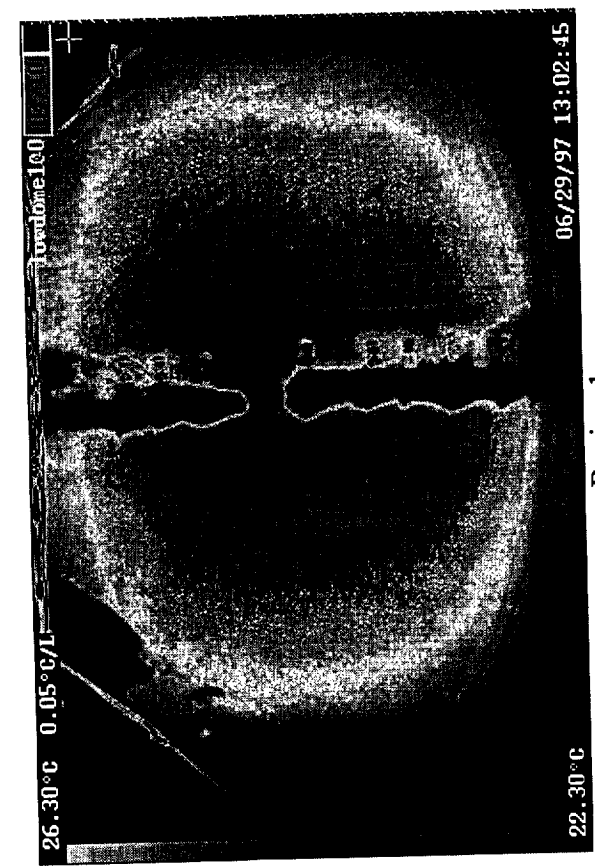
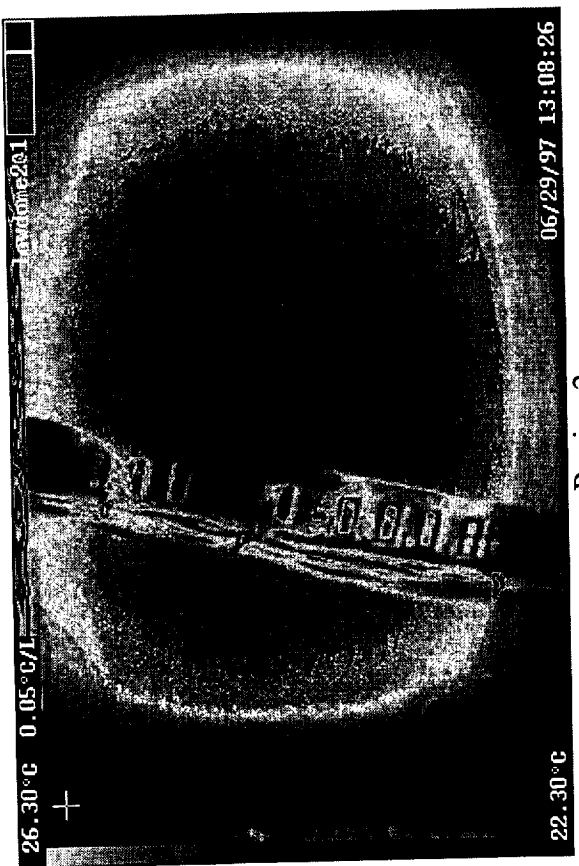


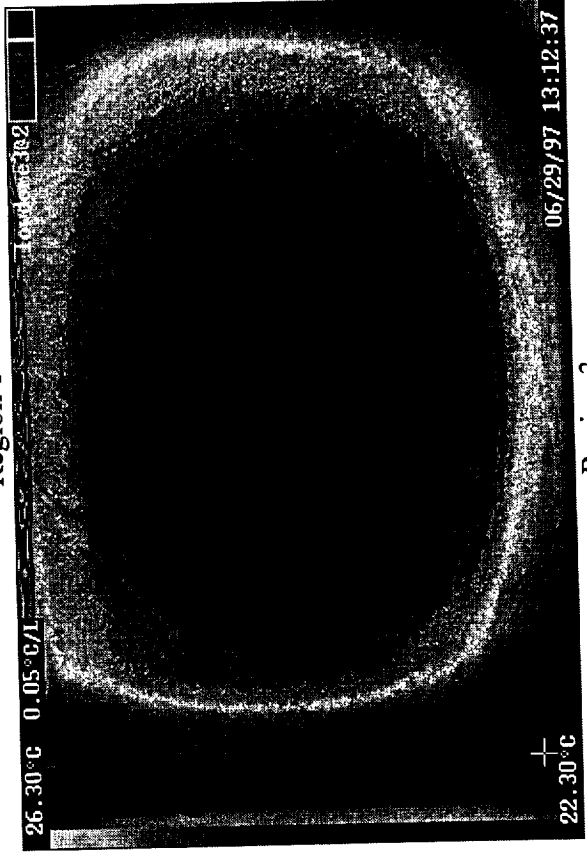
Figure 36. Thermogram map for the dome.



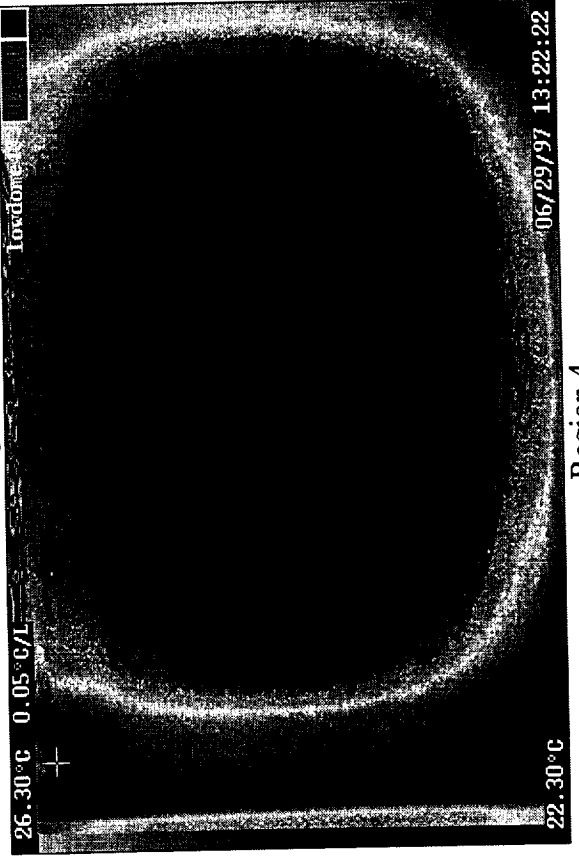
Region 1



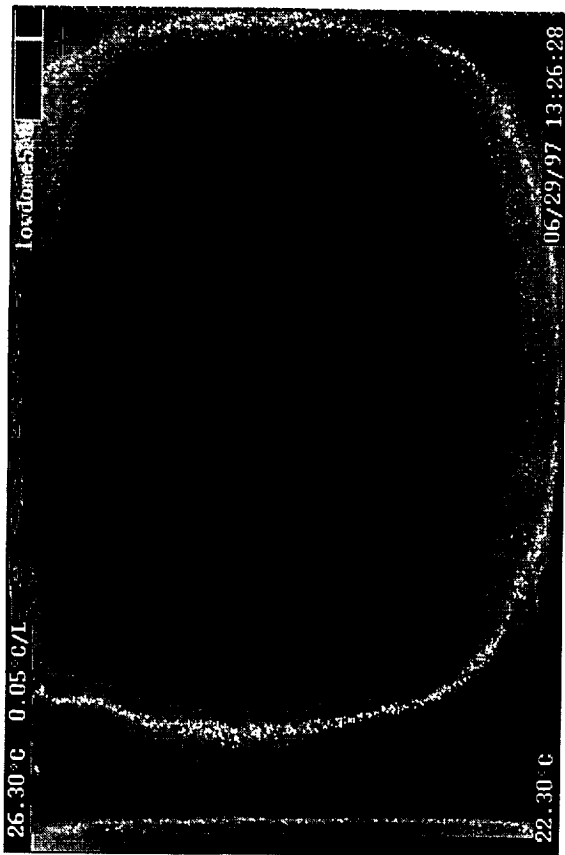
Region 2



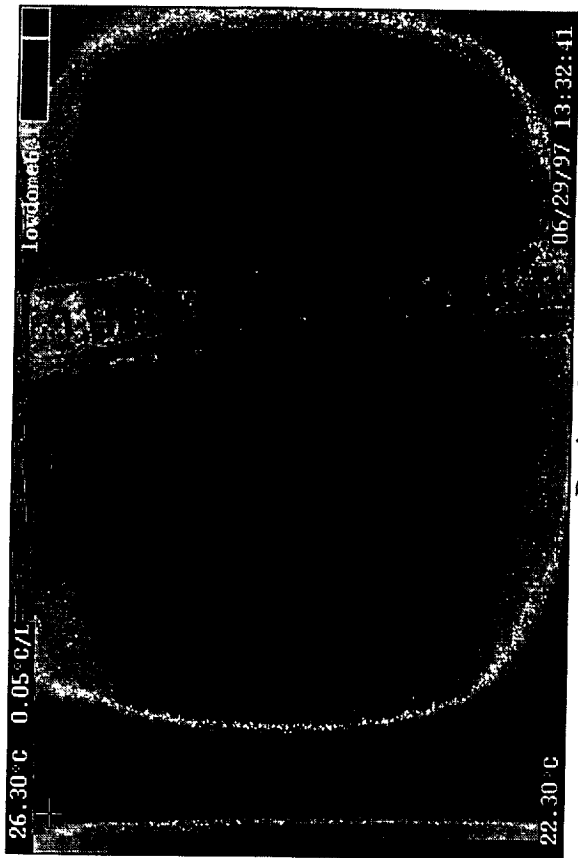
Region 3



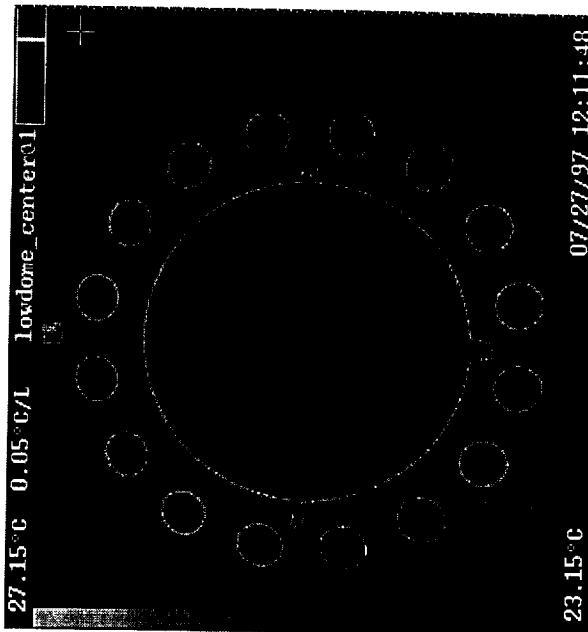
Region 4



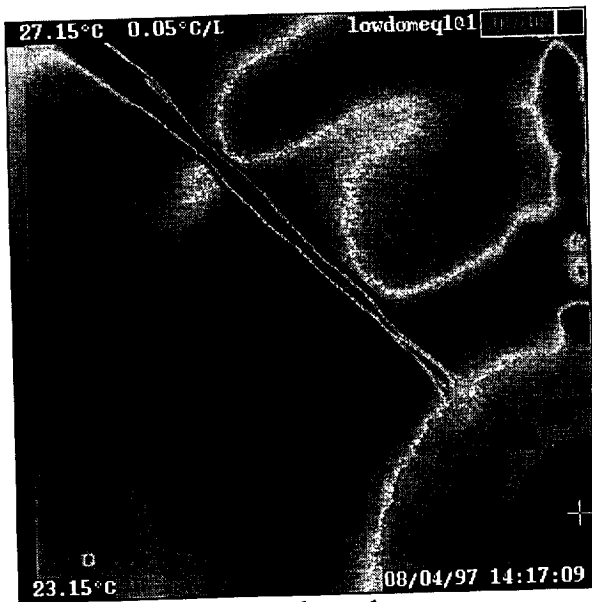
Region 5



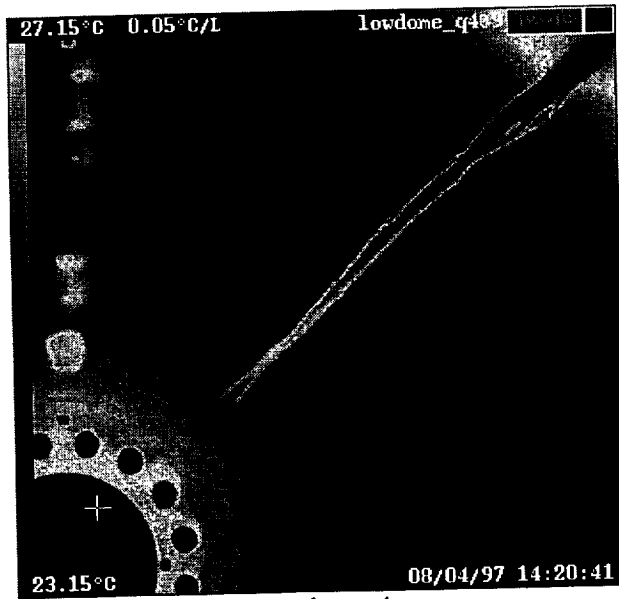
Region 6



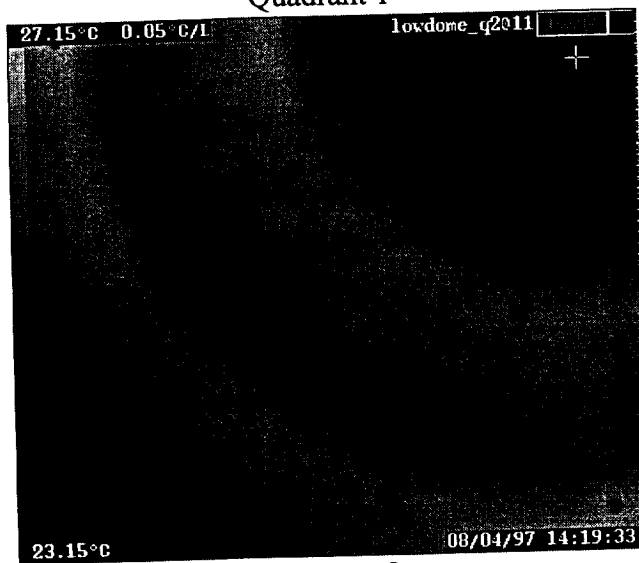
Center



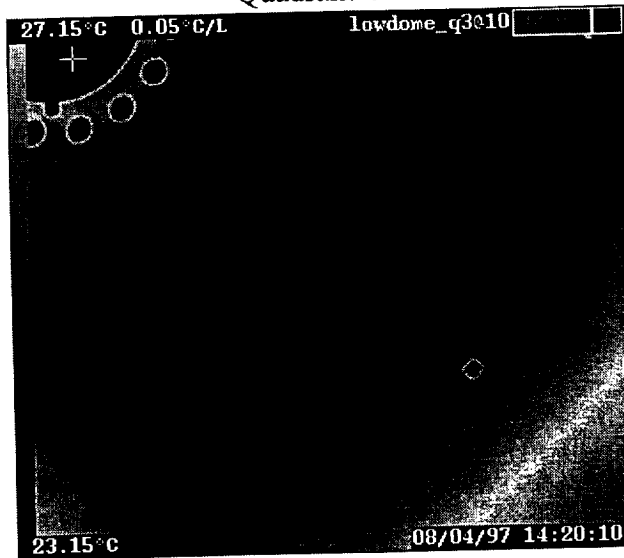
Quadrant 1



Quadrant 4



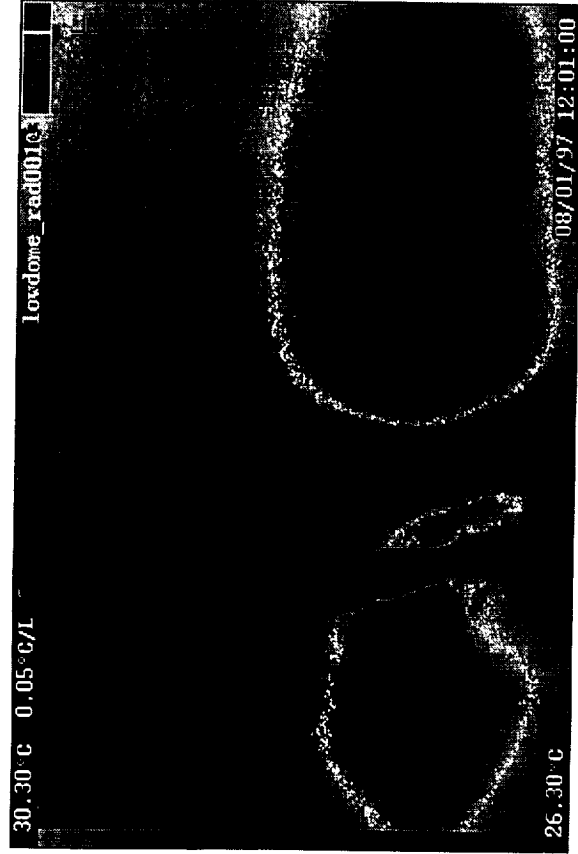
Quadrant 2



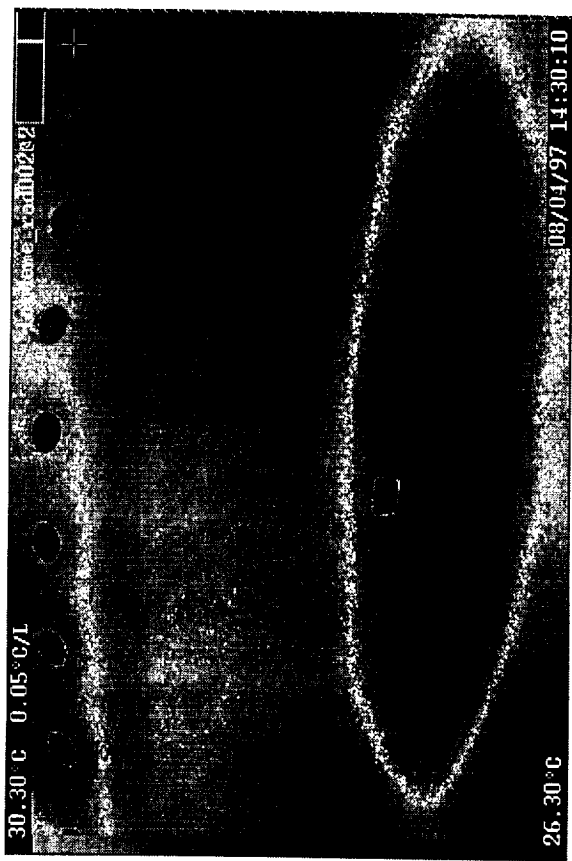
Quadrant 3



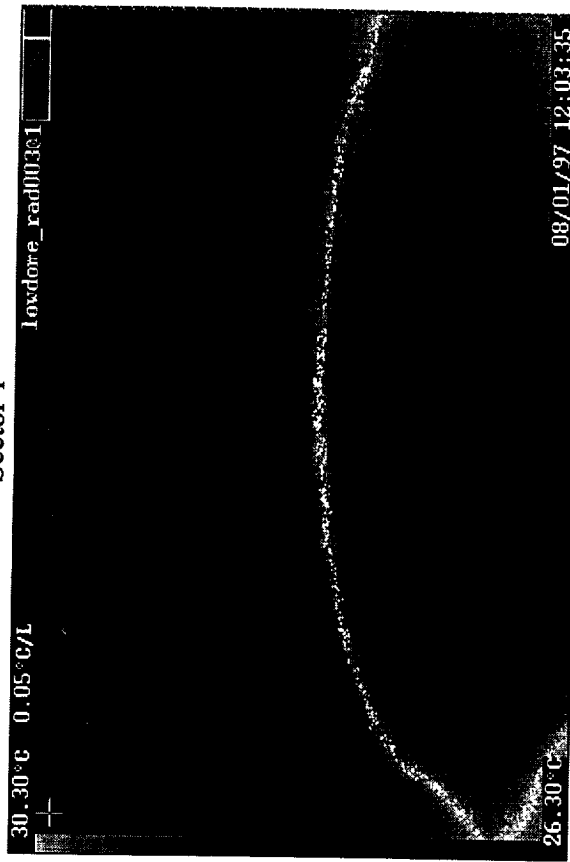
Sector 0



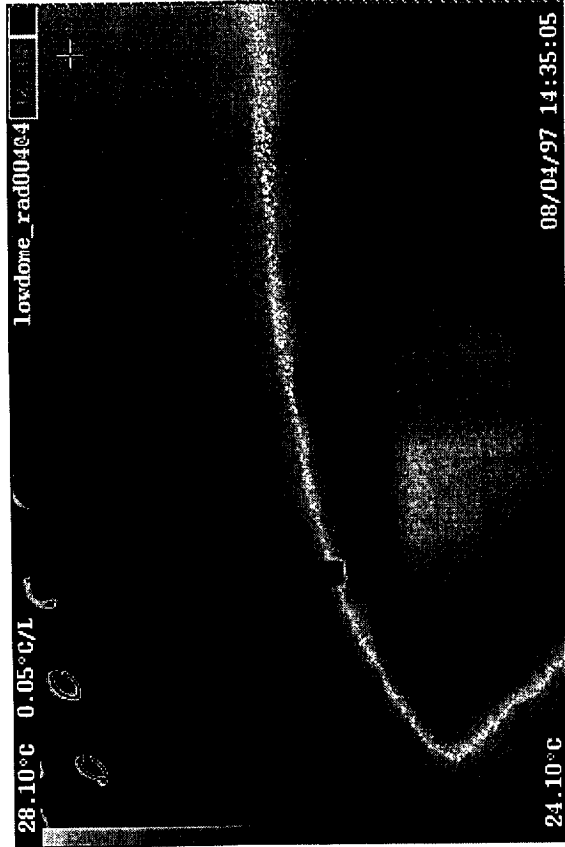
Sector 1



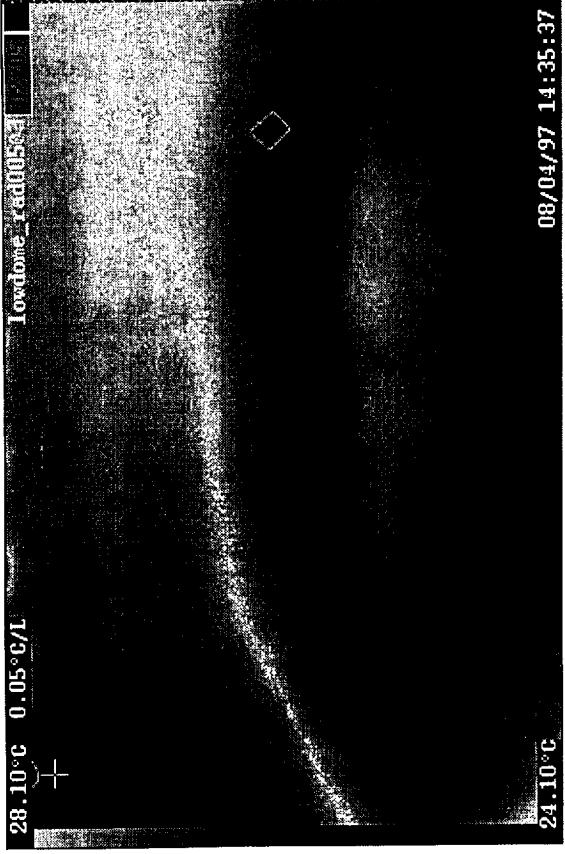
Sector 2



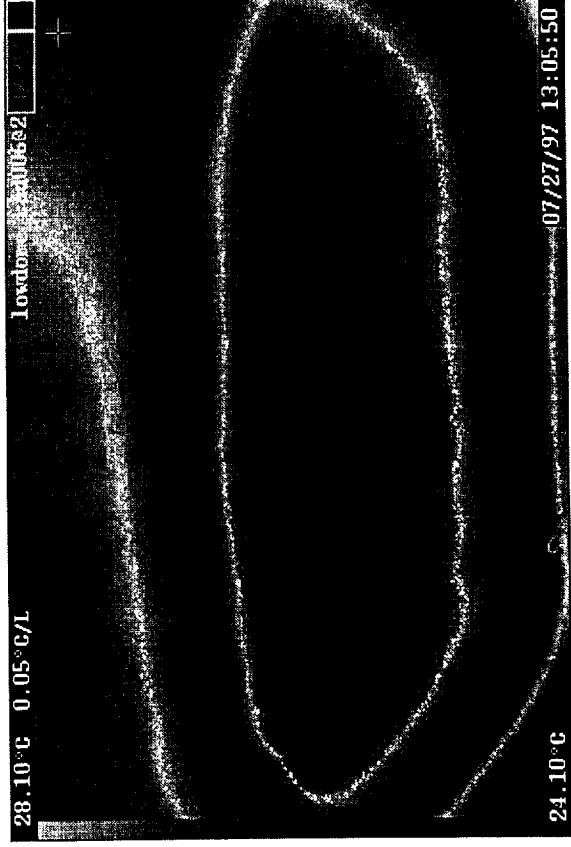
Sector 3



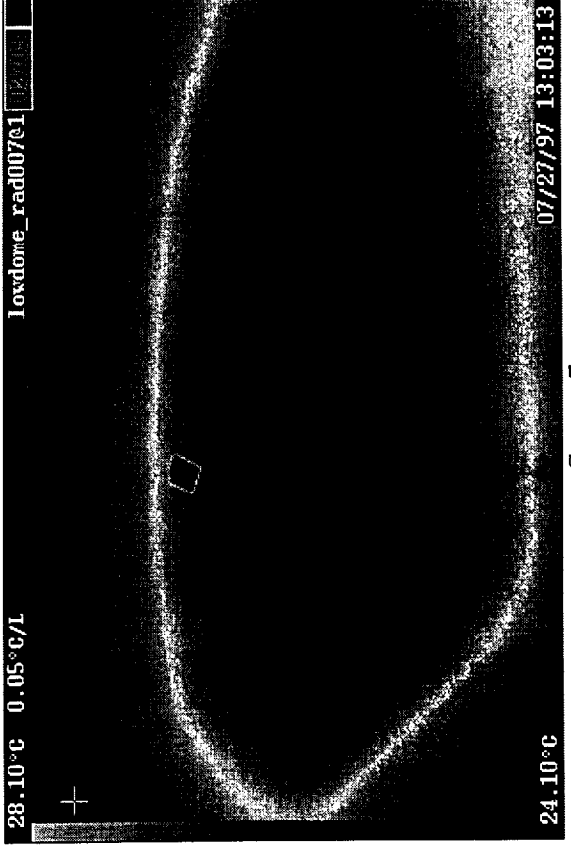
Sector 4



Sector 5



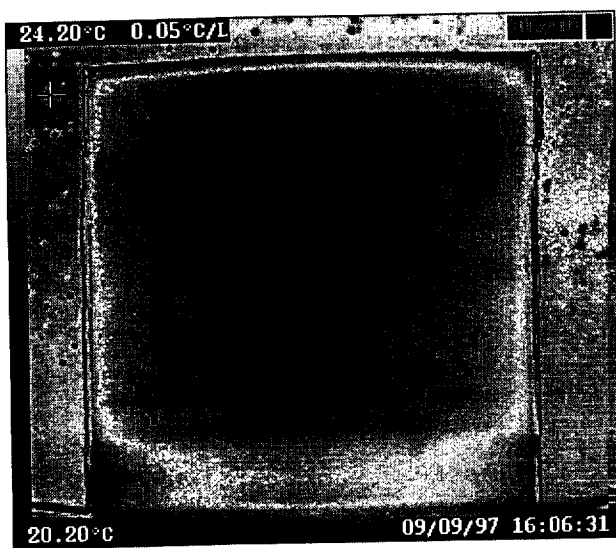
Sector 6



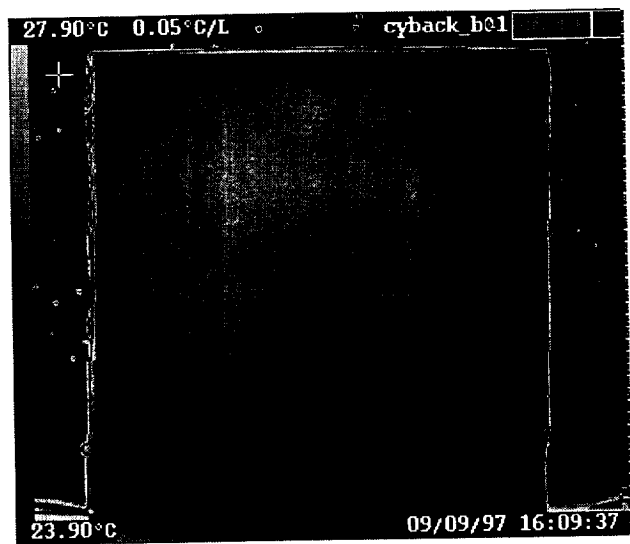
Sector 7

7.0 THERMOGRAPHIC INSPECTION OF GRAPHITE/EPOXY PANELS FOR THIOKOL

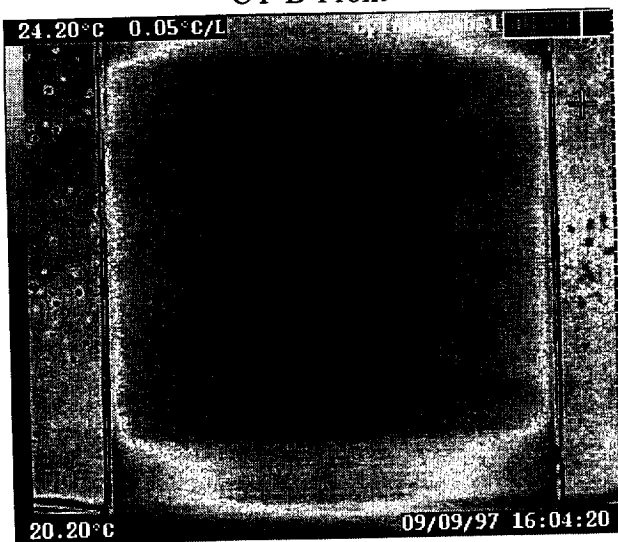
- Project description: Test panels built by THIOKOL.
- Material: Graphite/epoxy
- Lay-up schedule: Unknown
- Critical defect size: Unknown
- Inspected using flash thermography (Bales TIP)
- Imaged at a distance of 32 inches
- Power setting of 1400V
- Results: Several thermal abnormalities found. See thermograms.



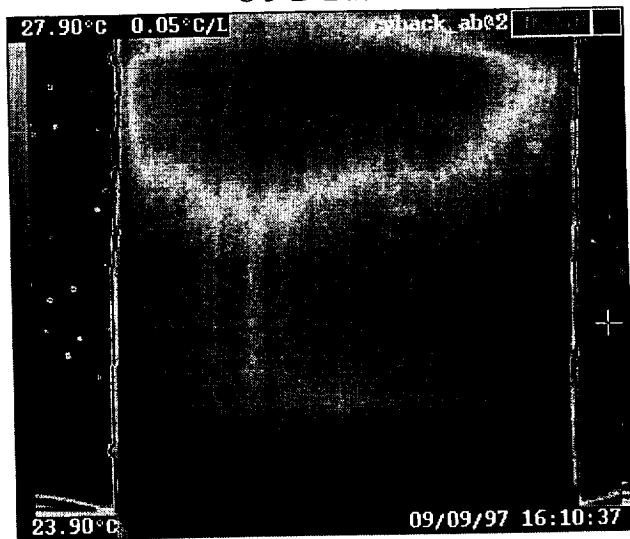
CY-B-Front



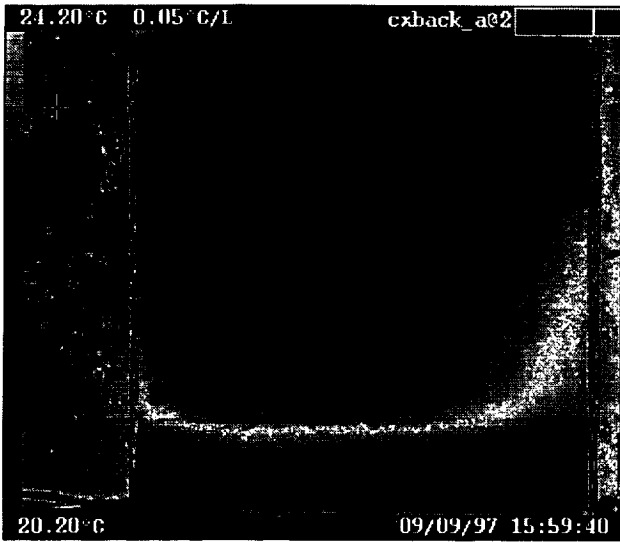
CY-B-Back



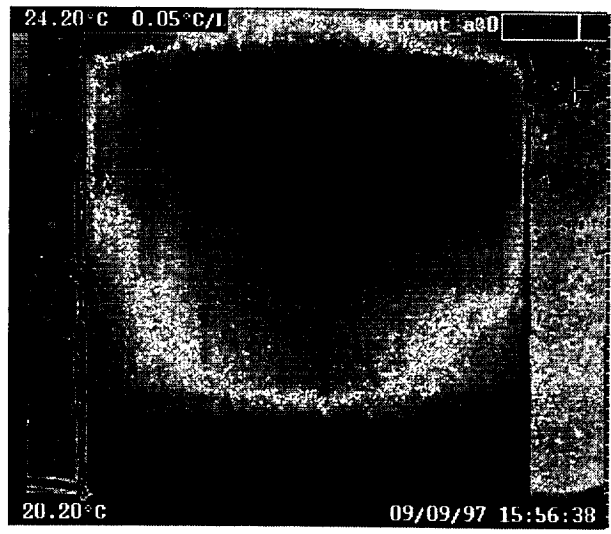
CY-AB-Front



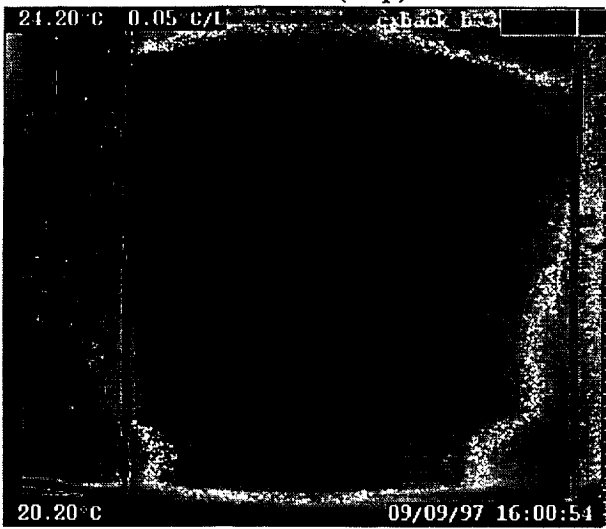
CY-AB-Back



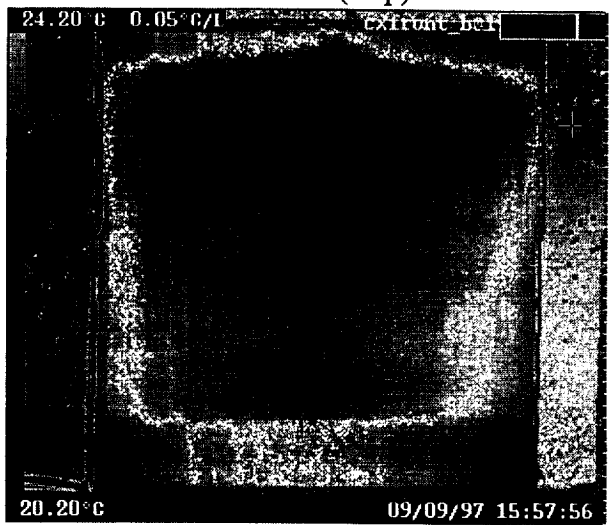
CX-Back (Top)



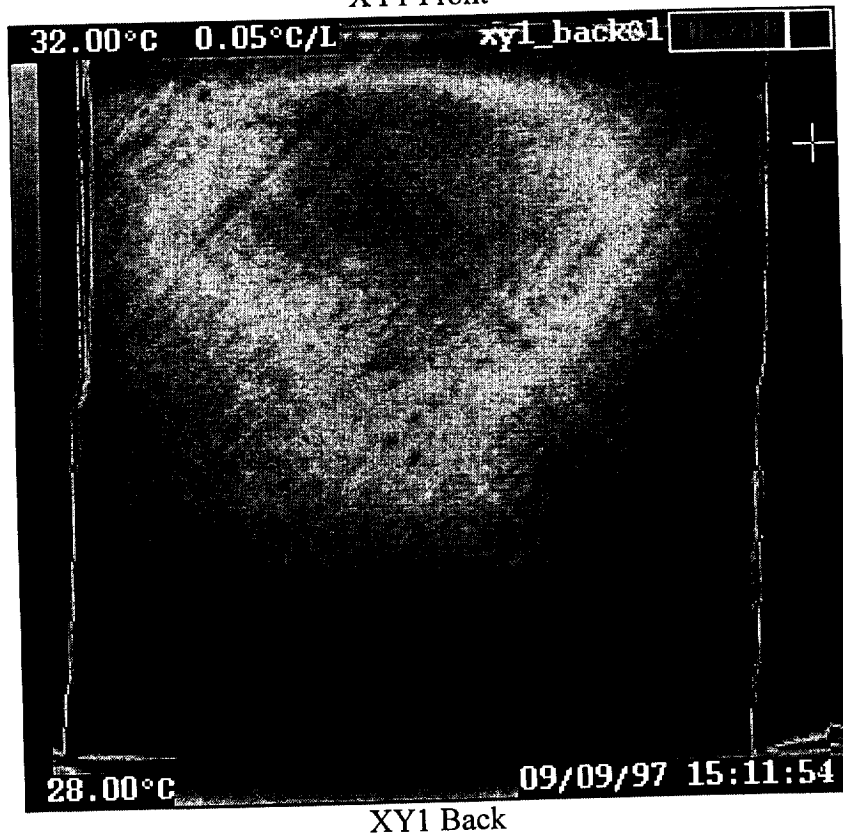
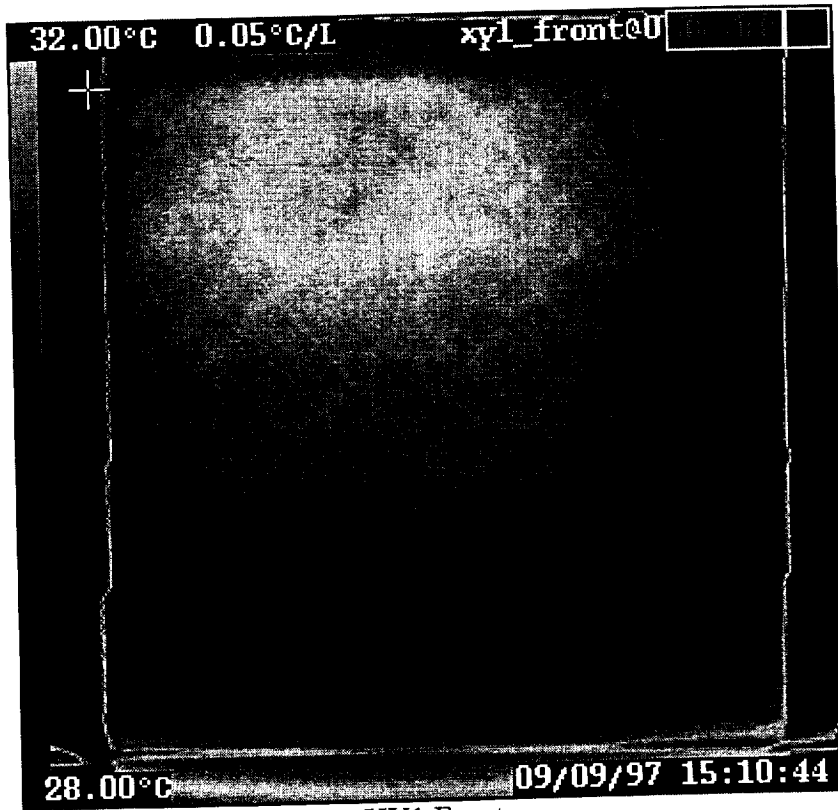
CX-Front (Top)



CX-Back (Bottom)

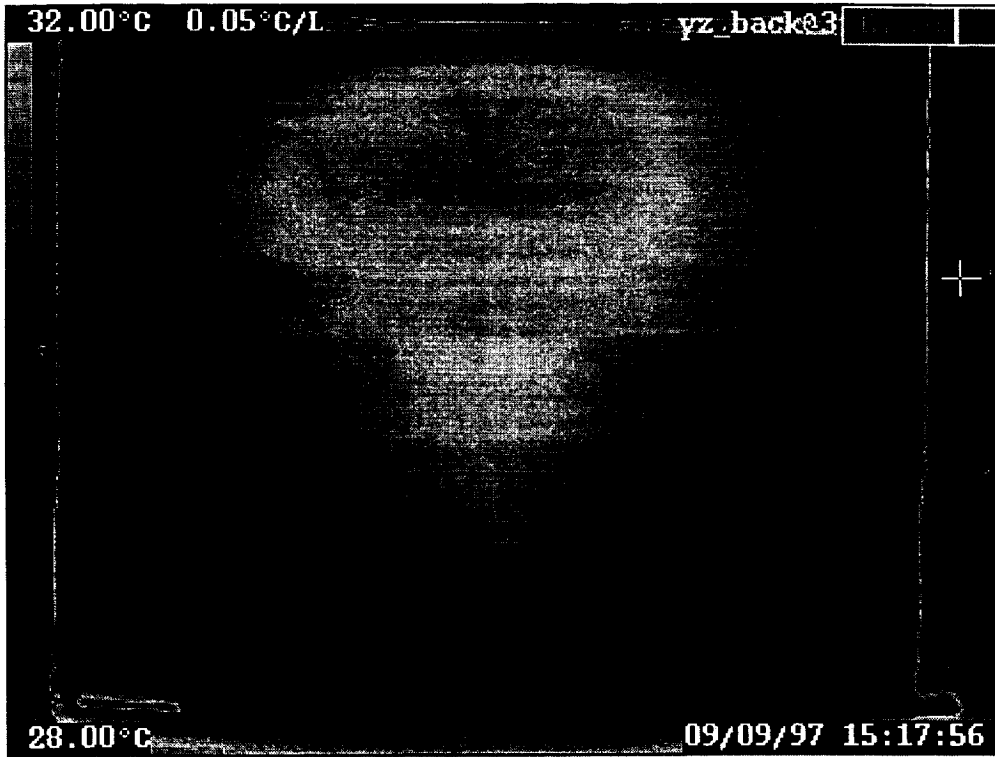


CX-Front (Bottom)

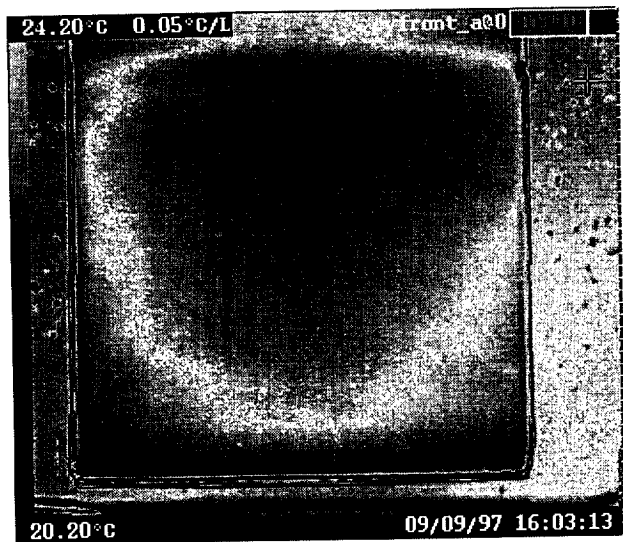




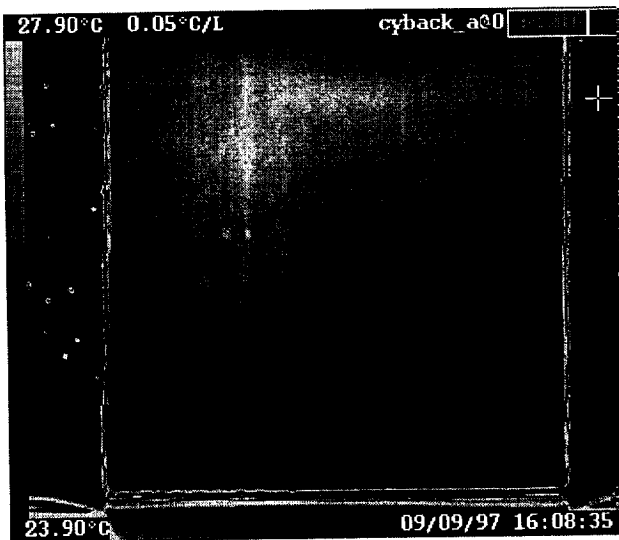
YZ Front



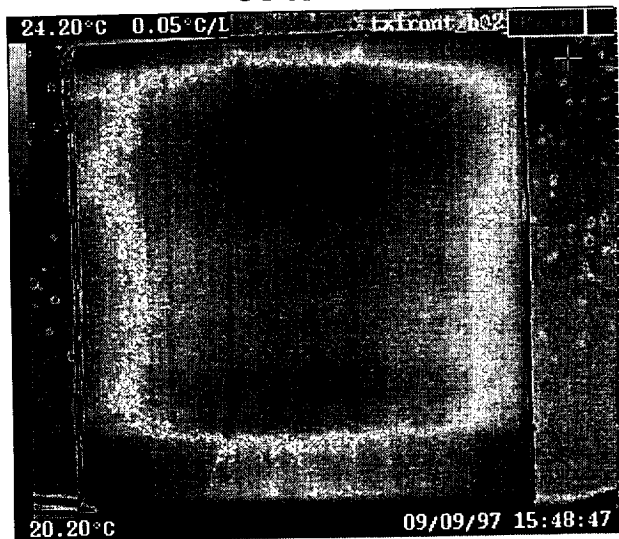
YZ Back



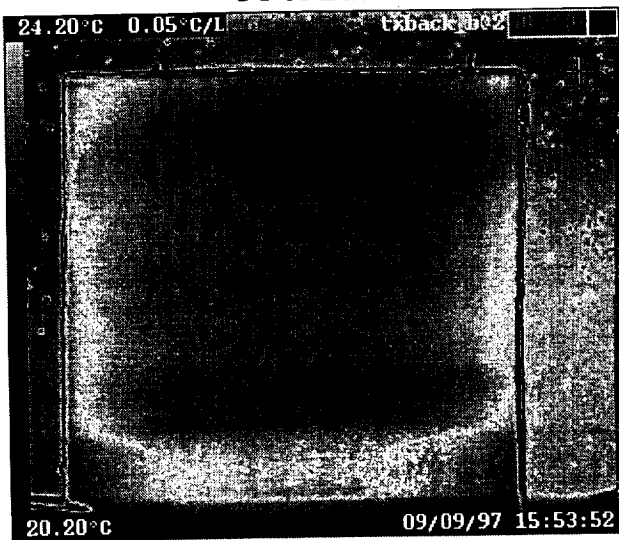
CY-A-Front



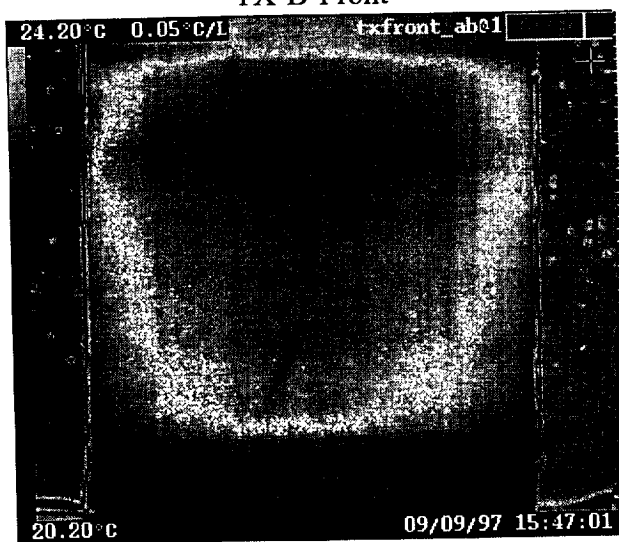
CY-A-Back



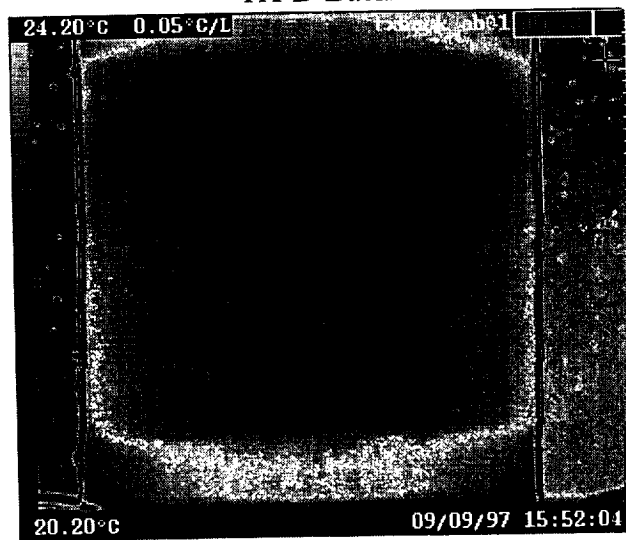
TX-B-Front



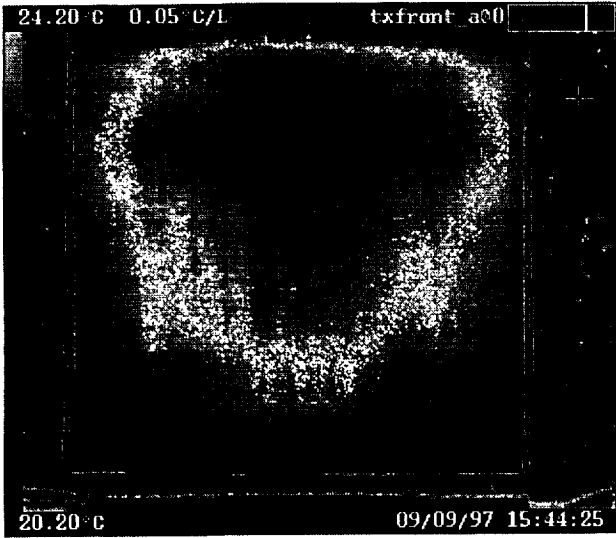
TX-B-Back



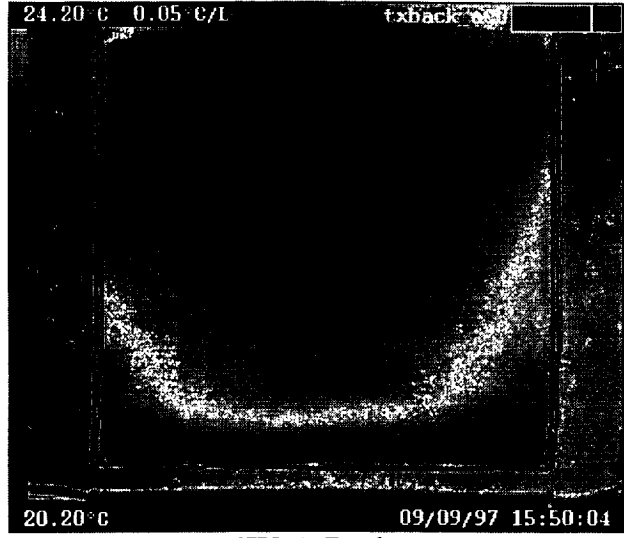
TX-AB-Front



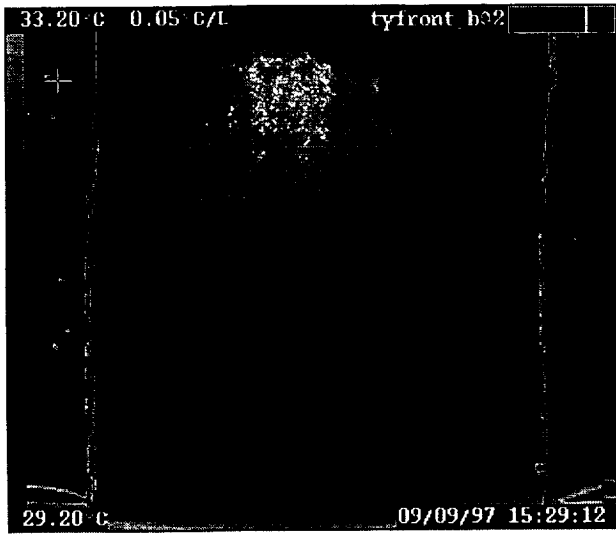
TX-AB-Back



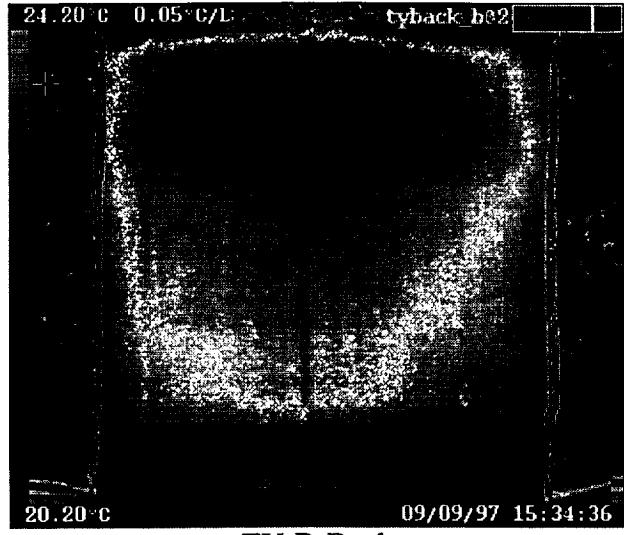
TX-A-Front



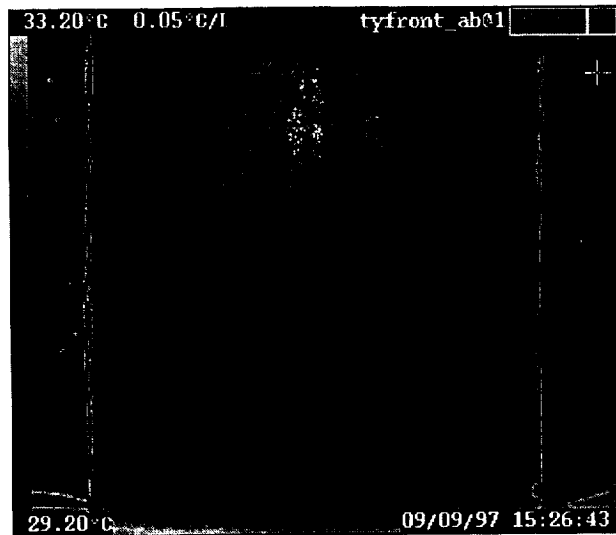
TX-A-Back



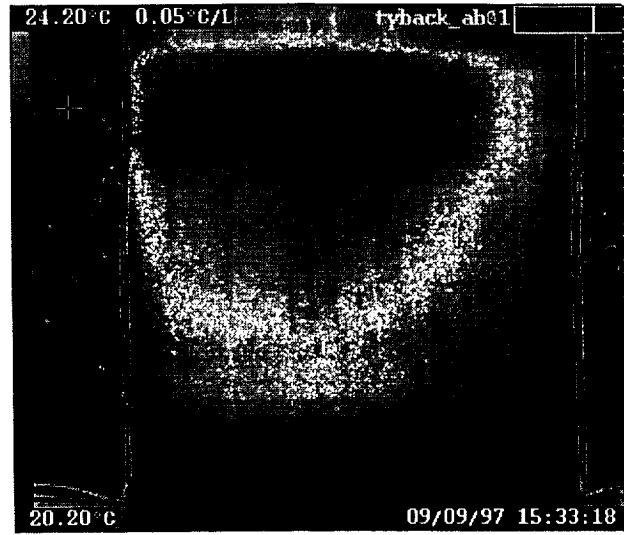
TY-B-Front



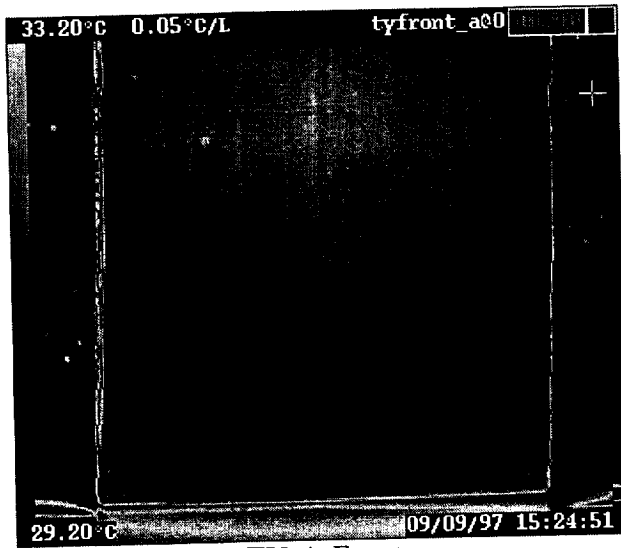
TY-B-Back



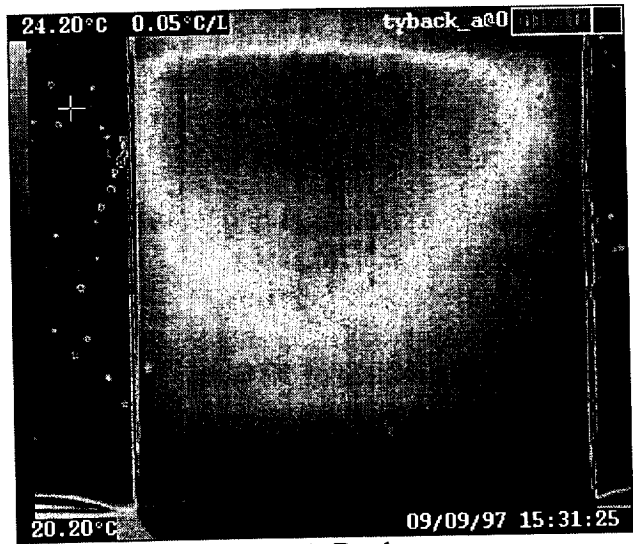
TY-AB-Front



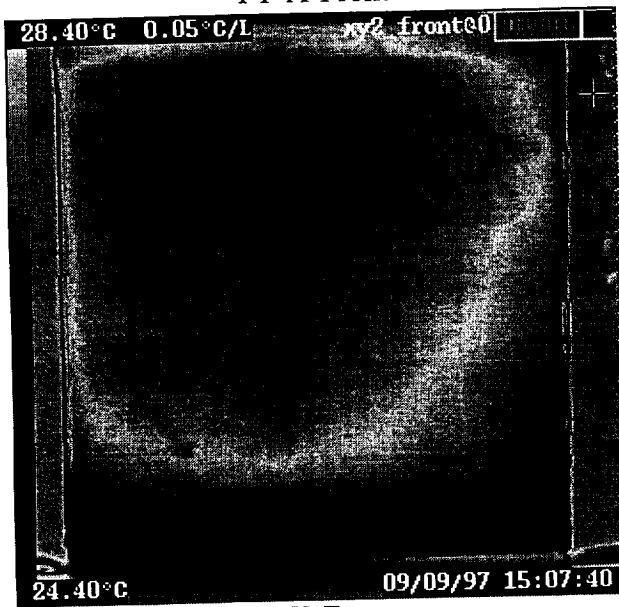
TY-AB-Back



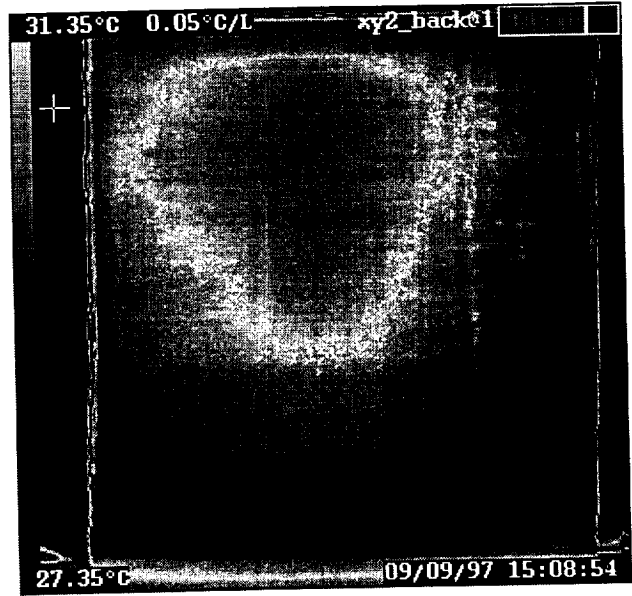
TY-A-Front



TY-A-Back



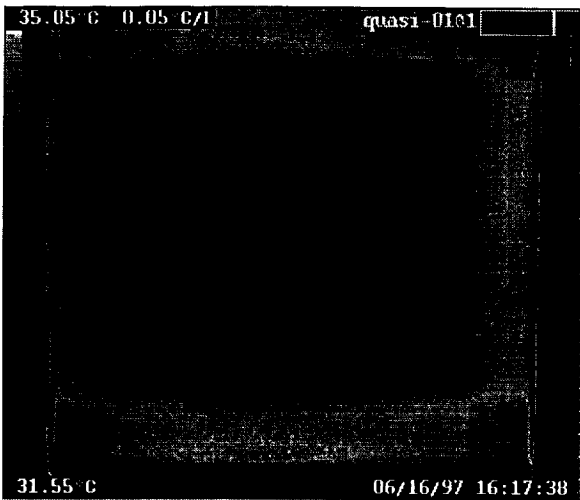
XY2 Front



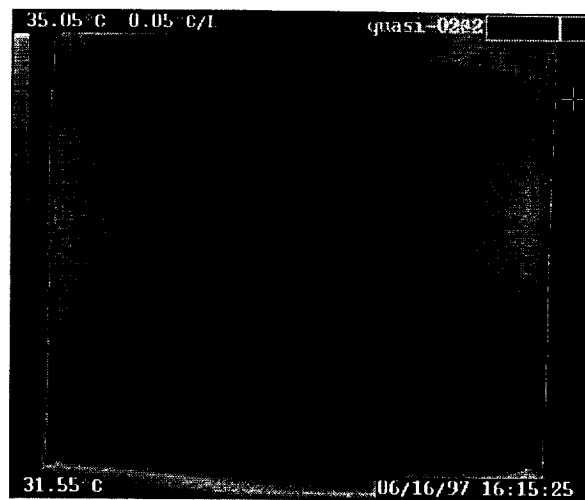
XY2 Back

8.0 THERMOGRAPHIC INSPECTION OF GRAPHITE PANELS FOR LOCKHEED-MARTIN

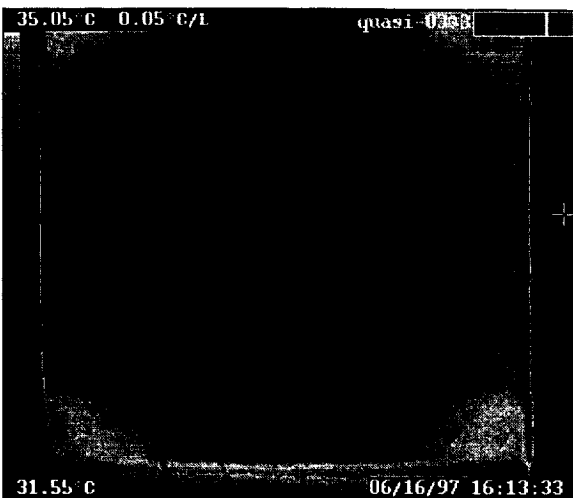
- Material: Unidirectional graphite/epoxy
Lay-up schedule: Unknown
- Critical defect size: Unknown
- Inspected using flash thermography from the label side (Bales TIP)
- Imaged at a distance of 32 inches
- Power setting of 1400V
- Thermograms taken at 100 msec. after flash
- Panels are oriented on thermograms upside down, i.e. label inverted in upper right hand corner
- No thermal abnormalities detected, only ply orientations apparent



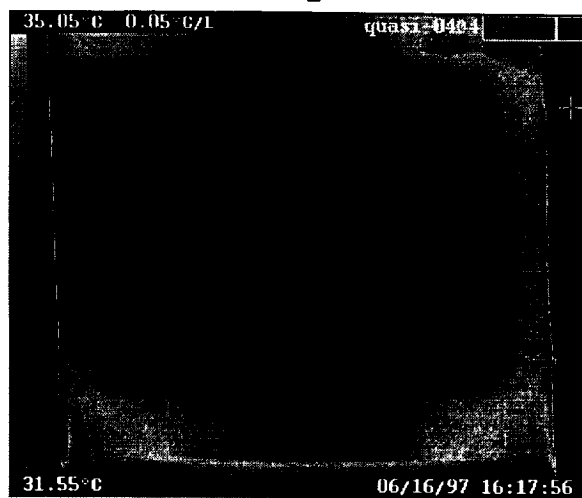
1



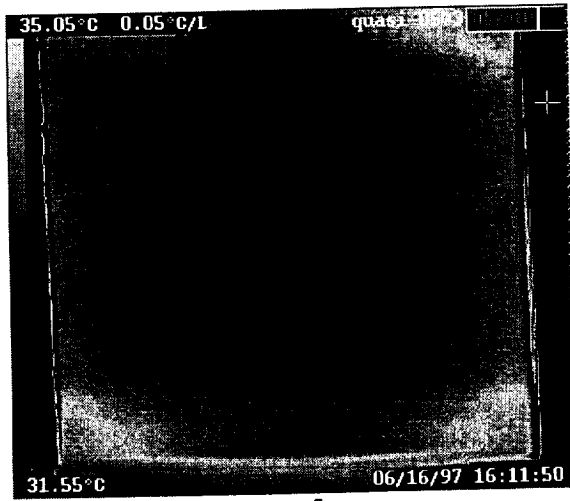
2



3



4



5

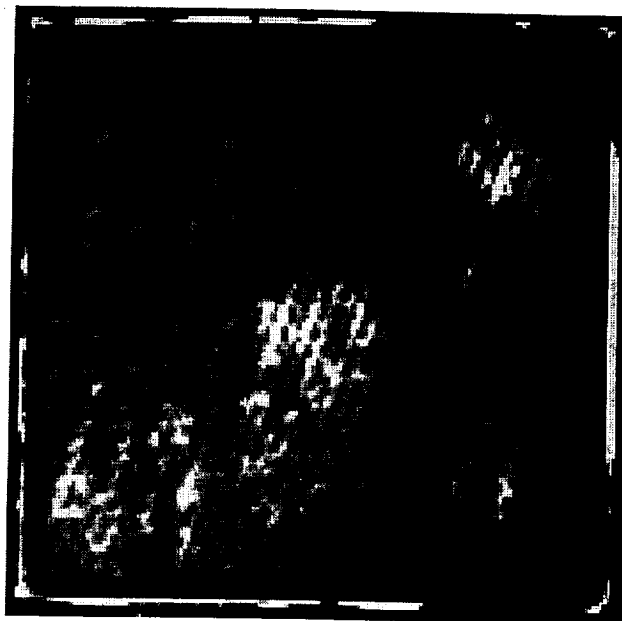
9.0 SOLID ROCKET BOOSTER NOSE CAP

9.1 THERMOGRAPHY OF SRB TEST COUPONS

Configuration: Amber Radiance 1 thermal camera (25 mm lens) running under Thermal wave Imaging software.



Core (Painted flat black)



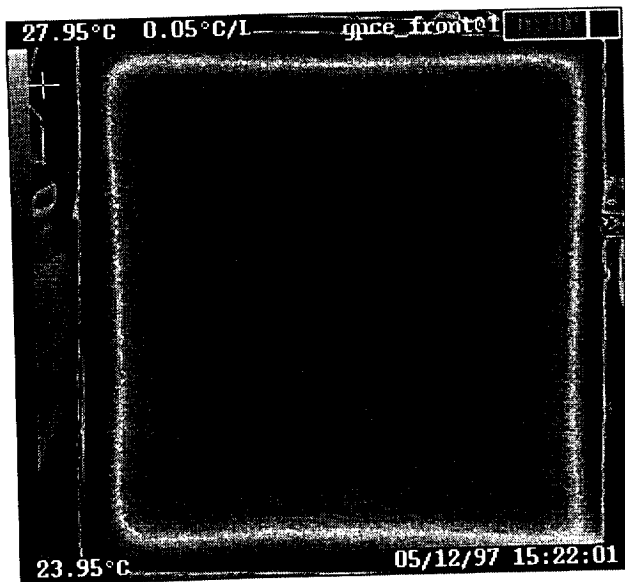
Face sheet

Notes: Writing on the core material made inspection difficult. Some of the affects of the writing were overcome by painting the surface with a water washable flat black paint. The paint helped to give the surface a uniform emissivity instead of the contrasting black letters on the yellow surface. Only part of the defects are pointed out in the thermogram.

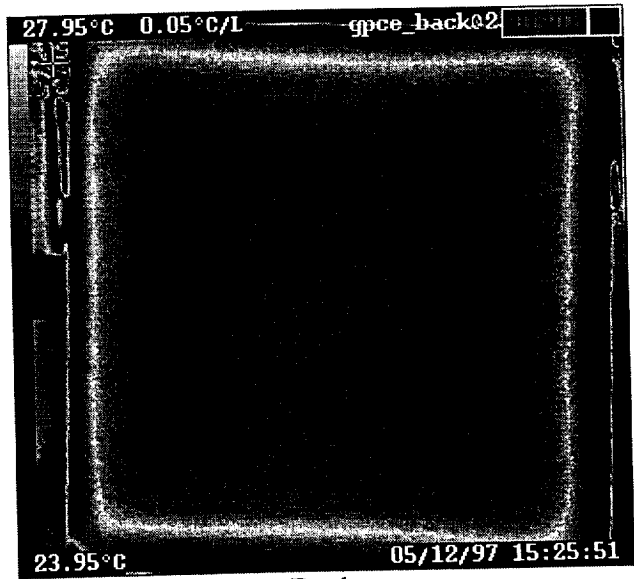
There appears to be two main defect regions in the face plate (center and upper right).

9.2 THERMOGRAPHY OF GRAPHITE/CYANIDE ESTER PANEL FOR SRB NOSE CAP

Configuration: Lamp heating (1000W)
Imaged at 20 inches using back side heating.



Front



Back

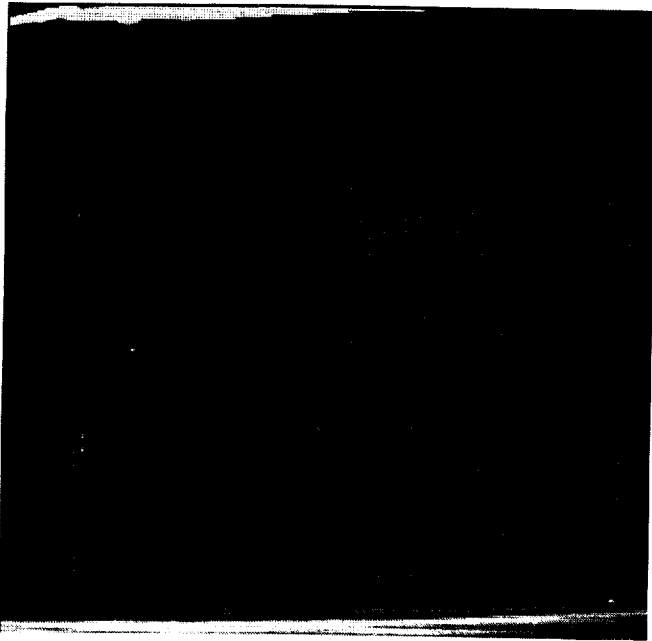
Discussion of results:

- Very efficient heat conduction through panel, requiring little exposure time to the heat lamp for inspection.
- Both thru-transmission (1000W quartz lamp) “shown above” and one-side (flash heating) inspections were performed.
- No thermal abnormalities were detected with either method indicating good bond between foam core and face plates.

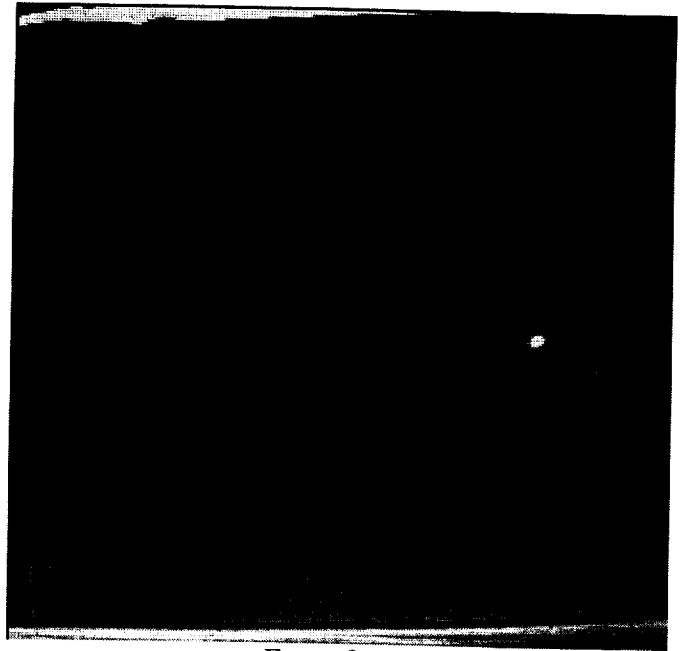
9.3 THERMOGRAPHY OF HG-10

Panel HG-10 featured a F650/AF-191K/8552 [Graphite/polyimide[foam filled honeycomb} glass/phenolic]lay-up. The panel was inspected with the Amber Radiance 1 with 25 mm lens running under Thermal Wave Imaging software. The heat source for this inspection was the Bales Scientific flash unit set to 1400V excitation level. The distance between the imager and test article was set at 32 inches. The surface of the sample was dulled with a water washable flat black paint.

The only thermal abnormality found was a small spot on the right side of the front face of the panel. This defect acts as a small void “delamination” at the edge of a bolt hole. No indications were found using through transmission heating (1000W heat lamp). A defect standard panel is needed to verify the depth of penetration of the flash heating



Rear face

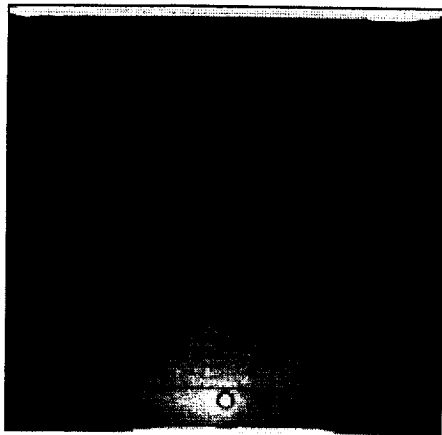


Front face

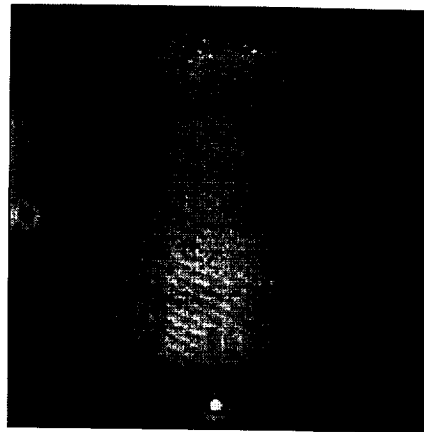
9.4 HOT GAS PANELS (HG15, HG16, HG17, HG18, HG19, HG20)

As with the HG-10 panel the thermal inspection of panels HG15 through 20 were performed with the Amber Radiance 1 with 25 mm lens running under Thermal Wave Imaging software. The heat source for these inspections was the Bales Scientific flash unit set to 1600V (maximum allowable) excitation level. Each panel was inspected from both sides. The side in the thermograms is labeled as (M => mesh side and B => back side). No surface preparation was used (i.e. flat black paint) to dull surface for these inspections.

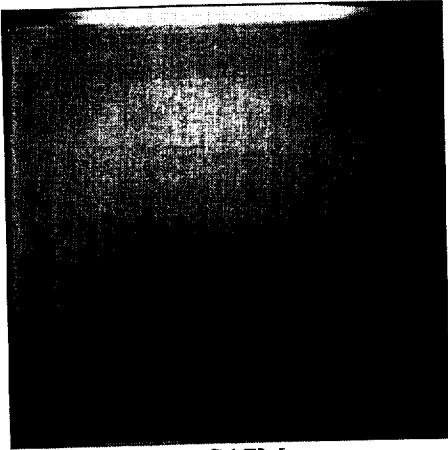
No abnormalities found in panels during inspection. The inspection were capable of detecting a 0.5 inch square piece of lead foil tape on side opposite camera during front side flash heating.



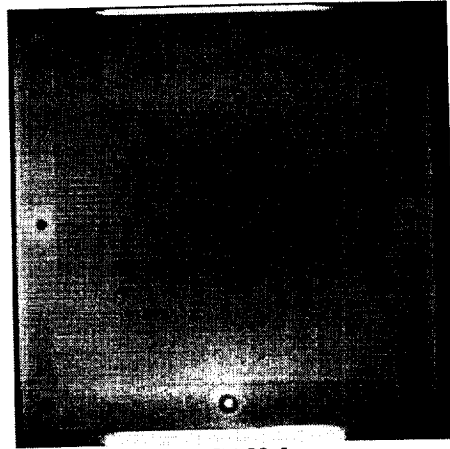
HG15M



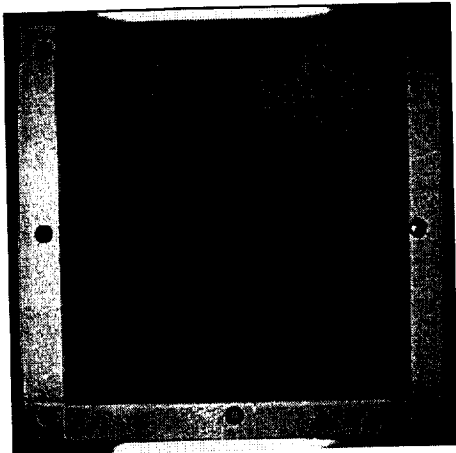
HG16M



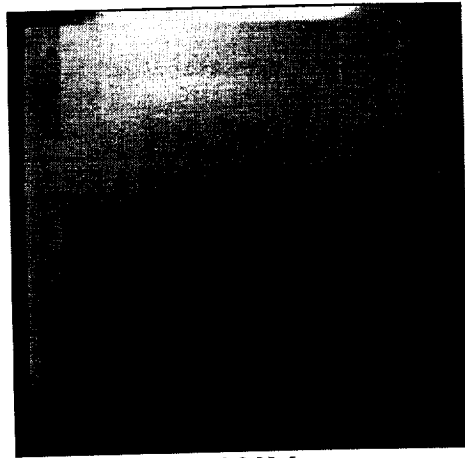
HG17M



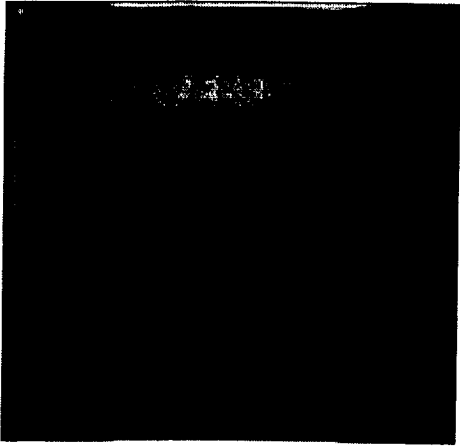
HG18M



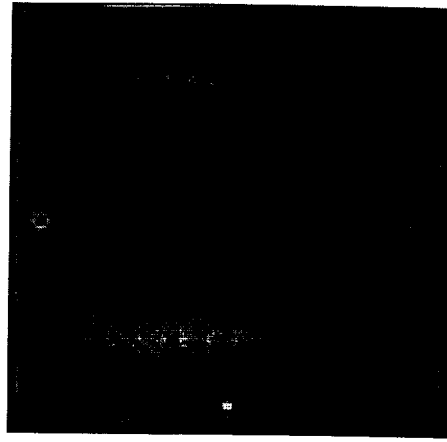
HG19M



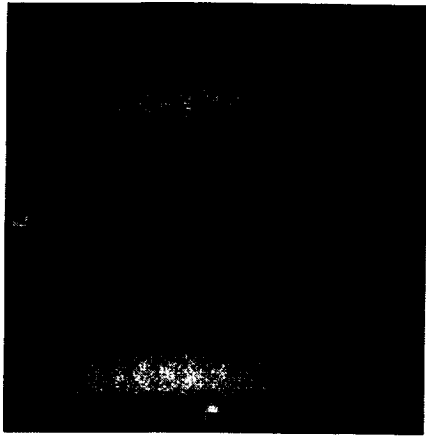
HG20M



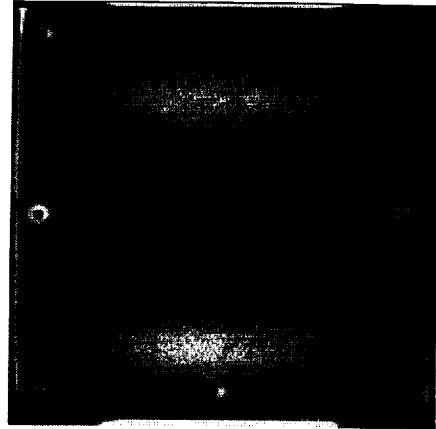
HG15B



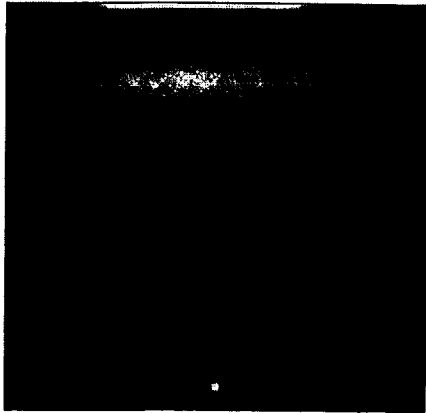
HG16B



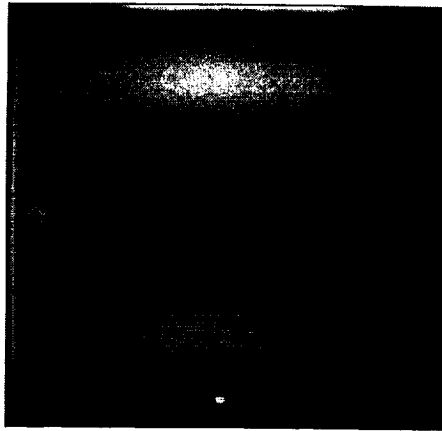
HG17B



HG18B



HG19B

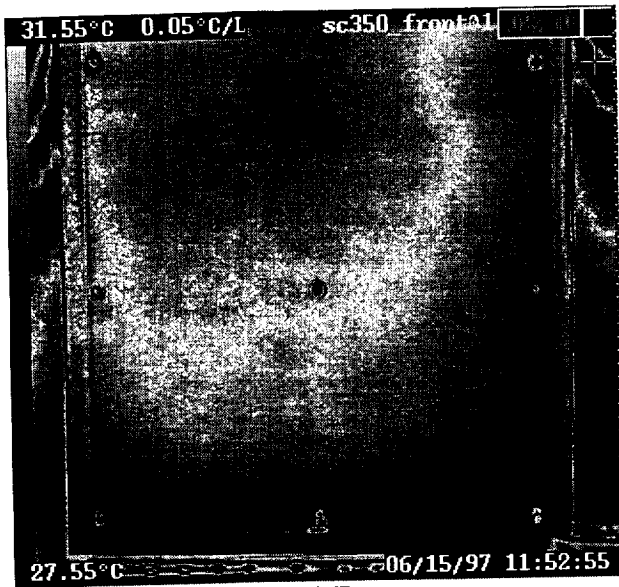


HG20B

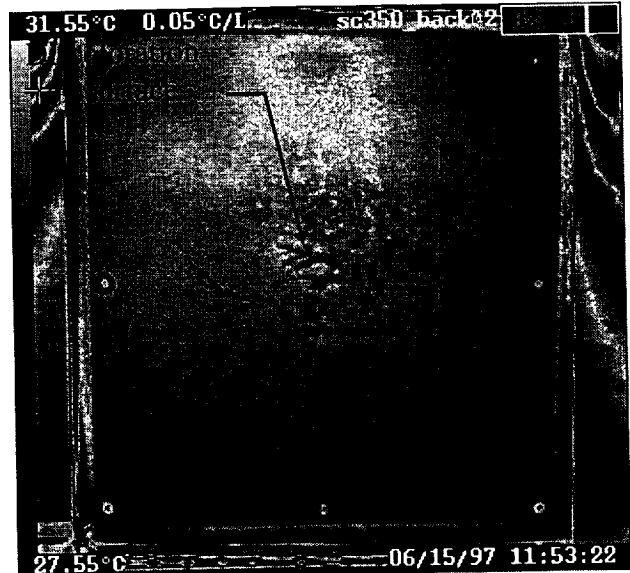
9.5 HOT GAS PANEL SC350 and SCGLASS

Inspected using the Bales TIP and single sided flash (power setting of 1400V) thermography at a distance of 32 inches.

Thermal abnormalities marked on images

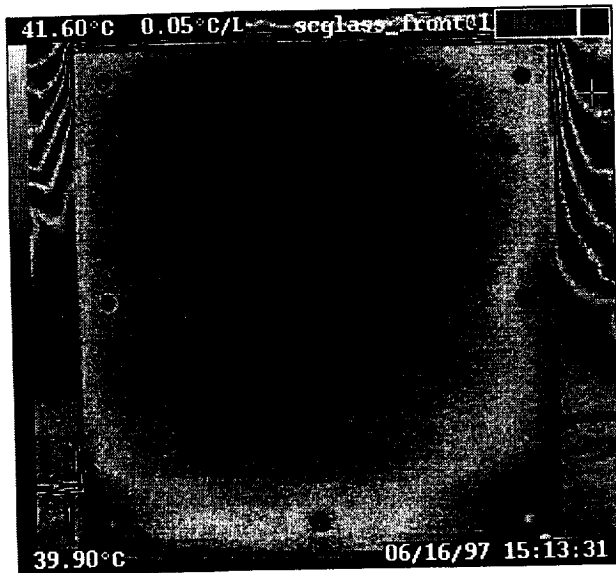


SC350 Front

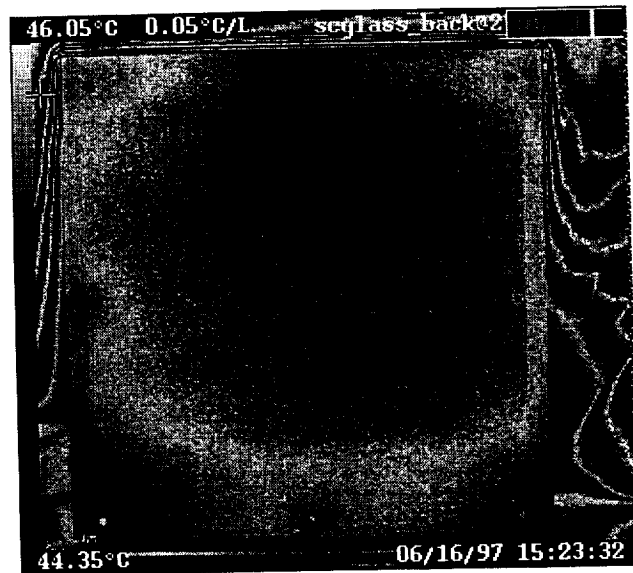


SC350 Back

Graphite/phenolic panel



SCGLASS Front



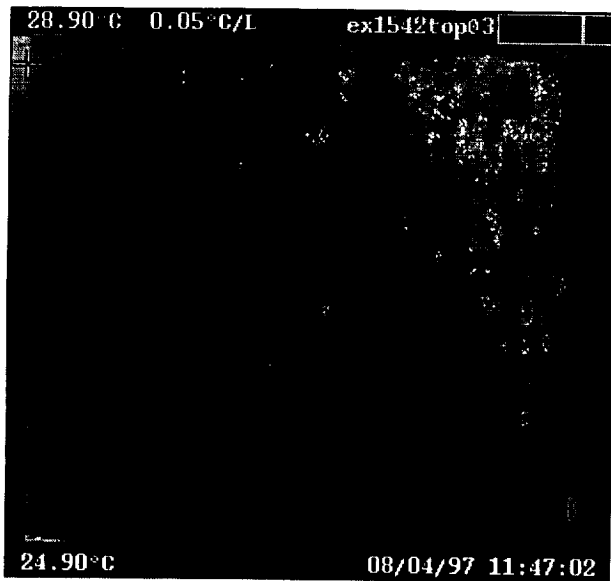
SCGLASS Back

Fiberglass/phenolic panel

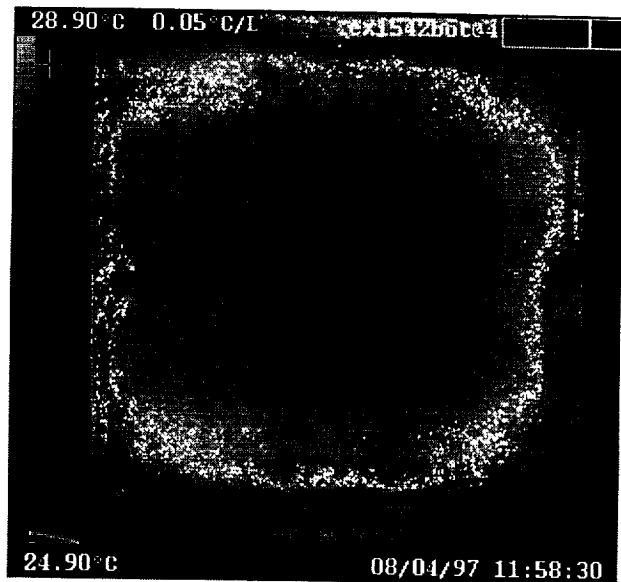
9.6 HOT GAS PANEL EX1542 and F650BMI (post treatment)

Inspected using the Bales TIP and flash (power setting of 1400V) thermography at a distance of 32 inches.

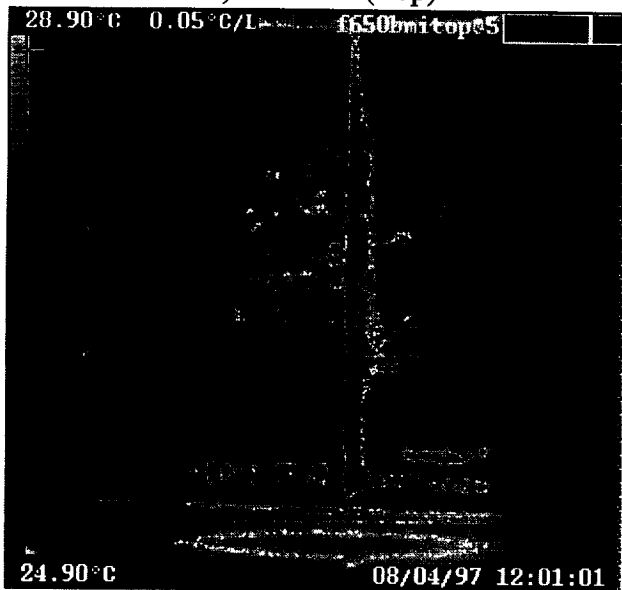
- Material:
- A) EX1542 Cynate ester/SC350G/3501-6/AS-4
 - B) F650 BMI Fab/SC350/8552 epoxy
 - C) Glass/Phenolic



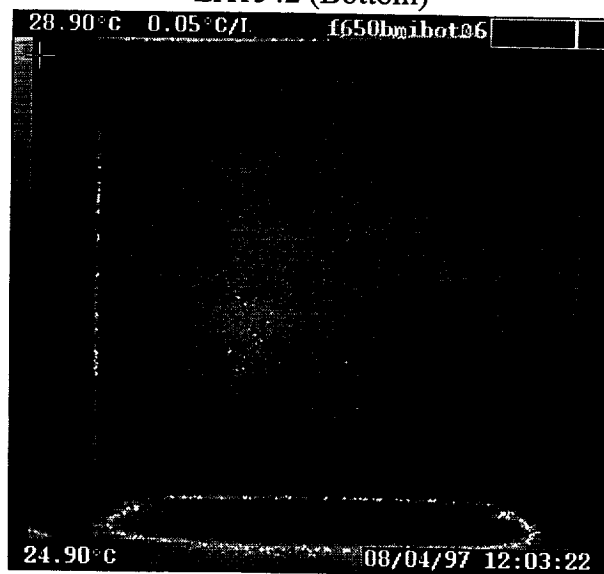
A) EX1542 (Top)



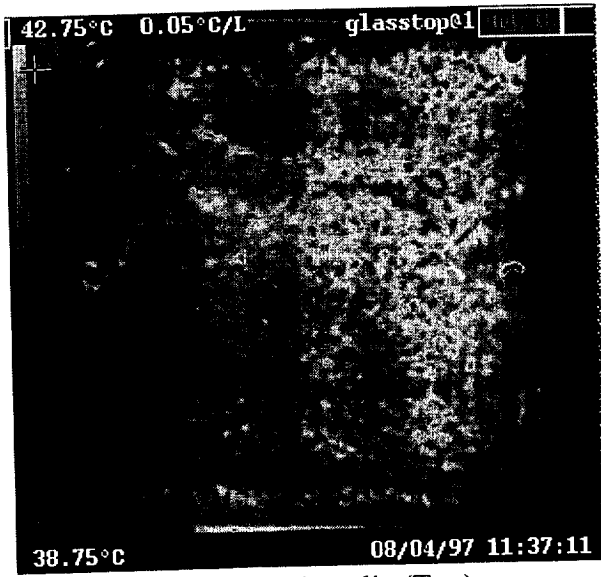
EX1542 (Bottom)



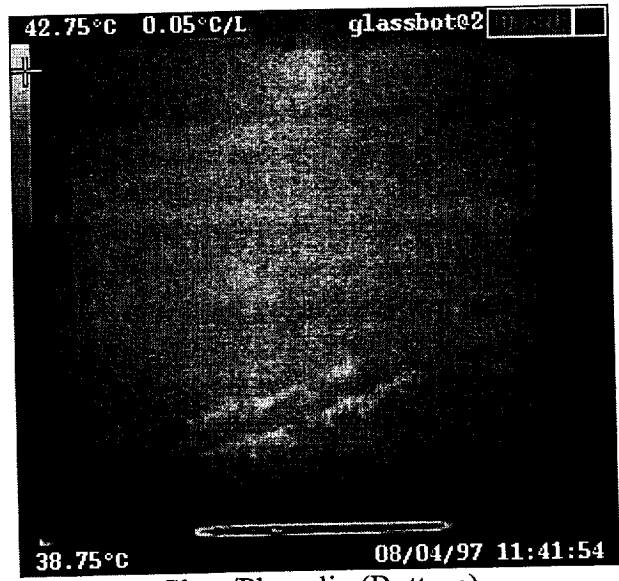
B) F650BMI (Top)



F650BMI (Bottom)



C) Glass/Phenolic (Top)



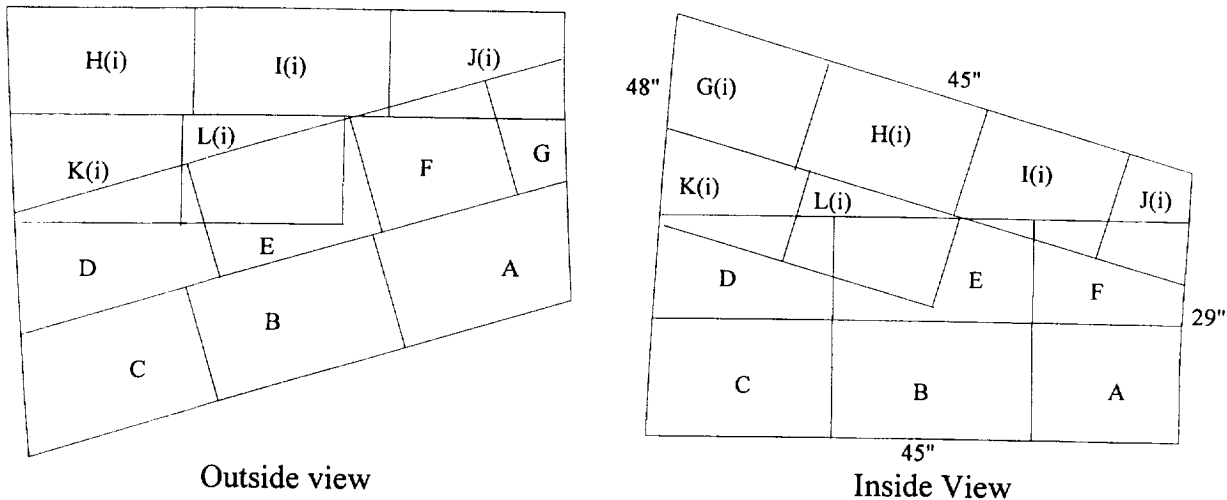
Glass/Phenolic (Bottom)

10.0 X-38 PANEL #9

A thermographic inspection was performed on the X38 test panel, SDK51375091; S/N 002. The panel was labeled as #9 and was intended to be the 2nd (outer) face sheet of a cored composite lay-up. The face sheet was fabricated using graphite/epoxy in at the Johnson Space Flight Center (JSC). The lay-up schedule and critical defect size was not provided by JSC

The panel was inspected using flash thermography from both sides. A single sided inspection was not possible as determined by the inability to detect lead foil tape on the back side of the panel during inspections. The panel was imaged at a distance of 32 inches using a Amber Radiance 1 thermal camera running under Thermal wave Imaging software. Flash heating was provided by a Bales Scientific Flash Unit set to a power setting of 1400V. With this arrangement the nominal inspection size was 12 inch tall by 18 inch wide and required 24 stations to provide complete coverage of the panel (Figure 37).

Some surface preparation was required to cover the gloss "yellow" finish on the mesh side of the panel. Here a "water washable" flat black paint was applied to increase the emissivity of the panel.



Outside view

Inside View

Note: The label (i) indicates that the panel was inverted to acquire thermograms.

Figure 37. X-38 Panel.

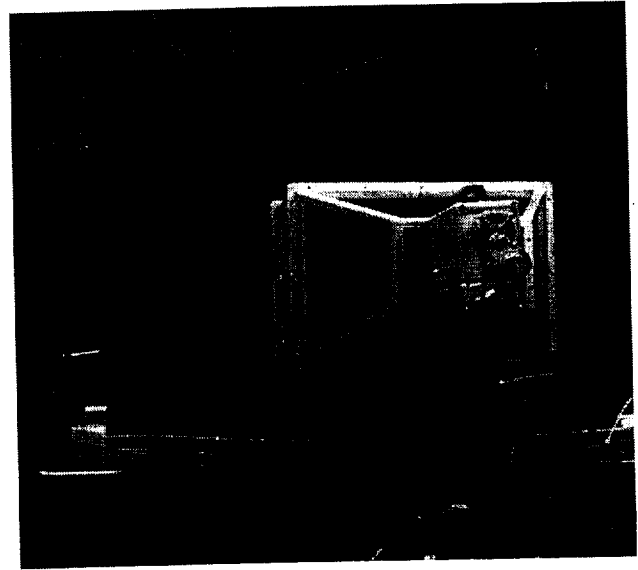


Figure 38. X-38 panel under inspection.

Two anomalies were found at image positions E and H on the inside of the panel. Each indication appeared to be close to the surface of the panel. The indications were not detected when the panel was examined from the opposite side. The indications are approximately 1/4 inch square.

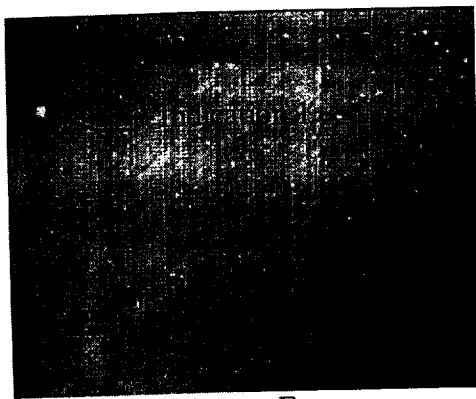


Image E.

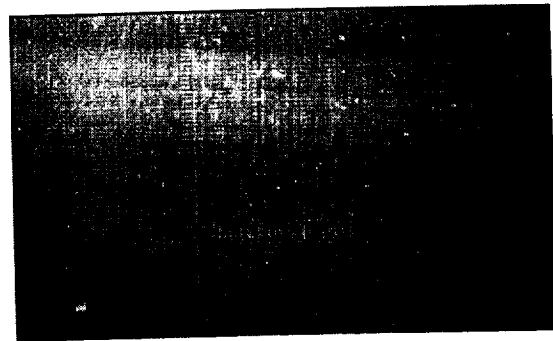


Image H.

Figure 39. Anomalies on X-38 panel.

A complete set of images from the inspection of the panel are provided for future reference.

Inside of panel

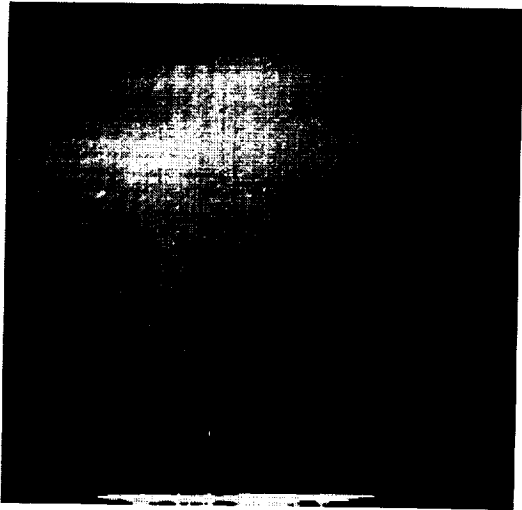


Image A.

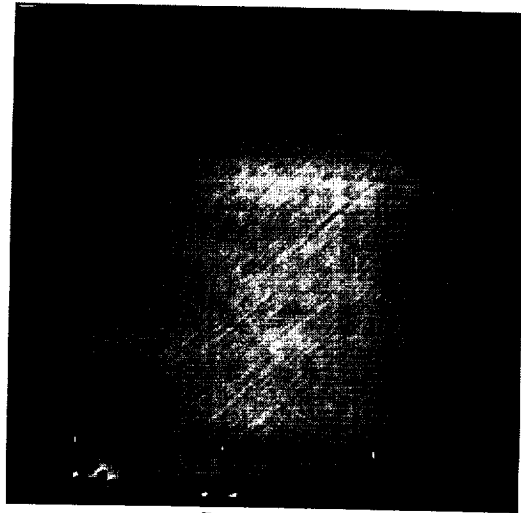


Image B.

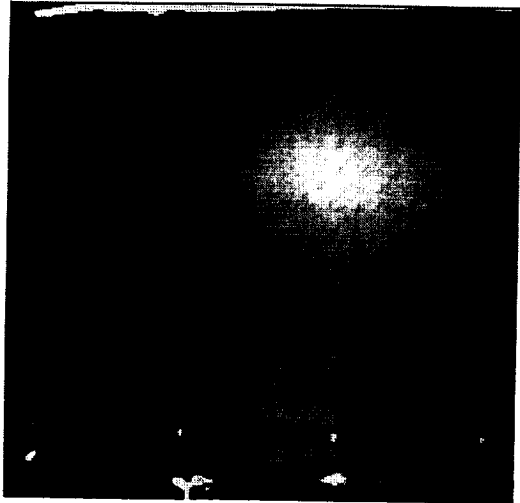


Image C.

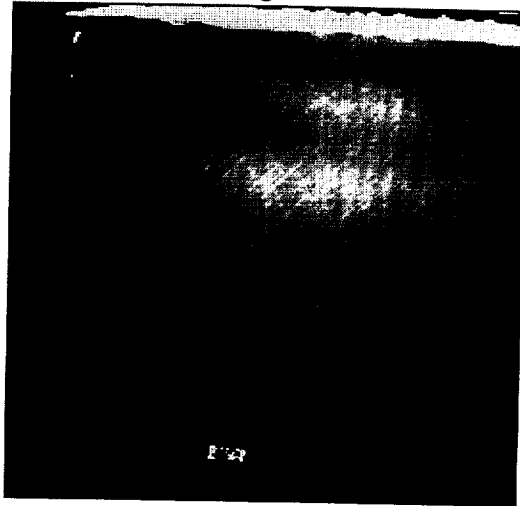


Image D.

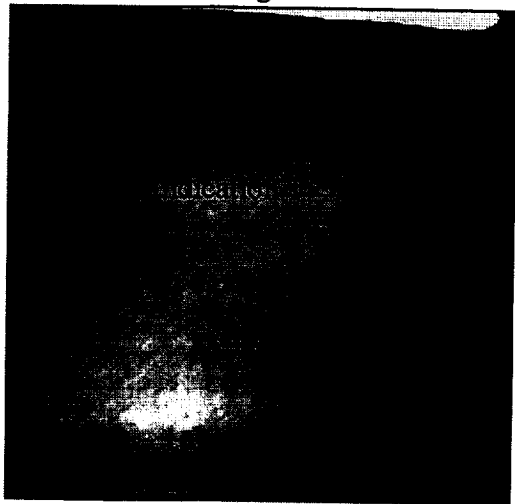


Image E.

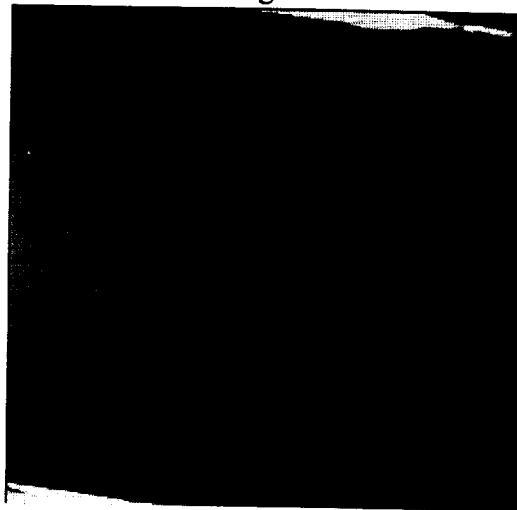


Image F.



Image G.

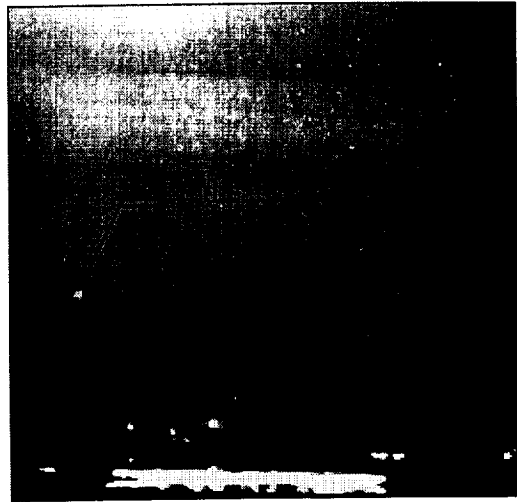


Image H.

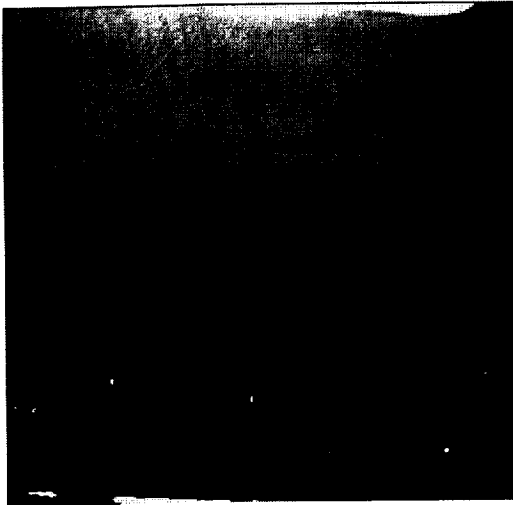


Image I.

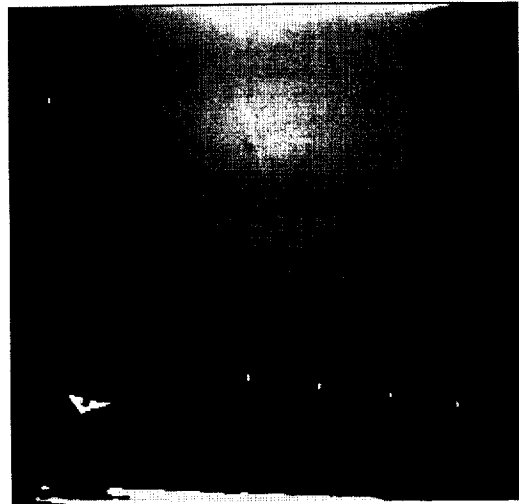


Image J.

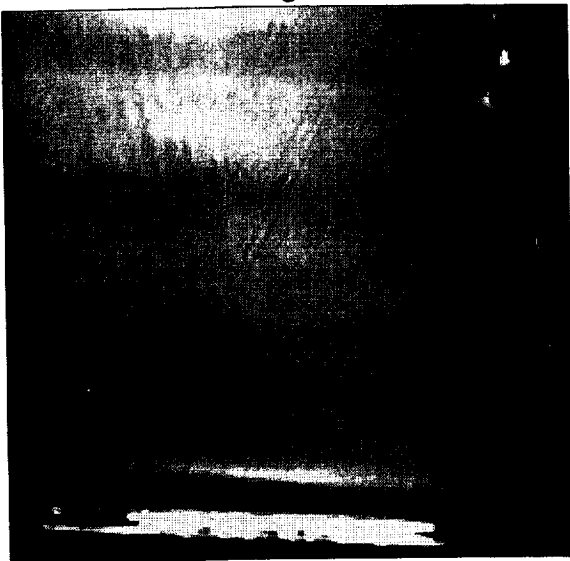


Image K.

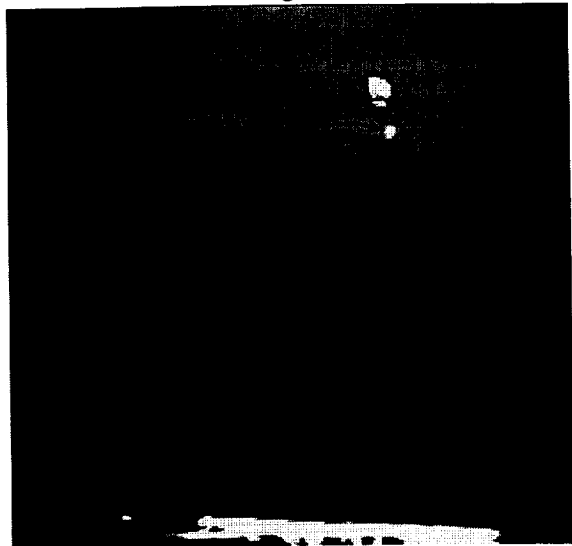


Image L.

Outside (Mesh side) of panel



Image A

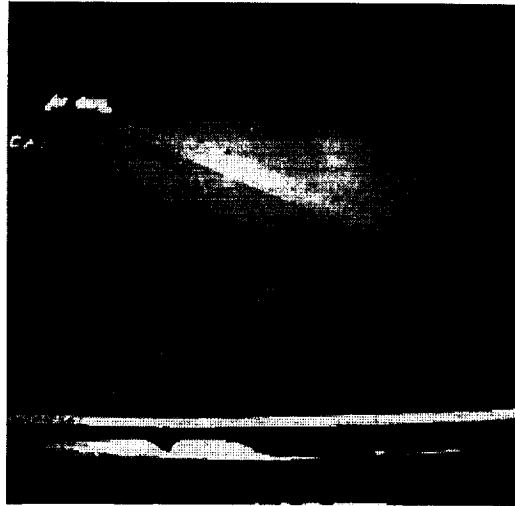


Image B

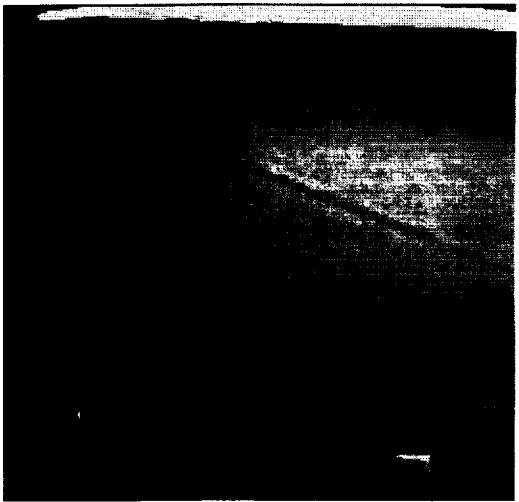


Image C

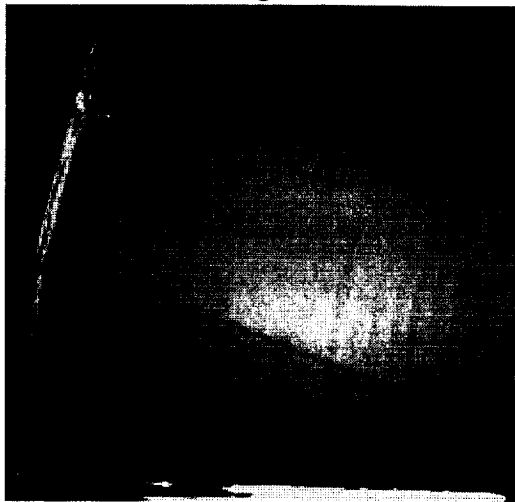


Image D

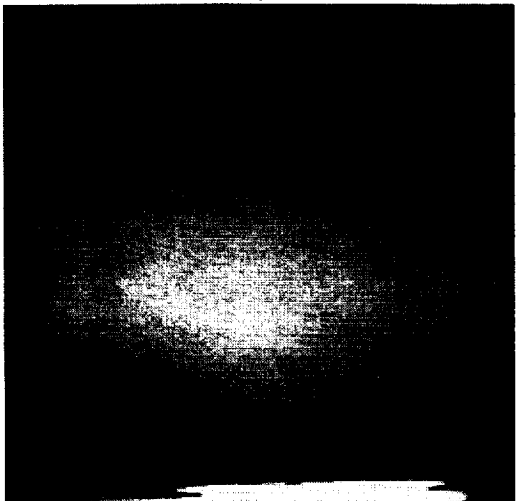


Image E



Image F

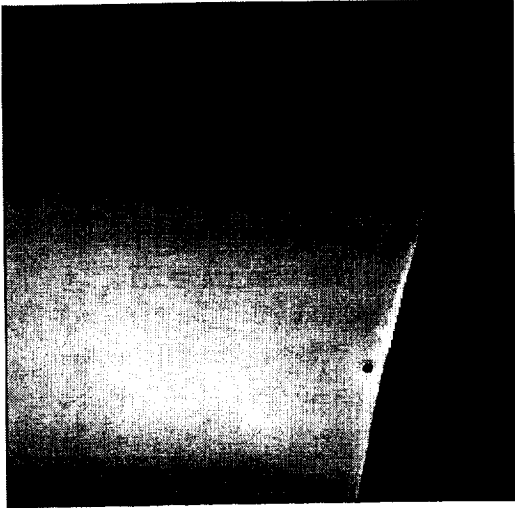


Image G

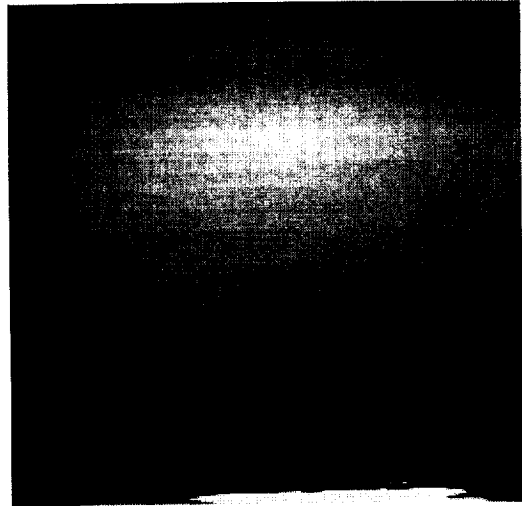


Image H

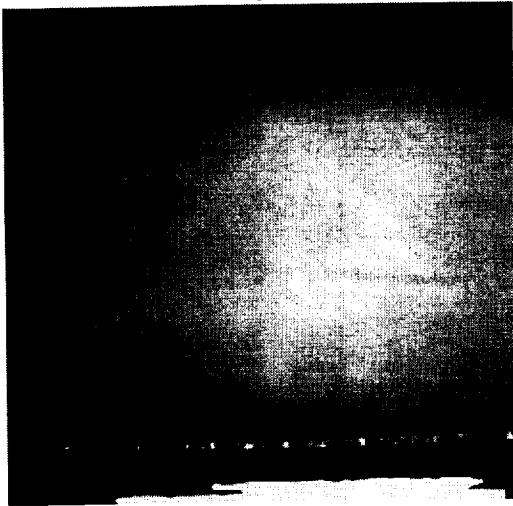


Image I

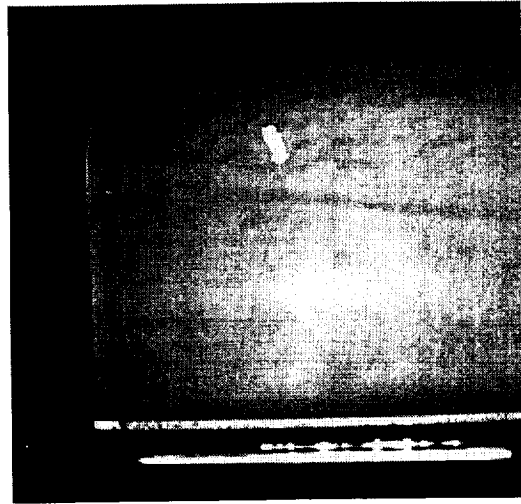


Image J

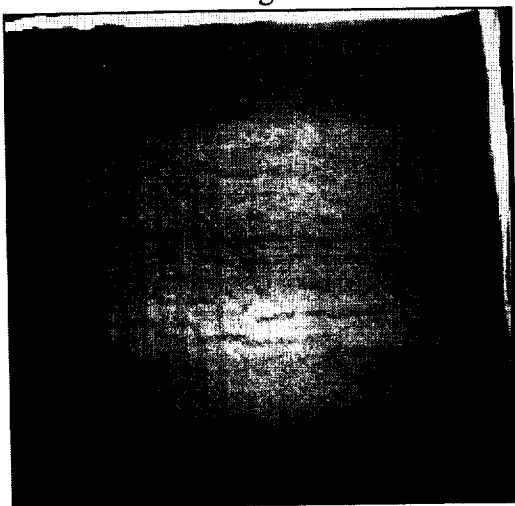


Image K

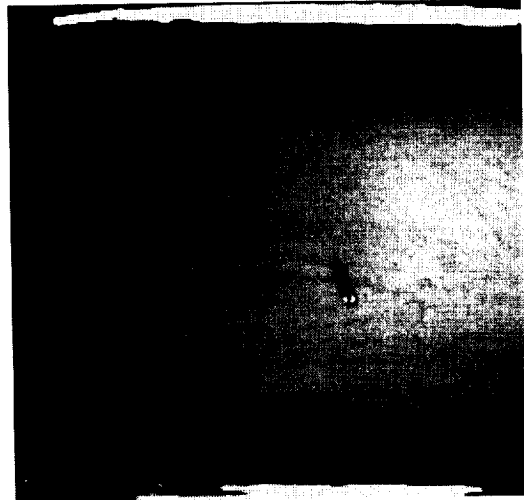


Image L

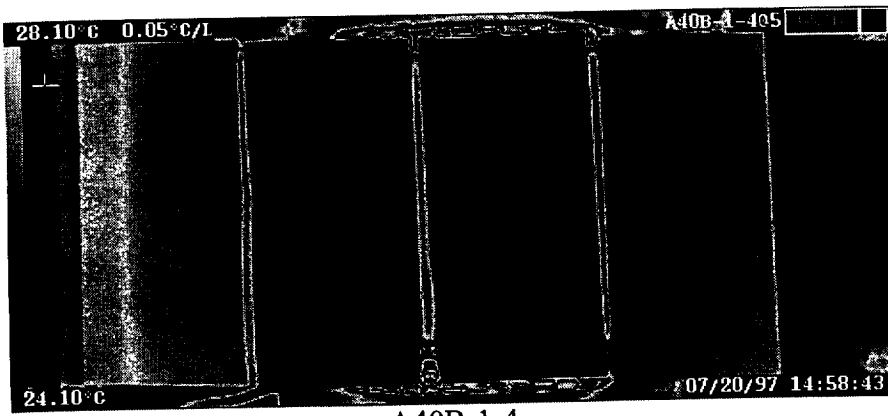
11.0 GRAPHITE/EPOXY DEBRIS IMPACT PANELS (PRE-IMPACT)

Ninety six 4" x 8" graphite/epoxy panels were thermographically inspected for manufacturing defects. These tests were intended to verify the quality of the material prior to impact loading. The heat source for the thermal inspection was generated by the Bales Scientific Flash Hood. The hood was set to an excitation power of 1400V and the acquisition rate was set to 20 msec/frame. The panels were placed 32 inches from the imager and heated from the viewing side. To accommodate the thickness of the panels both front and back side inspections were performed.

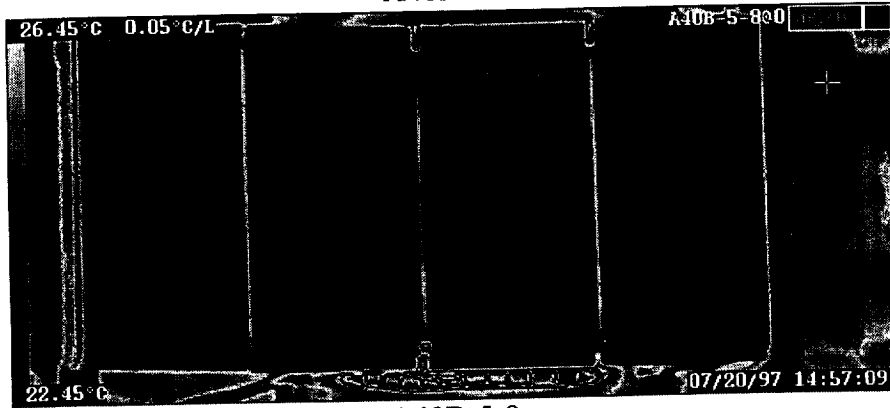
Out of the 192 inspections performed, only 10 anomalies were detected. These anomalies are identified in the following table and shown on the thermograms. The defect regions were identified on the samples with a white marker.

Defect Number	Panel
1	A40B-3
2	A40B-6
3	A40B-22
4	A24B-3
5	A24B-13
6	A24-1
7	A24-3
8	A24-6
9	A24-19
10	I16B-11

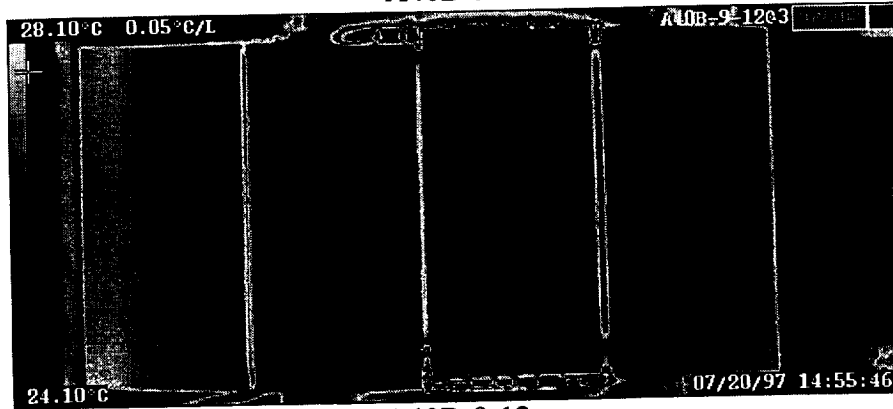
Designation	Gr/Ep	Plies	Orientation
I16	IM7/8552	16	[(0,+45.90.-45)s]2
I40	IM7/8552	40	[(0,+45.90.-45)s]5
A24	AS4/3501-6	24	[(0,+45.90.-45)s]3
A40	AS4/3501-6	40	[(0,+45.90.-45)s]5



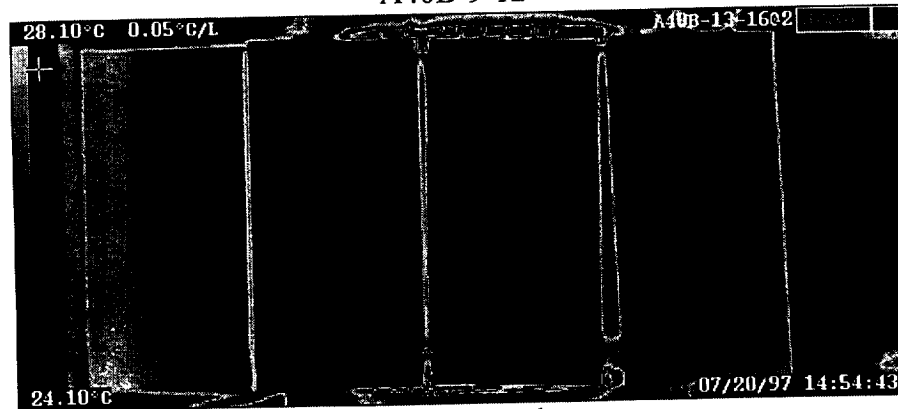
A40B-1-4



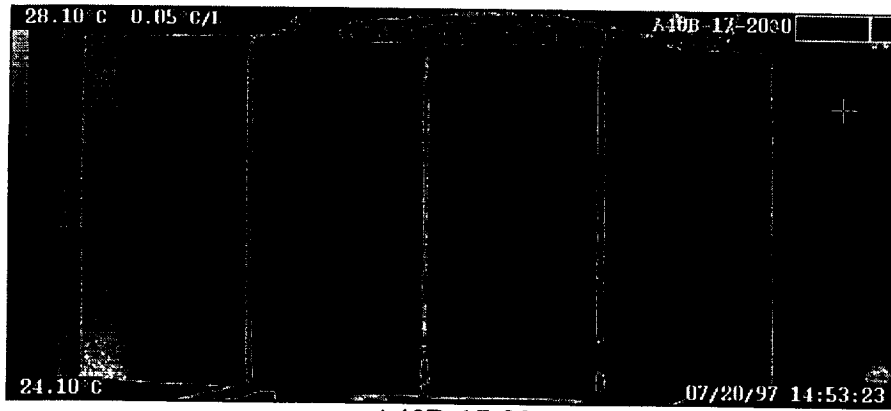
A40B-5-8



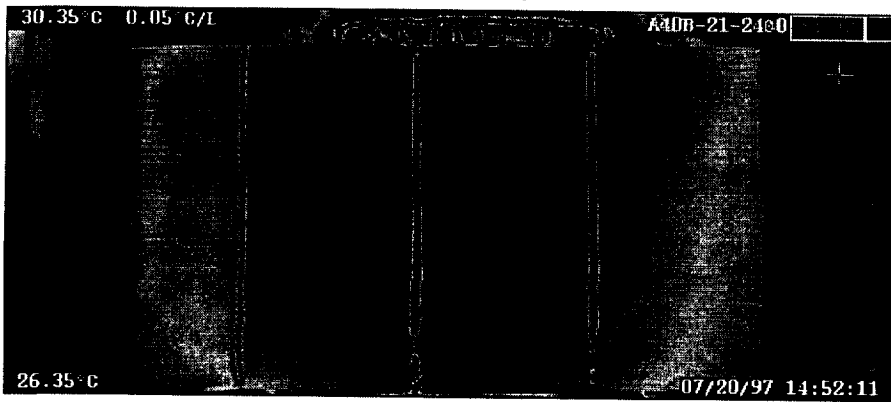
A40B-9-12



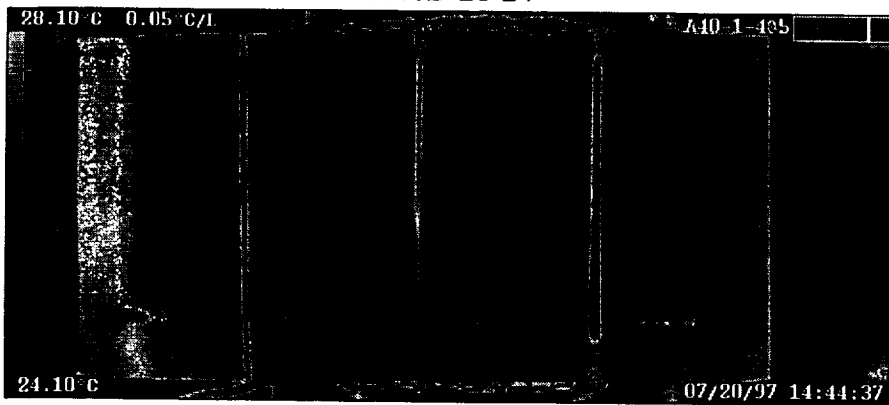
A40B-13-16



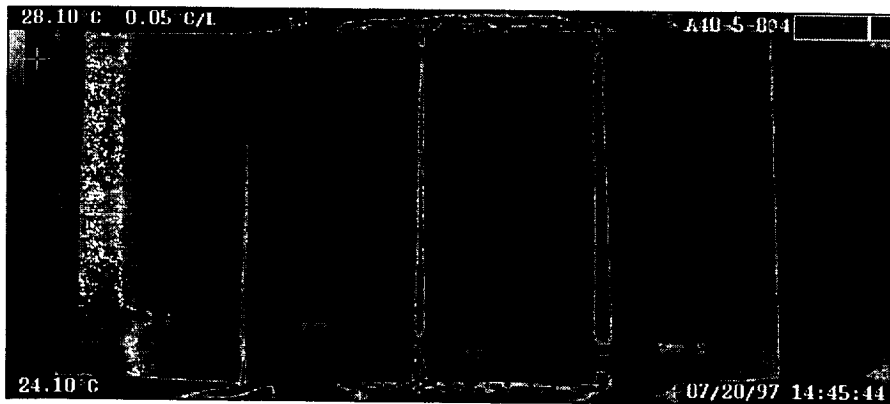
A40B-17-20



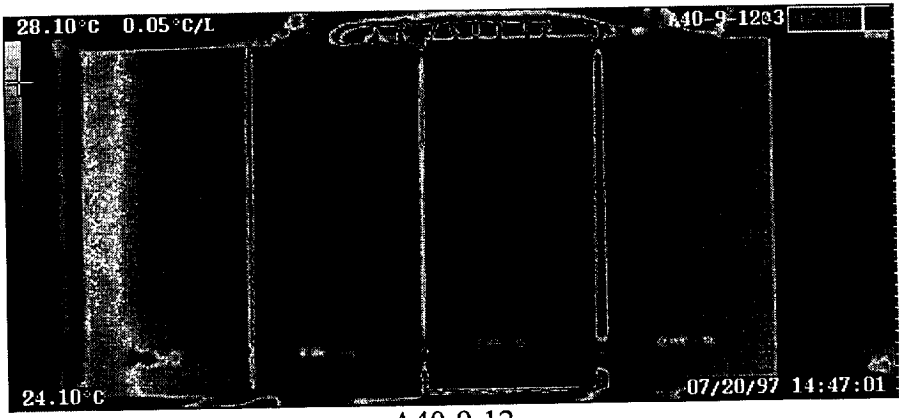
A40B-21-24



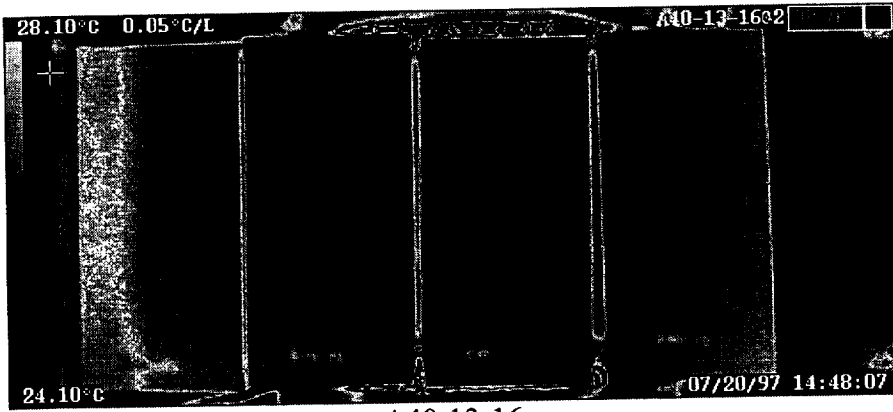
A40-1-4



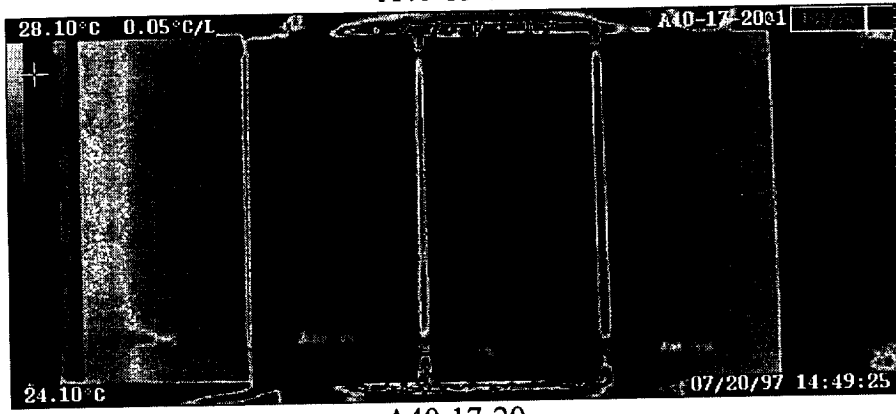
A40-5-8



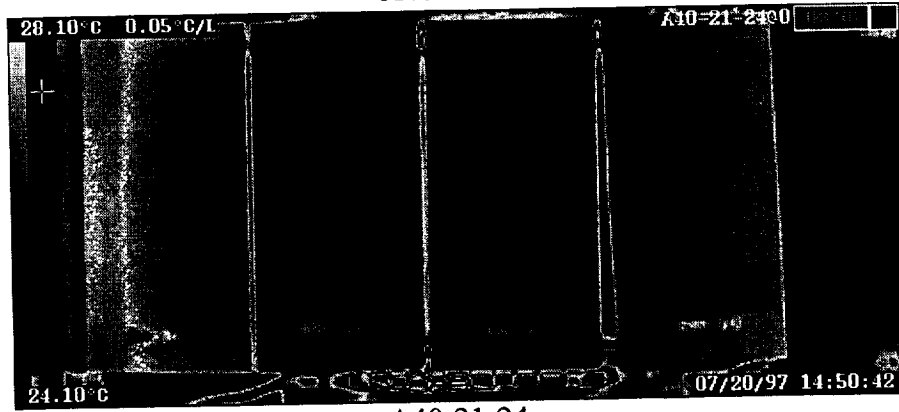
A40-9-12



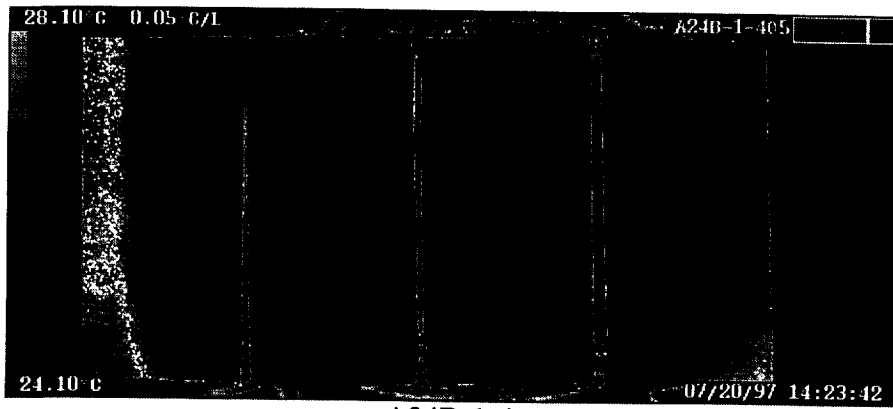
A40-13-16



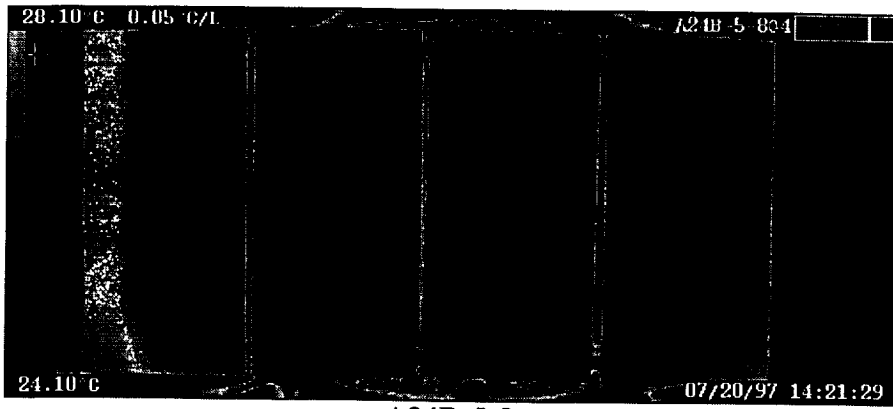
A40-17-20



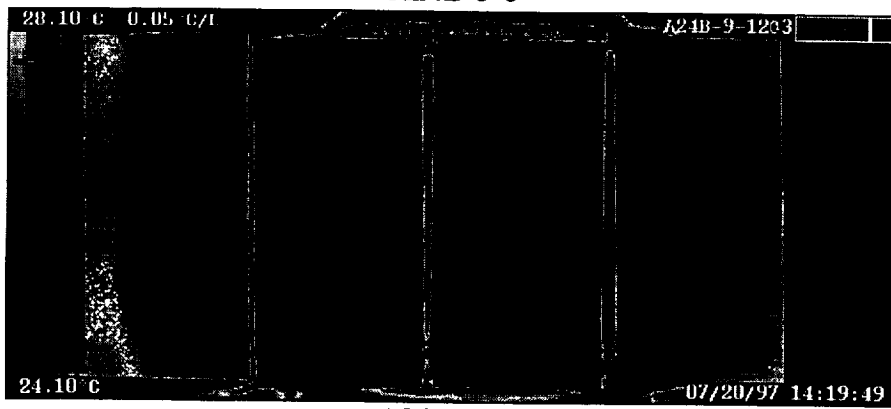
A40-21-24



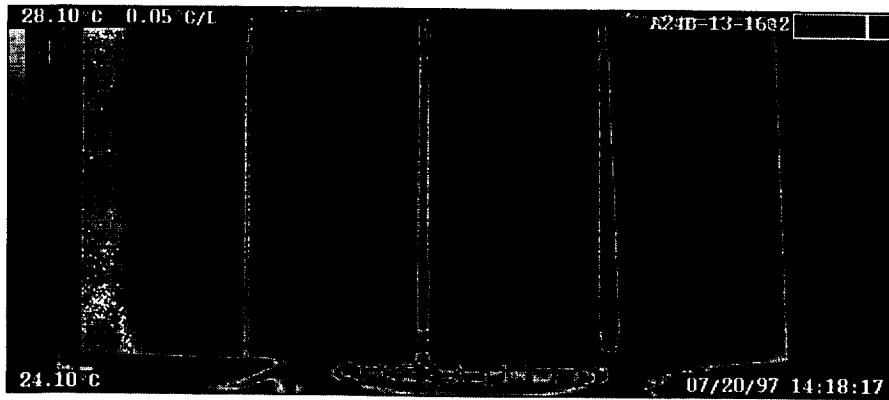
A24B-1-4



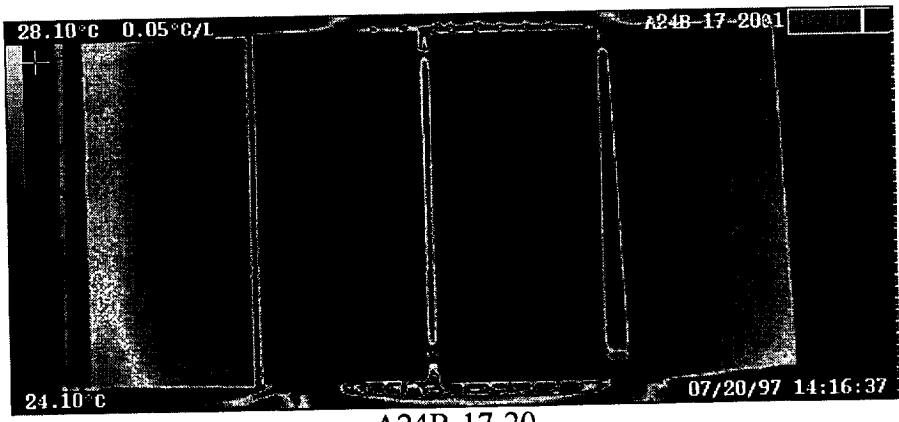
A24B-5-8



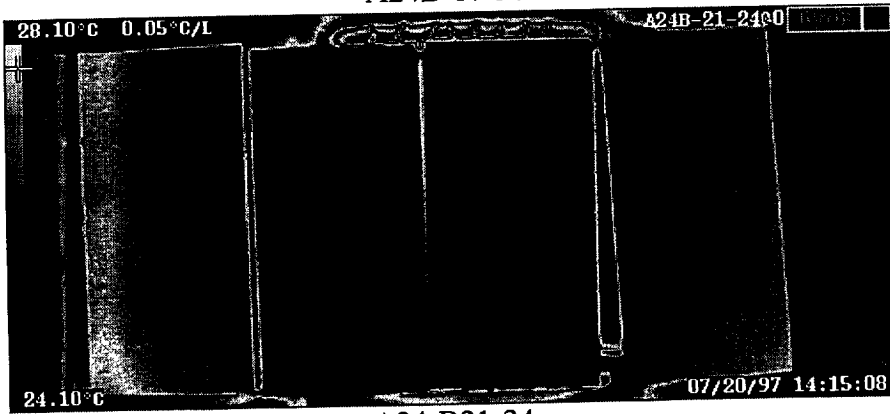
A24B-9-12



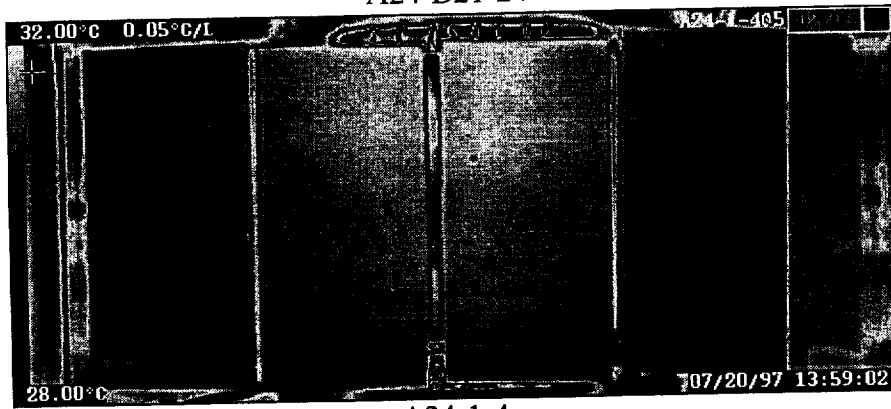
A24B-13-16



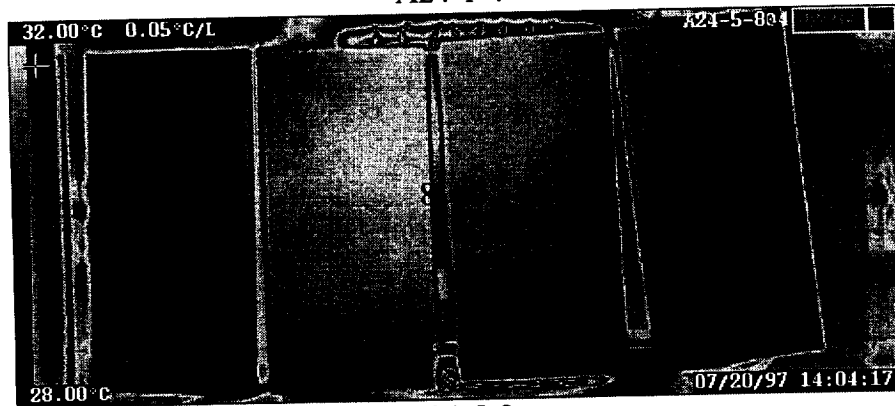
A24B-17-20



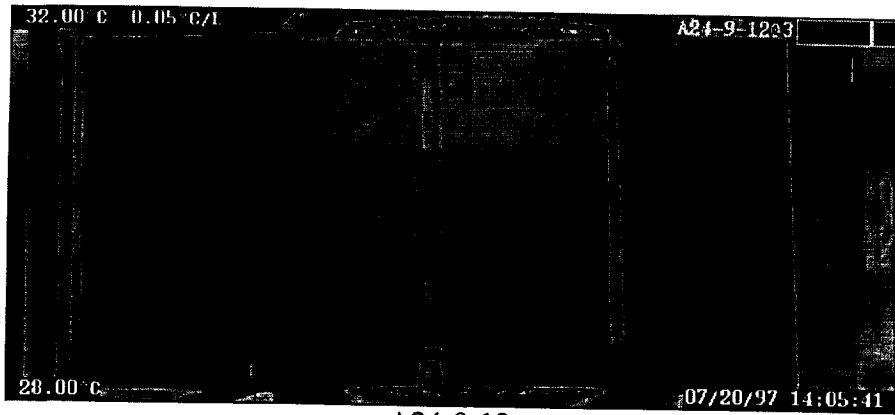
A24-B21-24



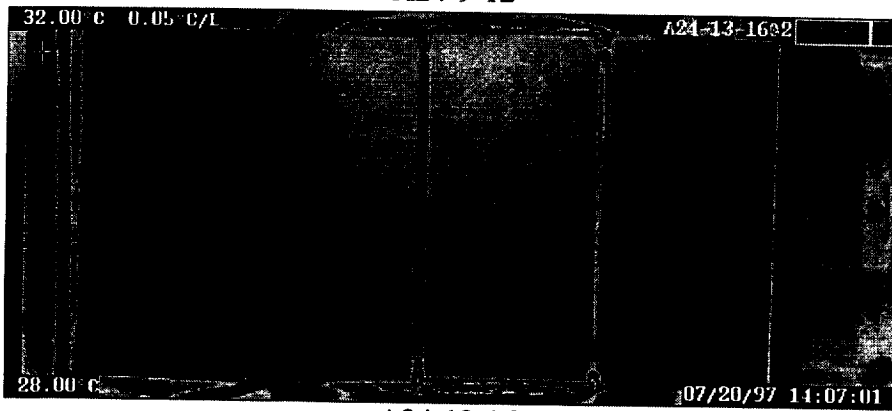
A24-1-4



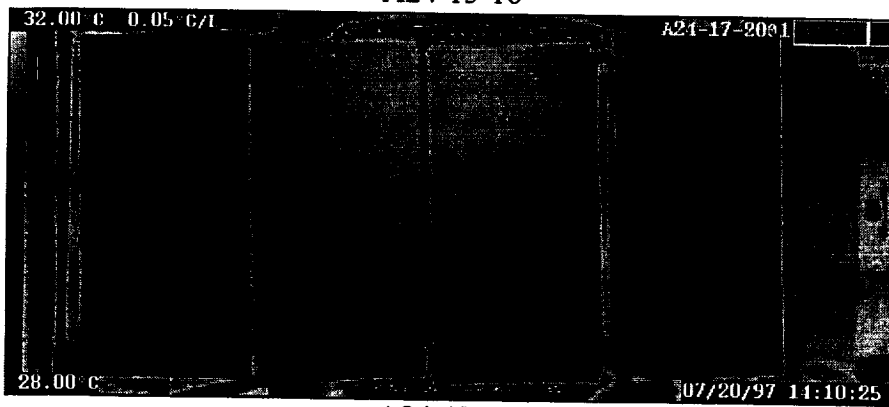
A24-5-8



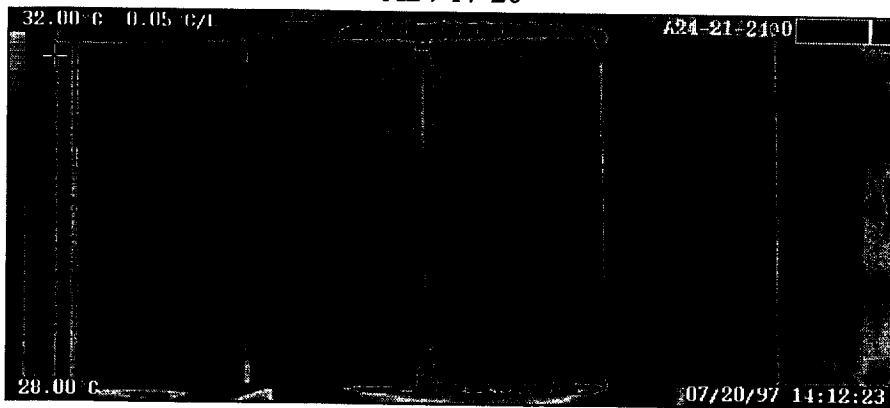
A24-9-12



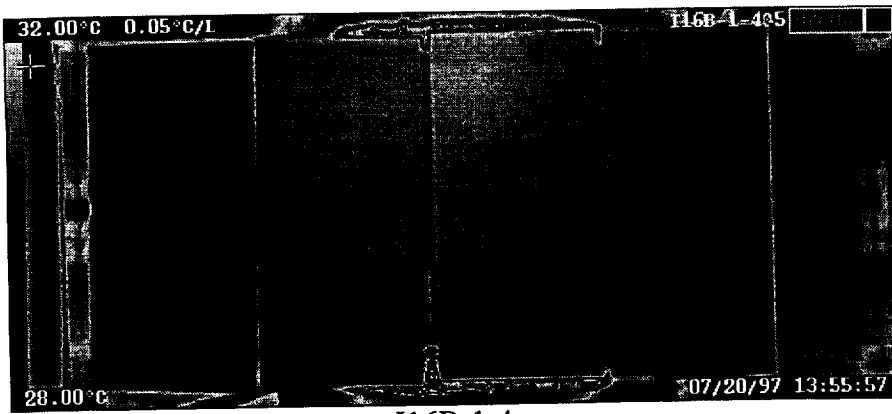
A24-13-16



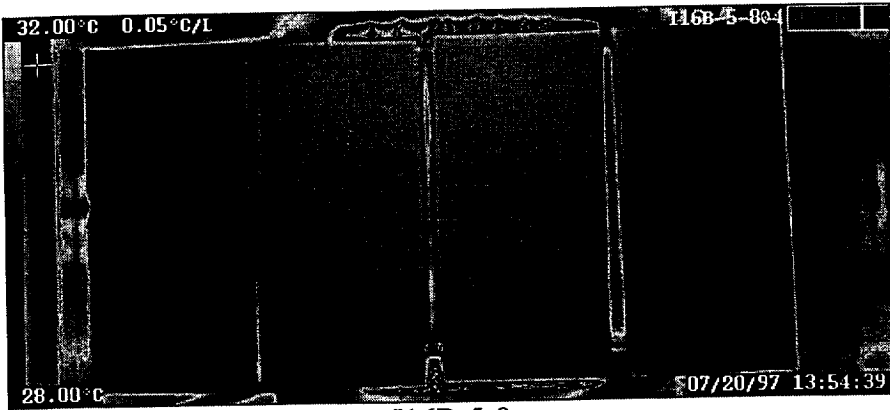
A24-17-20



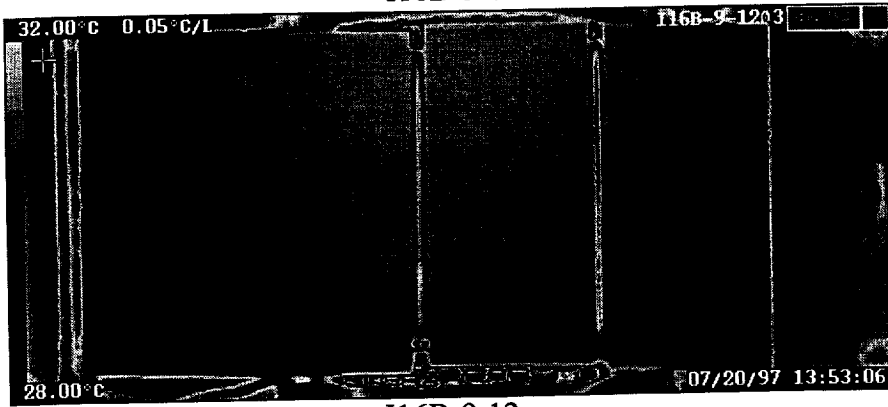
A24-21-24



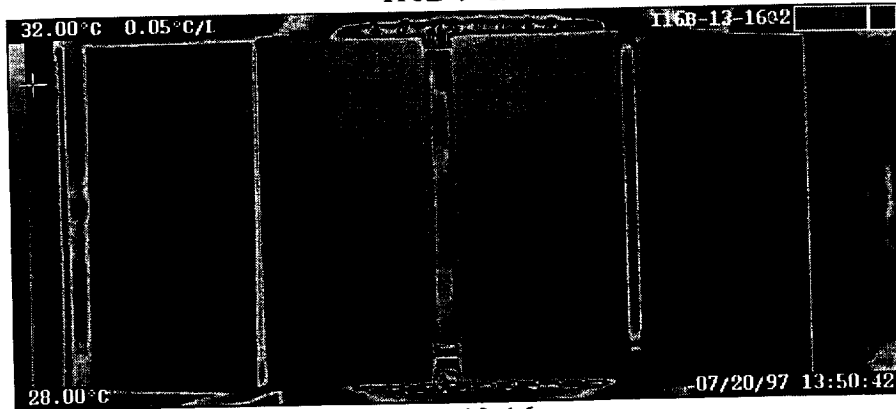
I16B-1-4



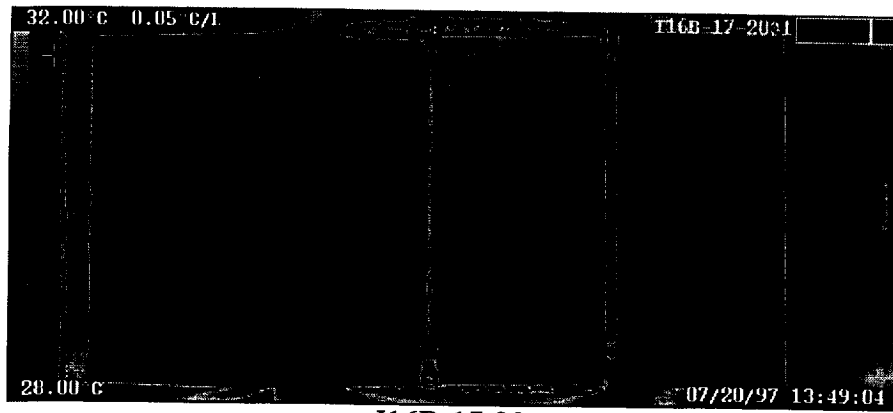
I16B-5-8



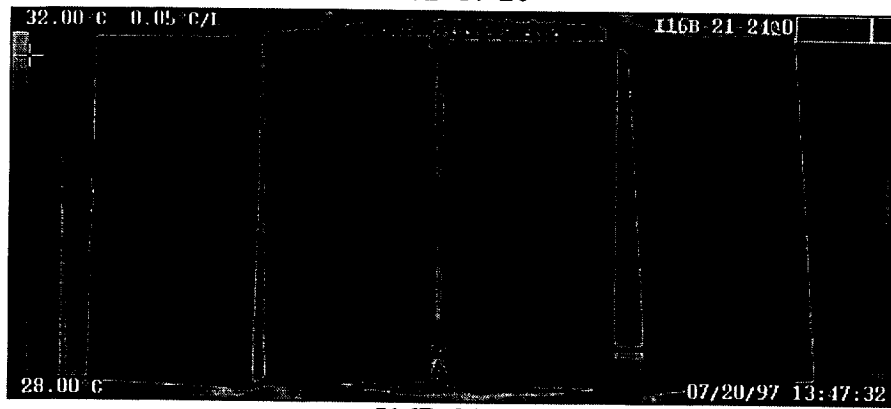
I16B-9-12



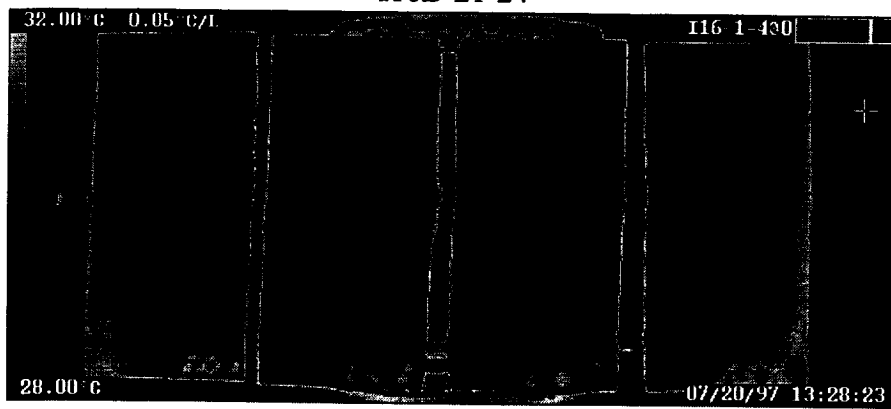
I16B-13-16



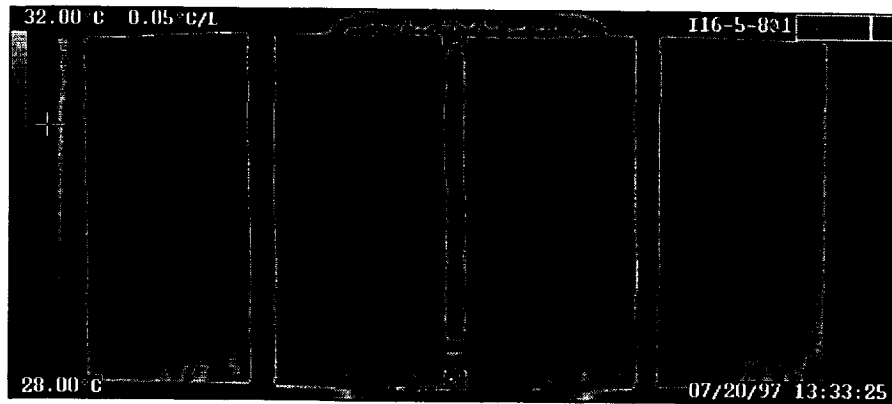
I16B-17-20



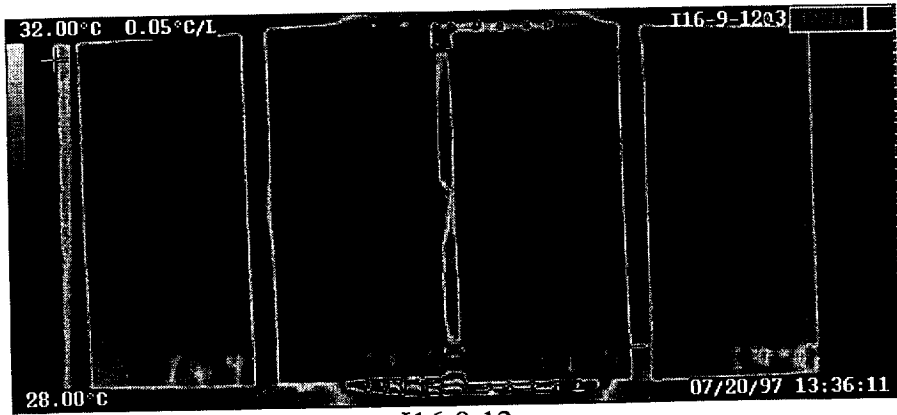
I16B-21-24



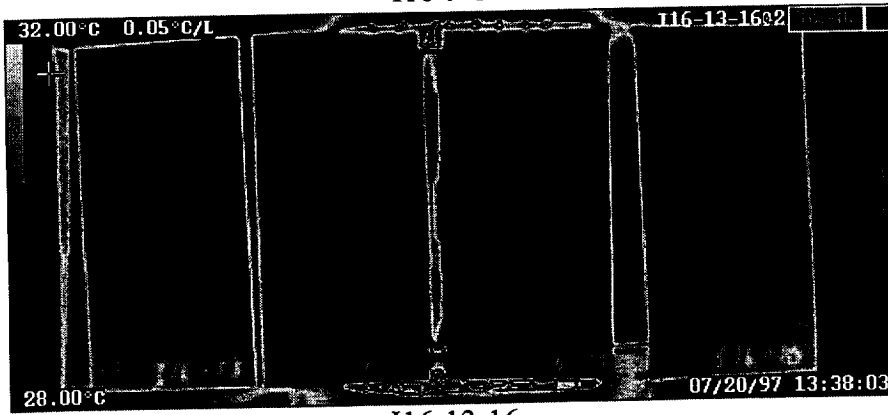
I16-1-4



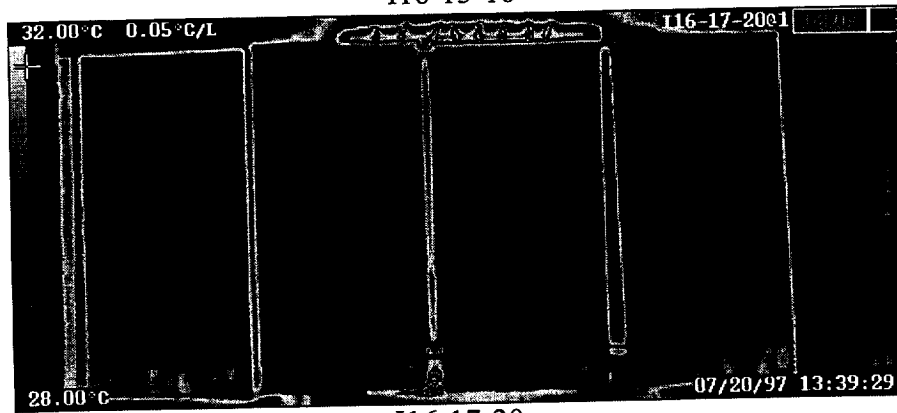
I16-5-8



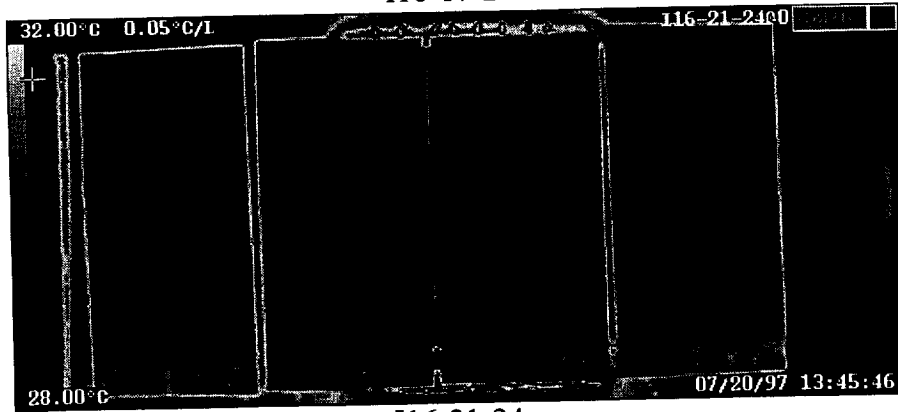
I16-9-12



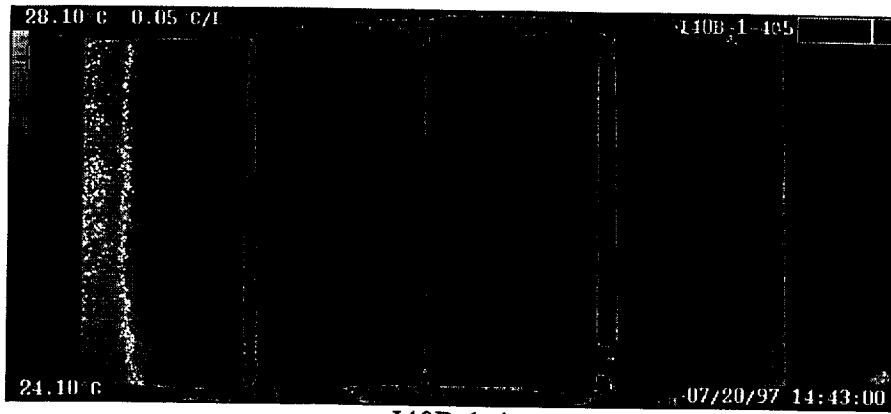
I16-13-16



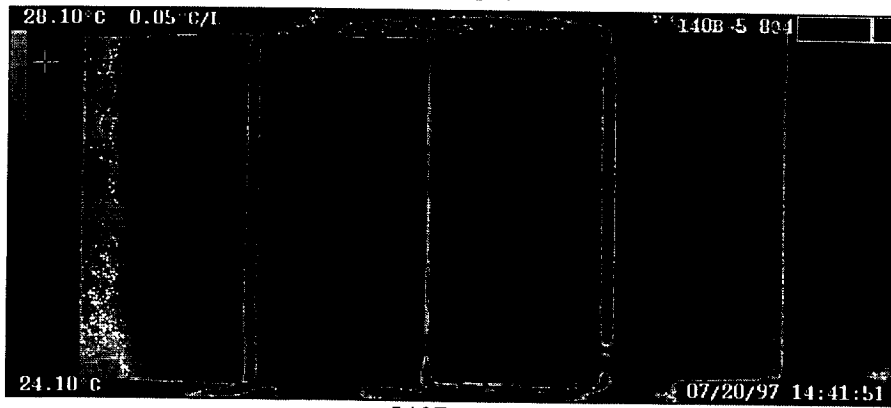
I16-17-20



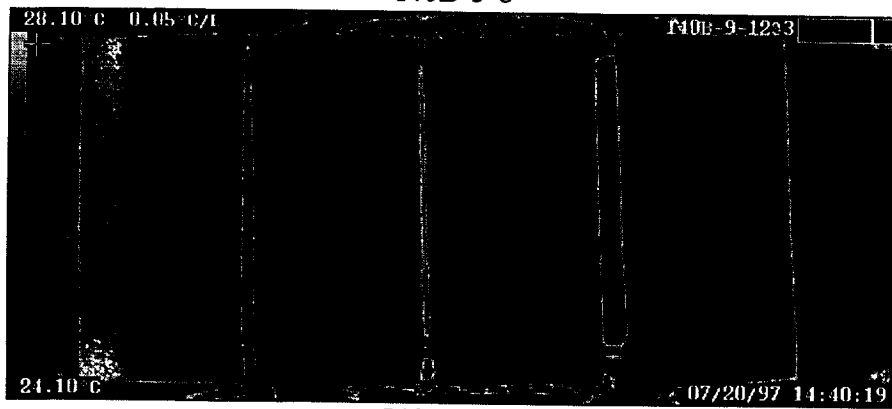
I16-21-24



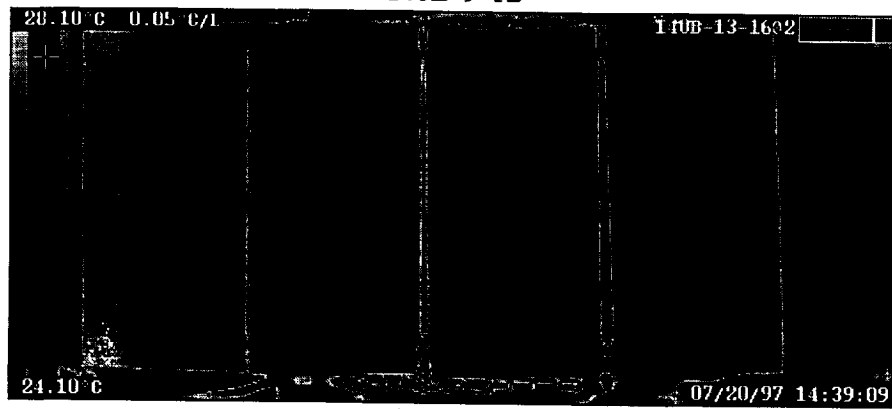
I40B-1-4



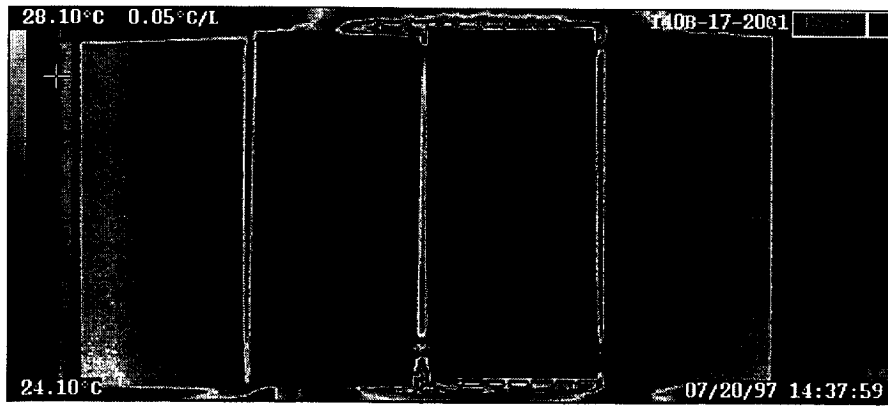
I40B-5-8



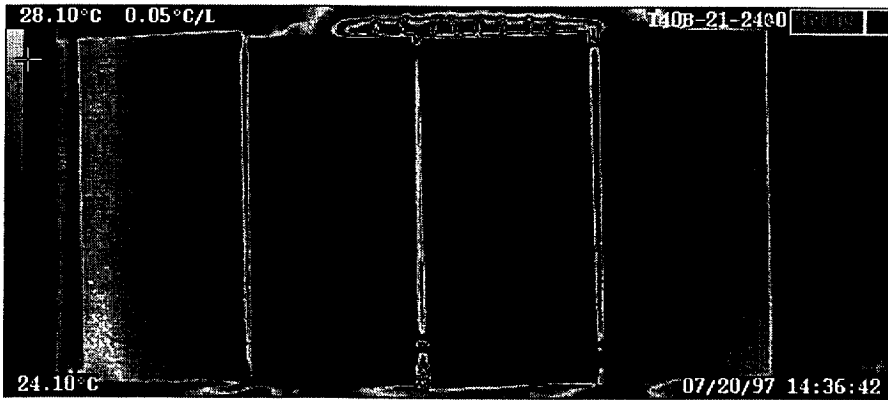
I40B-9-12



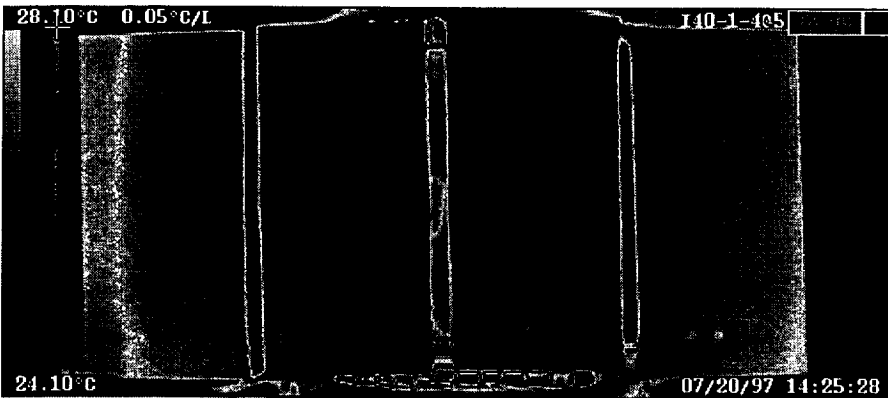
I40B-13-16



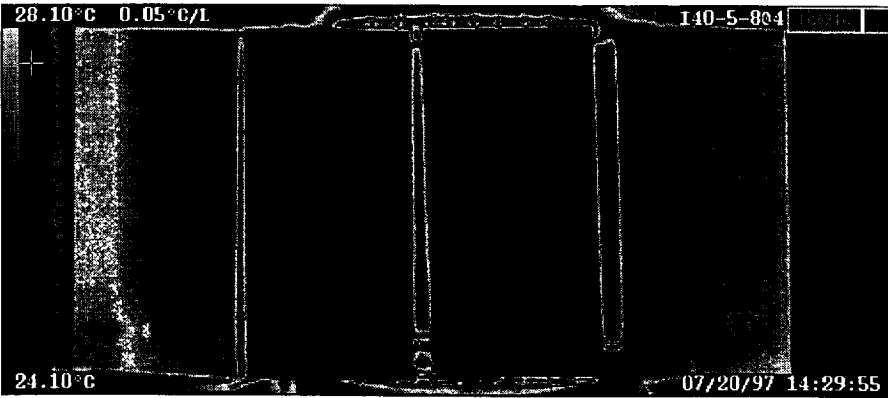
I40B-17-20



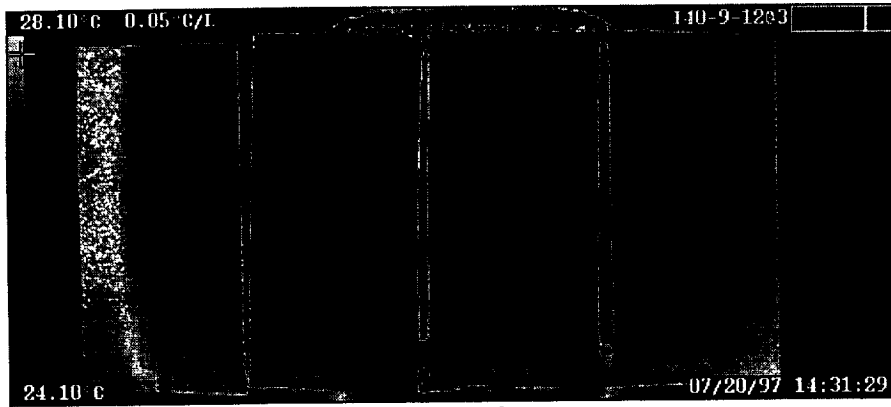
I40B-21-24



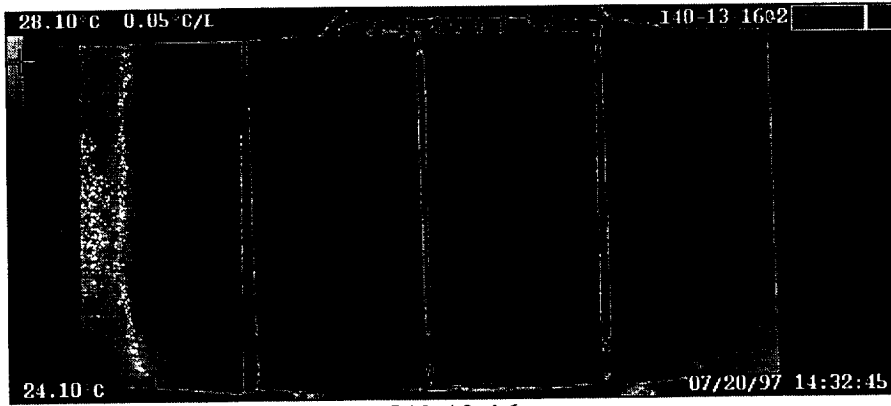
I40-1-4



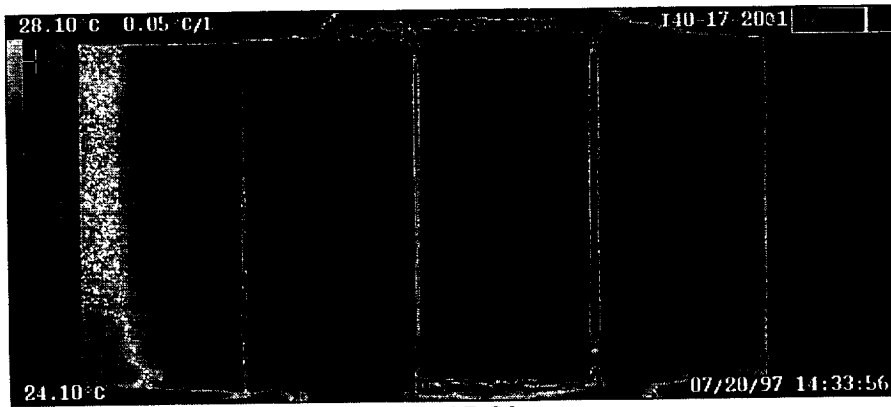
I40-5-8



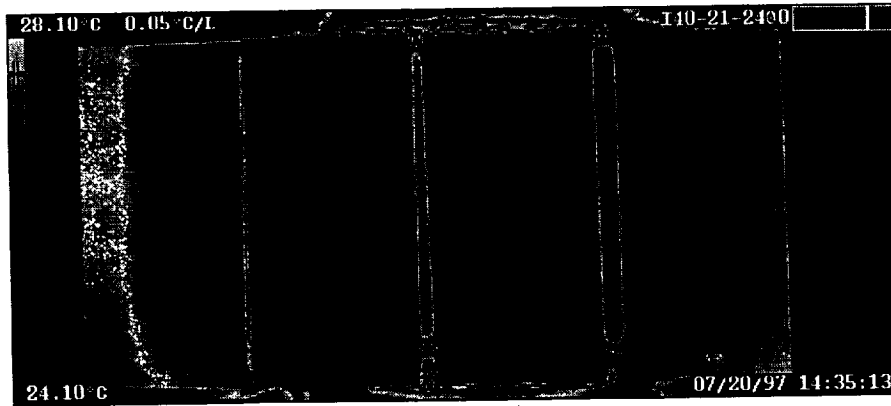
I40-9-12



I40-13-16



I40-17-20



I40-21-24